A Unifying Model for Cohesinopathies and Thalidomide Teratogenicity

A Unifying Model for Cohesinopathies and Thalidomide Teratogenicity

by

Annie Sanchez

A Dissertation

Presented to the Graduate and Research Committee

of Lehigh University

in Candidacy for the Degree of

Doctor of Philosophy

in

Cell and Molecular Biology

Lehigh University

May 2023

Approved and recommended for acceptance as a dissertation in partial fulfillment of the requirements for the degree of Doctor of Philosophy

Annie Sanchez
Identifying the Link Between Cohesinopathies and Thalidomide Teratogenicity

March 28, 2023

Defense Date

Dissertation Director
M. Kathyn Iovine, PhD

Approved Date

Committee Members

Robert V. Skibbens, PhD
(Co-advisor)

Michael J. Layden , PhD
(Internal Member)

Dale Dorsett, PhD
(External Member)

ACKNOWLEDGMENTS

First and foremost, I would like to thank my advisors, Dr. M. Kathryn Iovine and Dr. Robert V. Skibbens, for their time, mentorship, and support throughout my graduate career. Dr. Iovine's positivity and encouragement motivated me to continue and finish my Ph.D. Her guidance and support have been a driving force to my success in her lab. Her service and commitment to helping others left a long-lasting impact that has shaped my future goals. I couldn't have picked a better lab to be a part of. Dr. Skibbens has pushed me to be the best scientist I can be. His knowledge and enthusiasm for research was truly invaluable in my growth as a scientist. I thank you for all you both have done for me and for all the brilliant and fun discussions. I had the best of both worlds, and I learned so much from every interaction.

I would also like to thank the rest of my committee members, Dr. Michael Layden and Dr. Dale Dorsett. I thank you all for the discussions and guidance during committee meetings. I appreciate the time you spent with me and the feedback that improved my research and dissertation. I would also like to acknowledge the undergraduate students that helped me with this project, Elise Thren, Emma Anderson, and Fiona Mensching; your commitment and effort helped move this research forward. I would also like to acknowledge Dr. Shaswatti Battacharya, Dr. Mike Mfarej, Dr. Caitlin Hyland, Casey Field, and Lexi Perez for their friendship. You all shaped my time at Lehigh and made it a memorable and fun experience. I would also like to acknowledge the current graduate students in the Iovine Lab and Skibbens Lab, Alex Seaver, Victoria Hyland, and Gurvir Shing. I know the labs are in good hands, and I'm excited to see the work you will continue to do.

Lastly, I would like to thank my support system outside of Lehigh. To my friends and family, who have been with me through it all, I couldn't have done this without you. To my dad, I am forever grateful for all the sacrifices you made so I could be the person I am today. You are my biggest inspiration. To my brother, you have always been my best friend; I thank you for always believing in me and motivating me. And to my future husband, John, you have been through this whole thing with me. Words cannot express my appreciation for you. Thank you for taking care of ollie and frasier on my late days and weekends in the lab. Thank you for taking care of me on my bad days. Thank you for the laughs, the home, and the love you've given me. I can't wait for the next chapter of our lives.

I never imagined getting this far. I am thankful to everyone I've met along the way for you all have shaped me in some ways. I look forward to what the future has in store.

Annie Sanchez

May 2023

TABLE OF CONTENTS

LIST OF FIGURES AND TABLES

ABSTRACT

Roberts Syndrome (RBS) and Cornelia de Lange Syndrome (CdLS) are developmental conditions in humans collectively termed cohesinopathies. RBS and CdLS result in limb malformation, craniofacial abnormalities, cognitive disabilities, and defects in numerous internal organs, such as the GI tract and cardiac systems. Cohesinopathies arise due to improper cohesin function. Cohesin is a complex that plays a role in DNA tethering both in *cis* (along the same strand of DNA) and *trans* (between sister chromatids) mechanisms. DNA tethering is crucial for sister chromatid cohesin, DNA condensation, DNA repair, and transcriptional regulation. While the gene mutations resulting in cohesinopathies are well established, the downstream impacts of such mutations are largely unknown. Interestingly, the developmental defects arising from RBS and CdLS are highly similar to those due to thalidomide exposure during pregnancy. Thalidomide was a popular drug used to treat morning sickness in the late 1950s. Thalidomide exposure led to approximately 10,000 babies being born with severe developmental abnormalities. In this case, thalidomide blocks Cullin4 Ring Ligase (CRL4), a ubiquitin ligase that clears embryos of factors that adversely impact development. The downstream targets of CRL4 that lead to organ malformations are still elusive. Yet, thalidomide is an immunomodulatory (IMiD) drug that has proven effective in treatments of Hansen's Disease, leprosy, and myeloma. Thus, understanding the molecular mechanisms through which thalidomide acts is essential for drug discovery and new therapies.

Here, we investigate the role of cohesin in regulating the thalidomide target, CRL4. First, we report findings that the cohesin pathway impacts gene regulation of an essential CRL4

component. Second, we identify downstream targets of the cohesin/CRL4 axis that lead to organ malformation. These findings provide a unified molecular mechanism shared by thalidomide poisoning, and genetic outcomes that produce RBS and CdLS. This study provides a model to study multi-spectrum syndromes previously believed to be unrelated to each other. This research can help advance treatment options for rare diseases, as they may not be so rare after all.

CHAPTER 1

INTRODUCTION

1.1 The cohesin ring and function in development

Cohesin complex is made up of core proteins SMC1, SMC3, and RAD21/MCD1/SCC1 (Guacci et al., 1997; Michaelis et al., 1997; Tóth et al., 1999; Birkenbihl and Subramani 1992). The cohesin complex can bind DNA spontaneously, but auxiliary factors, such as SA1,2,, PDS5, ESCO2, HDAC8, and NIPBL, facilitate cohesion activation/deactivation and cohesin loading onto DNA (Ciosk 2000; Seitan 2006; Rollins 1999; Rollins 2004; Jeppsson 2014; Marston 2014; Skibbens 2016). Cohesins mediate the tethering of DNA segment, both in a *trans*- (intermolecular) and *cis*- (intramolecular) mechanism. Trans-DNA tethering is important for sister chromatid cohesion after DNA replication or in response to DNA damage. *Cis*-DNA tethering acts to create loops along the same strand of DNA for gene regulation and chromosome organization (Figure 1). Both *trans*- and *cis*- DNA tethering are a fundamental processes required for cell division and differentiation during multicellular organism development (Tanaka et al., 2000; Onn et al., 2008; Kakui and Uhlmann, 2018; Kim and Yu, 2020).

Multicellular organisms start off as a single cell that must divide and differentiate. Cell division allows for the replication of a single cell into identical daughter cells that will either continue to divide or differentiate to a specific cell fate. The DNA replication process occurs during the S-phase of the cell cycle; replicated chromosomes are segregated to daughter cells during mitosis. Sister chromatids must remain tethered together from replication until they are ready to separate in anaphase. Similarly, during DNA damage, cohesin is recruited to the DNA damage site to aid in repair through homologous recombination and genome-wide impedes cell cycle progression (Ström

et al., 2004; Ünal et al, 2004; Ström et al 2007; Ünal et al., 2008; Putnam and Kolodner, 2017). This *trans*- cohesion of chromosomes is mediated by the cohesin complex and auxiliary factors (Skibbens, 2009).

Importantly, cohesin plays another crucial role in development through its *cis*-DNA tethering mechanism. Gene regulation during development ensures genes are expressed at the appropriate times. This regulation allows for cells to take up specific functions or respond to different environments. Cohesin can facilitate gene regulation during development via long distance DNA looping (Rollins et al., 2004; Hadjur et al., 2009; Mishiro et al., 2009; Nativio et al., 2009; Hou et al., 2010). Studies in mammalian cells, show that cohesins interact with CCCTC-binding factor (CTCF), an important player in creating long range DNA interactions (Parelho et al., 2008; Rubio et al., 2008; Wendt and Peters, 2009; Hadjur et al., 2009; Hou et al., 2010; Kagey et al., 2011; Ball et al., 2014). There is evidence to suggest CTCF recruits cohesin for DNA loop stabilization (Wendt and Peters, 2009; Degner et al., 2011; Nativio et al., 2011; Majumder and Boss, 2011; Guo et al., 2012). These loops organize the chromosomes and allow for enhancers-promoter or suppressor interactions to regulate gene expression during development. In fact, cohesins can bind to about 18,000 new gene loci that help in the maternal to zygotic genome activation during development of zebrafish embryos (Meier et al., 2018). Not surprisingly, mutations in cohesin pathway can result in severe developmental maladies termed cohesinopathies.

1.2 The underlaying mechanism of cohesinopathies

Cohesinopathies are multi-spectrum developmental abnormalities which include Roberts Syndrome (RBS) and Cornelia de Lange Syndrome (CdLS). Cohesinopathies result in phocomelia (flipper-like appendages), microcephaly, cognitive disabilities, and defects in GI tract and numerous other internal organs. RBS and CdLS are cohesinopathies that result due to defects in the cohesin pathway. CdLS arises due to autosomal dominant disorders from heterozygous or X-linked mutations in cohesin subunits *SMC1A*, *SMC3*, *RAD21* or auxiliary factors *NIPBL* and *HDAC8* (Krantz et al., 2004; Tonkin et al., 2004; Gillis et al., 2004; Musio et al., 2006; Deardorff et al., 2007; Deardorff et al., 2012; Yuan et al., 2015). CdLS prevalence is at least 1 in every 10,000 live births with 65% of reported cases due to *NIPBL* gene mutations (Opitz, 1985; Krantz et al., 2004; Tonkin et al., 2004; Zakari et al., 2015). CdLS arises, in part, due to improper cohesin *cis*-DNA tethering which inhibits regulatory elements from regulating gene expression (Rollins et al., 1999; Krantz et al., 2004; Dorsett, 2010; Bose et al., 2012; Dorsett and Merkenschlager, 2013).

RBS on the other hand is an autosomal recessive disorder resulting from mutations in the cohesin acetyltransferase *ESCO2* (Establishment of Cohesion 1 homolog 2) (Van Den Berg and Franckle, 1993; Vega et al., 2005; Schüle et al., 2005; Gordillo et al., 2008). About 150 cases of RBS have been reported. There is a high mortality rate for RBS affected individuals, many infants with severe forms of RBS are stillborn or die shortly after birth (Schüle et al., 2005; Okpala et al., 2022). ESCO2 is evolutionarily conserved among vertebrates and the C terminus resembles the yeast Eco1/Ctf7 protein in yeast (Skibbens et al. 1999; Ivanov et al., 2002; Vega et al., 2005). ESCO2 activates cohesins through the acetylation of SMC3, a critical step for proper sister chromatid

cohesion and high fidelity chromosome segregation (Skibbens et al., 1999; Toth et al., 1999; Ivanov et al., 2002; Bellows et al., 2003; Hou and Zou, 2005; Rolef Ben-Shahar et al., 2008; Zhang et al., 2008). Unlike CdLS patients, which do not exhibit an increase in mitotic failure, RBS patient cells exhibit premature centromere separation, chromosome segregation defects, aneuploidy, elevated levels of apoptosis and reduced cell proliferation (Schüle et al., 2005; Vega et al., 2005; Gordillo et al., 2008; Horsfield et al., 2012; Mehta et al., 2013). Thus, it has been suggested that RBS arises due to defects in *trans*-DNA tethering. Alternatively, ESCO2 acetylation of SMC3 also is critical for regulating loop lengths during G1 (Dauban et al., 2020).

The prevailing model for RBS is through loss of proliferative stem cells due to cell death (Tomkins et al., 1979; Tomkins and Sisken, 1984; Brooker et al., 2014; Zakari et al., 2015; Percival et al., 2015; Afifi et al. 2016; Percival and Parant, 2016; Zhou et al., 2018; Colombo et al., 2019). Data from our labs, and others, support the alternative model that transcriptional deregulation contributes the suite of developmental abnormities in RBS, similarly to the mechanism that gives rise to CdLS (Choi et al. 2010; Leem et al., 2011; Monnich et al., 2011; Xu et al., 2013; Rahman et al., 2015; Banerji et al., 2016; Xu et al., 2016). A transcriptional role of Esco2 is found using the regenerative caudal fin of zebrafish to study skeletal defects associated with cohesinopathies show regulation of an important gene for bone and joint formation with both cohesin and Esco2 impairment (Banerji et al., 2016, 2017a). Additional evidence shows gene expression profiles of *rad21* null mutants and esco2 morphants show overlapping altered genes (Monnich et al., 2011). However, the effect of *rad21* and *esco2* reduction produced opposing effects, meaning upregulated expression of genes

in *rad21* mutants were downregulated in embryos reduced for Esco2 function and vice versa. While the contrasting directions of altered gene expressions led those authors to discount transcription dysregulation as causative fore RBS (Monnich et al., 2011; Bose et al., 2012), others considered that this difference may be due to the ability of cohesin to remain chromatin bound in *esco2* mutant but not in *rad21* mutants (Skibbens et al., 2013; Banerji et al., 2016; Banerji et al., 2017a). For instance, subsequent studies support the transcriptional role of Esco2. Recent studies show that Eco1 in yeast inhibits cohesin translocase activity, through a mechanism independent of Eco1's role in cohesion establishment (Dauban et al., 2020). This study showed Eco1 mediates cohesin dependent DNA loop extrusion in G1. Moreover, Esco2 regulates the Notch pathway to promote neuronal differentiation in human development and to promote embryogenesis in medaka studies (Leem et at., 2011; Morita et al., 2012). Given that any or all of these activities, when defective, may contribute to RBS phenotypes, further efforts to understand the mechanisms of cohesinopathies may advance treatments and prevention options.

1.3 Thalidomide causes developmental abnormalities through the CRL4 E3 Ligase

Interestingly, phenotypes observed in cohesinopathy patients are nearly identical to those that arise due to exposure to a pharmaceutical agent during pregnancy. α-N-phthalimidoglutarimide, also known as thalidomide, was an over-the-counter medication in the late 1950s advertised to be safe and effective in the relief of morning sickness during pregnancy. The in-utero exposure of thalidomide, however, led to approximately 10,000 newborns having severe birth defects world-wide. Thus

thalidomide is a teratogen that affects normal embryo development (Smithells and Newman, 1992; Vargesson, 2015). Thalidomide is also an IMiD with anti-inflammatory and anti-angiogenic properties that make this drug effective in the treatment of Hansen's disease, myeloma, and different autoimmune diseases (Sheskin, 1965; Sampaio et al., 1991; D'Amato at al., 1994; Tramontana et al., 1995; Mujagic et al., 2002).

A first glimpse into how thalidomide affects cellular processes was obtained by the identification of Cereblon (Crbn), a component of Cullin4-Ring Ligases (CRL4), as the drug binding target (Ito et al., 2010). Thalidomide is a small synthetic compound in which a chiral C3-carbon atom within the glutarimide gives rise to two optical isomers, (R) and (S), to produce a racemic mixture. Researchers found that (S)-enantiomer thalidomide can bind Crbn more effectively while the (R) enantiomer dimerizes, rendering it inactive in vivo (Tokunga et al., 2018). Inhibition of CRL4 by thalidomide impact the normal role of the E3 ligase, which is to ubiquitinate its substrates for regulation and tag them for proteasomal degradation. The accumulation of otherwise degraded substrates is likely the mechanism of thalidomide teratogenicity (Figure 2).

The CRL4 substrates responsible for aberrant development are largely unknown, but some downstream pathways impacted by thalidomide have been described (Ito et al., 2010; Ito et al., 2011; Zhu et al., 2011; Tokunaga et al., 2018; Asatsuma-Okumura et al., 2019; Cheng et al., 2019). For instance, downstream effects of thalidomide induce the decrease in both fibroblast growth factor 8 (fgf8), and vascular endothelial growth factor (vegf) expression as well as an increase in Reactive Oxidative Species (ROS) in tissues. All three (Fgf8, Vegf and ROS) are implicated as mechanisms for

teratogenic effects of thalidomide (D'Amato et al., 1994; Gupta et al., 2001; Yabu et al., 2005; Therapontos et al., 2009; Ito et al., 2011; Shortt et al., 2013, Gandhi et al., 2014).

Efforts to develop IMiDs with little to no teratogenic effects is ongoing. The Food and Drug Administration approved two thalidomide derivatives, lenalidomide and pomalidomide, for cancer treatments (Lederman, 2014). These derived IMiDs show stronger immunomodulatory properties than thalidomide but little success has been made in preventing embryotoxicity (Muller et al., 1996; Muller et al., 1999; Corral et al., 1999; D'Amato et al., 2013). All novel IMiDs act on CRL4 such that resistance to IMiDs treatments in cancer patients is correlated to reduced levels of Crbn (Zhu et al., 2011; Lopez-Girona et al., 2012; Heintel et al., 2013). More research suggests IMiDs not only prevent targeting of endogenous CRL4 substrates, but IMiD binding to Crbn induces neo-substrate targeting (An et al., 2017; Asatsuma-Okumura et al., 2019). This model has been pursued to explain the anti-inflammatory properties that make IMiDs effective in disease treatment. Together, this research suggests that both the teratogenic and beneficial effects of thalidomide occur through the direct binding of IMiDs to Crbn, mediating CRL4 activity.

1.4 CRL4 E3 Ligase affects developmental processes

CRL4 E3 Ligases are the most common types of E3 Ligases in eukaryotes. Regardless, all E3 Ligases require an ubiquitin activating enzyme (E1) and a ubiquitin conjugating enzyme (E2). E1 requires ATP to covalently bind the small 76 amino acid protein, ubiquitin (Ub). Once bound, Ub is transferred to the E2 enzyme. In association

with E2, E3 covalently attaches Ub to a target protein substrate. Polyubiquitination of proteins leads to proteasomal degradation while mono-ubiquitination has been implicated in modification of protein functions or trafficking (Fang and Weissman, 2004; McCall et al., 2008; Jackson and Xiong, 2009).

The CRL4 E3 Ligase targeted by thalidomide is composed of Ring Box 1 (RBX1/ROC1), Cullin-4 (Cul4) protein, DNA Damage Binding Protein 1 (Ddb1), and Crbn. Crbn represents 1 of more than 30 known Ddb1-Cul4 Associated Factor (DCAF) that bind DDB1 through a WD40 β-propeller domain (McCall et al., 2008). DCAFs serve as substrate receptors for CRL4 E3 Ligases and allows for CRL4 complexes to interact with a large network of proteins to regulate a variety of different processes in the cell (Petroski and Deshaies, 2005; Angers et al., 2006; Lee and Zhou, 2007; Zimmerman et al. 2010). More than 90 proteins in mammals contain the WD40 domain, although their role as possible DCAFs, has yet to be validated (McCall et al., 2008).

Mutations in CRL4 E3 Ligases affect many cellular processes including DNA damage response, gene expression regulation, chromatin remodeling, and embryonic development (Ou et al., 2002; Petroski and Deshaies, 2005; Bosu et al., 2008; Ito et al., 2010; Jiang et al., 2012; Yu et al., 2015). Investigating the roles of CRL4 in development is thus challenging due to the many cellular processes that CRL4 affects. Germline knockouts of *ddb1* or *cul4* in murine models result in embryonic lethality that corresponds to increased apoptosis and attenuated proliferation (Cang et al., 2006; Chen et al., 2012; Jiang et al., 2012; Liu et al., 2012). However, knockdown studies in different model systems demonstrate that some endogenous targets of CRL4 (like

CDT1, c-Jun, HOXA9, H3 and CHK1) play roles in cell cycle progression, chromatin remodeling, and cell differentiation, all important processes in development (Higa et al., 2006; Waning et al., 2008; Leung-Pineda et al., 2009; Yu et al., 2015).

Multicellular organism development involves a series of coordinated events that result in the formation of specific tissues and organs. Cellular differentiation occurs due to the selective regulation of gene expression. Cells have many regulatory mechanisms that control access to DNA, RNA transcription, and protein regulation. These events depend on concentrations of interacting proteins which leads to the expression or silencing of genes (Cacace et al. 2012; Murugan and Kreiman 2012; Costa et al. 2013; Neuert et al. 2013). Cullin-Ring Family Ligases play a role in protein turnover that facilitates cell cycle progression and gene regulation important for developmental processes (Clurman et al., 1996; Roodbarkelari et al., 2010; Hua and Viestra, 2011). Not surprisingly mutations impacting CRL4 are implicated to congenital disabilities in humans. For instance, X-linked intellectual disabilities (XLID) are linked to mutations in *CUL4* genes in humans (Cabezas et al., 2000; Tarpey et al., 2007). XLID causes several developmental abnormalities including mental retardation, short stature, craniofacial abnormalities, and impaired speech. The high embryonic mortality rate of mutations in CRL4 demonstrate the importance of this E3 Ligase in developmental processes and the crucial need to further investigate CRL4 downstream effects leading to aberrant developmental pathways.

1.5 Zebrafish as a model for thalidomide teratogenicity and cohesinopathy studies

The zebrafish embryo is a useful model to study developmental processes in a vertebrate system. The rapid development of zebrafish and the introduction of molecular techniques for genetic manipulation, like genome editing tools and morpholino (MO) mediated knockdowns, make zebrafish ideal to study development (Nasevicius and Ekker, 2000; Hwang et al., 2013; Seruggia and Montoliu, 2014). Zebrafish have a rapid life cycle and can live up to 5 years (Figure 1.3). About 70% of protein coding genes found in human have a zebrafish analog, while 84% of genes associated with human disease have a zebrafish counterpart (Howe et al., 2013). Zebrafish embryogenesis consists of several major developmental stages: zygote, cleavage, blastula or shield stage, gastrula, segmentation, pharyngula, hatching and early larval period.

The zygote period starts with fertilization of the egg, leading to cytoplasmic movement that initiates animal and vegetal polarization. The zygotic stage is characterized as the one-cell stage where the animal pole becomes a clearer 'bubble' on top of the yolk granule-rich vegetal pole. The first cleavage occurs at around 40 minutes post fertilization. Once in the cleavage stage, the dividing cells, or blastomeres, go through rounds of cell division about every 15 minutes. The zebrafish embryo cleavage stage is a meroblastic process, meaning that the cells are not completely cleaved from one another and remain interconnected by cytoplasmic bridges. This stage is complete after about 2 hours post fertilization (hpf) and the blastula stage starts after 8 rounds of zygotic cell cycles. During the blastula or shield stage, blastomeres lose cytoplasmic bridges, cell cycle progression slows, and cells become asynchronous. It is at this stage that the maternal to zygotic (MZT) transition occurs and the influence

of maternally inherited mRNA and proteins decrease while zygotic transcription increases (Langley et al., 2014). Epiboly begins at the end of the blastula stage and leads to the formation of the three layers that eventually give rise to the ectoderm, mesoderm, and endoderm. The gastrula stage starts when the zebrafish embryo is at 50% epiboly (~5hpf). It is during the gastrula stage that cell differentiation and commitment initiates. The embryo tail bud formation (at ~10hpf) marks the end of the epiboly stage. The segmentation period occurs from 10hpf to 24hpf. This stage is characterized by somite development, organogenesis, and embryo elongation. The pharyngula period describes the stage where zebrafish embryos develop the classic vertebrate features like bilateral organization and a well-developed notochord. Eyes, fins and otic vesicle start forming during this period and the embryo body straightens. Cartilage, vasculature, and pigment cells differentiate, and the embryo exhibits bouts of swimming at this stage. The hatching period varies by embryos but usually occurs about 48hpf. During the hatching period, cartilage forming the pharyngeal arches of the jaw protrude the mouth out and the pectoral fins elongate. At 72hpf, zebrafish embryos enter the larval stage and have completed most of their morphogenesis. Larvae continue to grow rapidly and are considered sexually matured by the time they are 3 months old (Kimmel at al., 1995).

Zebrafish remain a useful model for cohesinopathy studies (Ghiselli et al., 2006; Horsfield et al., 2007; Rhodes et al., 2010; Muto et al., 2011; Monnich et al., 2011; Deardorff et al., 2012; Banerji et al., 2016; Banerji et al., 2017a). For instance, knockdowns of Esco2 and the cohesin subunit, Rad21, in zebrafish produced phenotypes associated with human cohesinopathies such as decreased head and eye

sizes, decreased truck size and defects in cardiac and gut development (Ghiselli et al., 2006; Horsfield et al., 2007; Rhodes et al., 2010; Muto et al., 2011; Monnich et al., 2011; Deardorff et al., 2012).

Not only are zebrafish useful for genetic disease analysis, but are increasingly used for pharmacological studies and early drug development (Chakraborty et al., 2009). Previous studies using mice models do not recapitulate the teratogenic effects of thalidomide and other IMiDs. However, zebrafish studies have been widely used to study thalidomide and other IMiDs teratogenic effects. Treatment of zebrafish with IMiDs, leads to eye and otic vesicle defects, decreased trunk and pectoral fin size and defects in vasculature development (Ito et al., 2010; Cheng et al., 2011; Beedie et al., 2016). These phenotypes in zebrafish recapitulate the effects of thalidomide during embryogenesis in humans.

1.6 Hypothesis and Research Objectives

RBS and CdLS are developmental conditions that highly resemble thalidomide teratogenicity phenotypes. Despite the similarities, a connection between these genetically induced and drug-derived developmental conditions has not been thoroughly investigated. Emerging evidence, however, suggests shared molecular mechanisms. For instance, thalidomide susceptibility in humans is correlated to mutations in Esco2 (Gomes et al., 2019). Thalidomide acts through the inhibition of proper CRL4 function (Ito et al., 2010). At present, the Fgf8 downregulation, and the ROS response of thalidomide are linked to CRL4 function (Yabu et al., 2005; Li et al., 2011; Ito et al., 2010; Shortt et al., 2013). Interestingly, CdLS zebrafish models also

exhibit *fgf8* downregulation during limb development (Muto et al., 2014). While RBS cells, along with zebrafish and yeast models of cohesin pathway mutations, suggest increased ROS levels compared to controls (Xu et al., 2013; McKay et al., 2019; Ren et al., 2005; Ren et al., 2008). Further evidence supporting a shared molecular pathway between cohesinopathies and thalidomide through the CRL4 E3 ligase are findings that show Esco2, the cohesin acetylase, is a target of CRL4 (Minamino et al., 2018; Sun et al., 2019). However, an impact of Esco2 on CRL4 has never been reported.

Given the role of cohesin in gene regulation, and other research supporting the transcriptional role of Esco2, my research aims to explore transcriptional regulation of CRL4 E3 Ligase genes in cohesinopathy disease models. My findings (discussed in the next chapters) are the first to provide a link between cohesinopathies and thalidomide teratogenicity through deregulation of an essential component of CRL4, *ddb1* (Figure 1.4). My work sheds light into the mechanism that lead to abnormal development in RBS and CdLS individuals, and further links these conditions to a pharmacological-based mechanism that may provide new inroads to treatments.

1.7 Figures and Tables

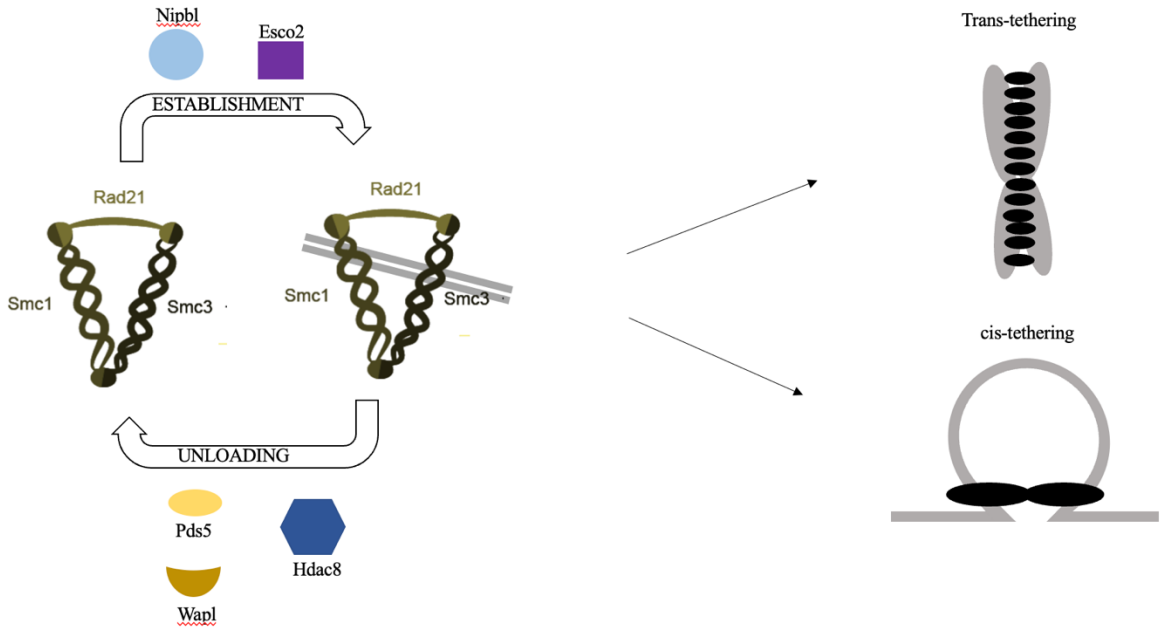

Figure 1.1. The cohesin complex and its function. Cohesin is made up of multiple core subunits, Smc1, Smc3 and Rad21 (SA and . Auxiliary proteins help cohesin loading/unloading (Nipbl, Wapl, Hdac8, Pds5, SA) onto DNA and establishment (Esco2). (right) Cohesin (Black circles) functions in both *cis*- and *trans*- DNA (grey) tethering mechanisms. *trans*- DNA tethering holds sister chromatids together after DNA replication and in response to DNA damage. *cis*- DNA tethering help organize in chromosome and plays a role in transcriptional regulation.

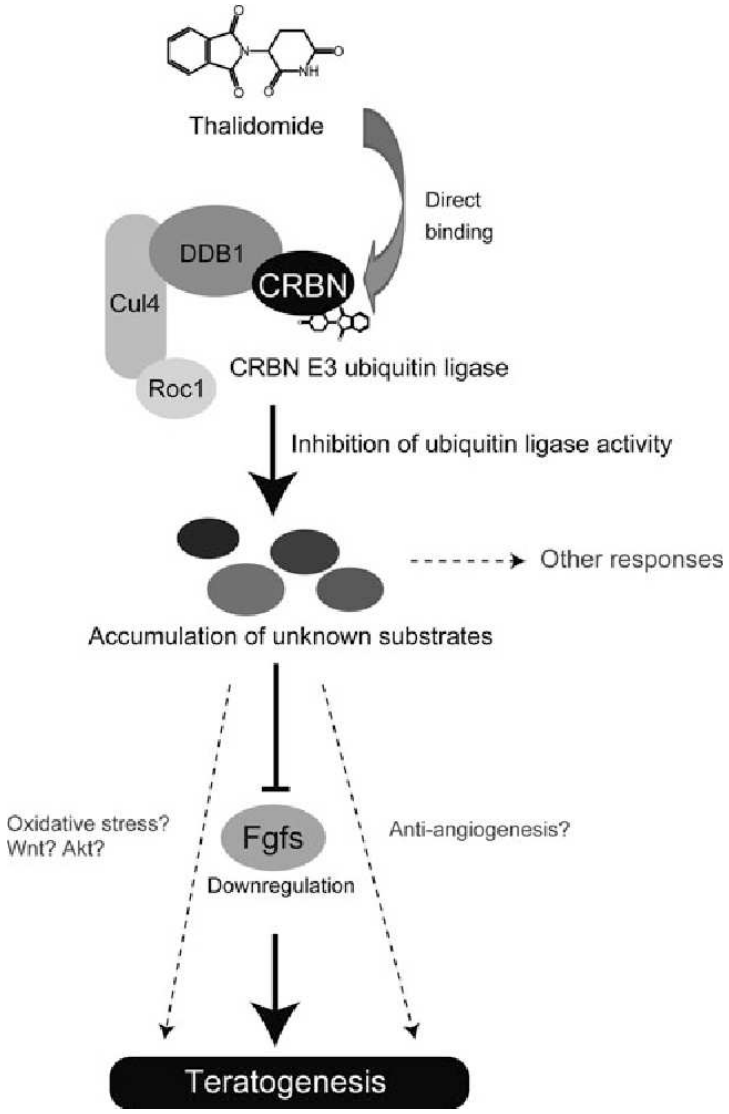

Figure 1.2. Proposed mechanism for thalidomide teratogenicity and immunomodulatory activities. Thalidomide directly binds Crbn resulting in alterations to endogenous CRL4 function. Accumulation of otherwise degraded proteins is suggested to cause changes is cellular processes.

Source: Ito et al. 2011

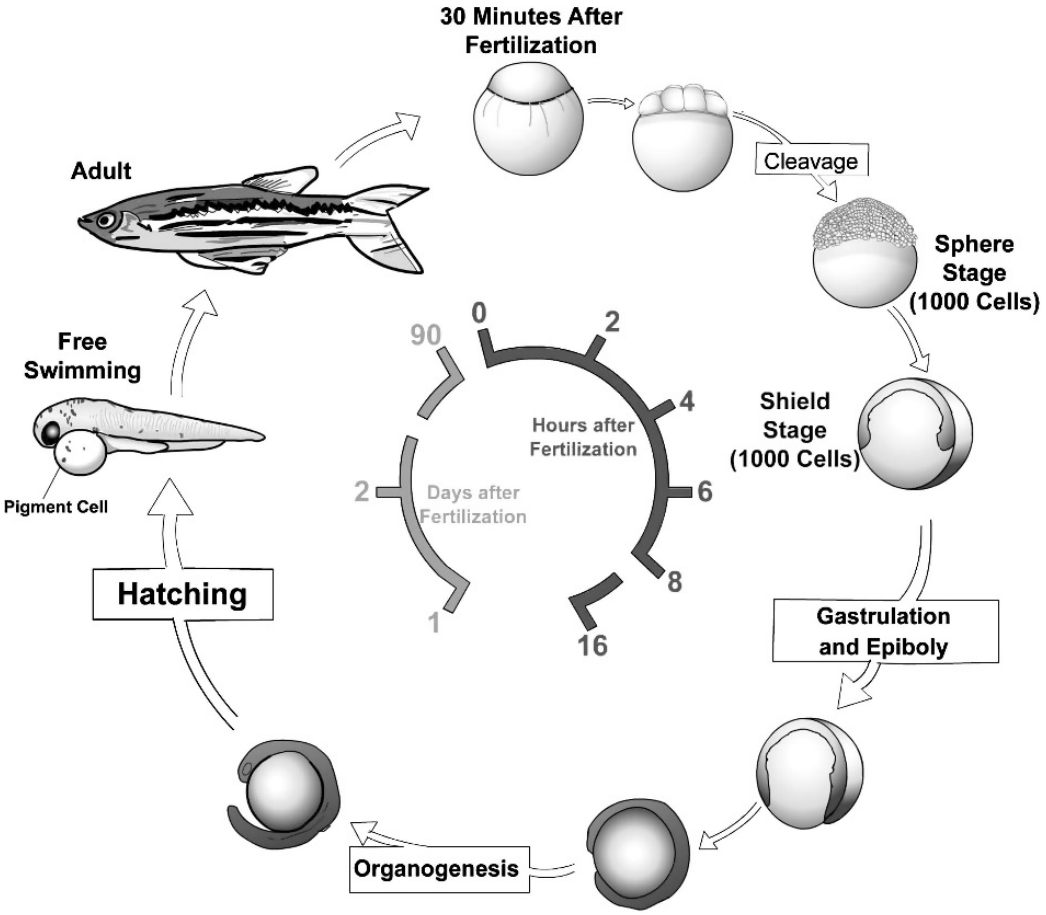

Figure 1.3. The zebrafish life cycle. Zebrafish develop rapidly, reaching sexual maturity by the time they reach three months of age. Zebrafish can live up to 5 years.

Source: D'Costa and Shepherd, 2009

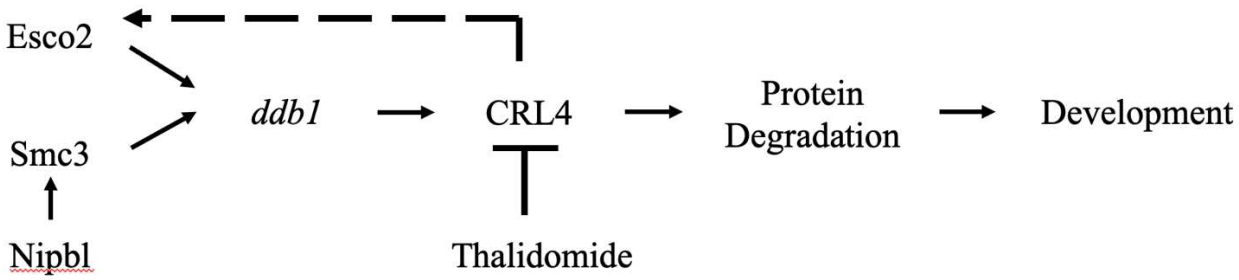

Figure 1.4. Proposed molecular cohesin/CRL4 pathway. Esco2, Smc3 and Nipbl regulate *ddb1* expression. Ddb1 is a subunit of CRL4, the thalidomide drug target. The role of CRL4 is to tag proteins with Ubiquitin, which targets them for proteasomal degradation, an important process during development. Dashed line represents evidence from Minamino et al., 2018 and Sun et al., 2019 that CRL4 regulates Esco2 protein.

1.8 References

Afifi HH, Abdel-Salam GM, Eid MM, Tosson AM, Shousha WG, Abdel Azeem AA, Farag MK, Mehrez MI, Gaber KR. Expanding the mutation and clinical spectrum of Roberts syndrome. *Congenit Anom (Kyoto)*. 2016 Jul;56(4):154-62. doi: 10.1111/cga.12151. PMID: 26710928.

An J, Ponthier CM, Sack R, Seebacher J, Stadler MB, Donovan KA, Fischer ES. pSILAC mass spectrometry reveals ZFP91 as IMiD-dependent substrate of the $CRL4^{CRBN}$ ubiquitin ligase. *Nat Commun*. 2017 May 22;8:15398. doi: 10.1038/ncomms15398. PMID: 28530236; PMCID: PMC5458144.

Angers S, Li T, Yi X, MacCoss M.J, Moon R.T, Zheng N. Molecular architecture, and assembly of the DDB1–CUL4A ubiquitin ligase machinery. *Nature* 443**,** 590–593 (2006). https://doi.org/10.1038/nature05175. PMID: 16964240.

Asatsuma-Okumura T, Ito T, Handa H. Molecular mechanism of cereblon-based drugs. *Pharmacol Ther*. 2019 Oct;202:132-139. doi: 10.1016/j.pharmthera.2019.06.004. Epub 2019 Jun 14. PMID: 31202702

Ball AR Jr, Chen YY, Yokomori K. Mechanisms of cohesin-mediated gene regulation and lessons learned from cohesinopathies. *Biochim Biophys Acta*. 2014 Mar;1839(3):191-202. doi: 10.1016/j.bbagrm.2013.11.002. Epub 2013 Nov 22. PMID: 24269489; PMCID: PMC3951616.

Banerji R, Eble DM, Iovine MK, Skibbens RV. Esco2 regulates cx43 expression during skeletal regeneration in the zebrafish fin. *Dev Dyn.* 2016 Jan;245(1):7-21. doi: 10.1002/dvdy.24354. Epub 2015 Nov 25. PMID: 26434741.

Banerji R, Skibbens RV, Iovine MK. Cohesin mediates Esco2-dependent transcriptional regulation in a zebrafish regenerating fin model of Roberts Syndrome. *Biol Open.* 2017a Dec 15;6(12):1802-1813. doi: 10.1242/bio.026013. PMID: 29084713; PMCID: PMC5769645.

Banerji R, Skibbens RV, Iovine MK. How many roads lead to cohesinopathies? *Dev Dyn.* 2017b Nov;246(11):881-888. doi: 10.1002/dvdy.24510. Epub 2017 May 22. PMID: 28422453.

Beedie SL, Rore HM, Barnett S, Chau CH, Luo W, Greig NH, Figg WD, Vargesson N. In vivo screening and discovery of novel candidate thalidomide analogs in the zebrafish embryo and chicken embryo model systems. *Oncotarget.* 2016 May 31;7(22):33237-45. doi: 10.18632/oncotarget.8909. PMID: 27120781; PMCID: PMC5078090.

Bellows AM, Kenna MA, Cassimeris L, Skibbens RV. Human EFO1p exhibits acetyltransferase activity and is a unique combination of linker histone and Ctf7p/Eco1p chromatid cohesion establishment domains. *Nucleic Acids Res.* 2003 Nov 1;31(21):6334-43. doi: 10.1093/nar/gkg811. PMID: 14576321; PMCID: PMC275453.

Birkenbihl RP, Subramani S. Cloning and characterization of rad21 an essential gene of Schizosaccharomyces pombe involved in DNA double-strand-break repair. *Nucleic Acids Res.* 1992 Dec 25;20(24):6605-11. doi: 10.1093/nar/20.24.6605. PMID: 1480481; PMCID: PMC334577.

Bose T, Lee KK, Lu S, Xu B, Harris B, Slaughter B, Unruh J, Garrett A, McDowell W, Box A, Li H, Peak A, Ramachandran S, Seidel C, Gerton JL. Cohesin proteins

promote ribosomal RNA production and protein translation in yeast and human cells. *PLoS Genet.* 2012;8(6):e1002749. doi: 10.1371/journal.pgen.1002749. Epub 2012 Jun 14. PMID: 22719263; PMCID: PMC3375231.

Bosu DR, Kipreos ET. Cullin-RING ubiquitin ligases: global regulation and activation cycles. *Cell Div.* 2008 Feb 18;3:7. doi: 10.1186/1747-1028-3-7. PMID: 18282298; PMCID: PMC2266742.

Brooker AS, Berkowitz KM. The roles of cohesins in mitosis, meiosis, and human health and disease. *Methods Mol Biol*. 2014;1170:229-66. doi: 10.1007/978-1-4939-0888-2_11. PMID: 24906316; PMCID: PMC4495907.

Cabezas DA, Slaugh R, Abidi F, Arena JF, Stevenson RE, Schwartz CE, Lubs HA. A new X linked mental retardation (XLMR) syndrome with short stature, small testes, muscle wasting, and tremor localizes to Xq24-q25. *J Med Genet.* 2000 Sep;37(9):663-8. doi: 10.1136/jmg.37.9.663. PMID: 10978355; PMCID: PMC1734699.

Cacace F, Paci P, Cusimano V, Germani A, Farina L. Stochastic modeling of expression kinetics identifies messenger half-lives and reveals sequential waves of coordinated transcription and decay. *PLoS Comput Biol.* 2012;8(11):e1002772. doi: 10.1371/journal.pcbi.1002772. Epub 2012 Nov 8. PMID: 23144606; PMCID: PMC3493476.

Cang Y, Zhang J, Nicholas SA, Bastien J, Li B, Zhou P, Goff SP. Deletion of DDB1 in mouse brain and lens leads to p53-dependent elimination of proliferating cells. *Cell.* 2006 Dec 1;127(5):929-40. doi: 10.1016/j.cell.2006.09.045. PMID: 17129780.

Chakraborty C, Hsu CH, Wen ZH, Lin CS, Agoramoorthy G. Zebrafish: a complete animal model for in vivo drug discovery and development. *Curr Drug Metab.* 2009 Feb;10(2):116-24. doi: 10.2174/138920009787522197. PMID: 19275547.

Chen CY, Tsai MS, Lin CY, Yu IS, Chen YT, Lin SR, Juan LW, Chen YT, Hsu HM, Lee LJ, Lin SW. Rescue of the genetically engineered Cul4b mutant mouse as a potential model for human X-linked mental retardation. *Hum Mol Genet.* 2012 Oct 1;21(19):4270-85. doi: 10.1093/hmg/dds261. Epub 2012 Jul 3. PMID: 22763239.

Cheng J, Gu YJ, Wang Y, Cheng SH, Wong WT. Nanotherapeutics in angiogenesis: synthesis and in vivo assessment of drug efficacy and biocompatibility in zebrafish embryos. *Int J Nanomedicine*. 2011;6:2007-21. doi: 10.2147/IJN.S20145. Epub 2011 Sep 15. PMID: 21976976; PMCID: PMC3181060.

Cheng J, Guo J, North BJ, Tao K, Zhou P, Wei W. The emerging role for Cullin 4 family of E3 ligases in tumorigenesis. *Biochim Biophys Acta Rev Cancer*. 2019 Jan;1871(1):138-159. doi: 10.1016/j.bbcan.2018.11.007. Epub 2018 Dec 30. PMID: 30602127

Choi HK, Kim BJ, Seo JH, Kang JS, Cho H, Kim ST. Cohesion establishment factor, Eco1 represses transcription via association with histone demethylase, LSD1. *Biochem Biophys Res Commun*. 2010 Apr 16;394(4):1063-8. doi: 10.1016/j.bbrc.2010.03.125. Epub 2010 Mar 21. PMID: 20331966.

Ciosk R, Shirayama M, Shevchenko A, Tanaka T, Toth A, Shevchenko A, Nasmyth K. Cohesin's binding to chromosomes depends on a separate complex consisting of

Scc2 and Scc4 proteins. *Mol Cell*. 2000 Feb;5(2):243-54. doi: 10.1016/s1097-2765(00)80420-7. PMID: 10882066.

Clurman BE, Sheaff RJ, Thress K, Groudine M, Roberts JM. Turnover of cyclin E by the ubiquitin-proteasome pathway is regulated by cdk2 binding and cyclin phosphorylation. *Genes Dev*. 1996 Aug 15;10(16):1979-90. doi: 10.1101/gad.10.16.1979. PMID: 8769642.

Colombo EA, Mutlu-Albayrak H, Shafeghati Y, Balasar M, Piard J, Gentilini D, Di Blasio AM, Gervasini C, Van Maldergem L, Larizza L. Phenotypic Overlap of Roberts and Baller-Gerold Syndromes in Two Patients With Craniosynostosis, Limb Reductions, and ESCO2 Mutations. *Front Pediatr*. 2019 May 28;7:210. doi: 10.3389/fped.2019.00210. PMID: 31192177; PMCID: PMC6546804.

Corral LG, Haslett PA, Muller GW, Chen R, Wong LM, Ocampo CJ, Patterson RT, Stirling DI, Kaplan G. Differential cytokine modulation and T cell activation by two distinct classes of thalidomide analogues that are potent inhibitors of TNF-alpha. *J Immunol*. 1999 Jul 1;163(1):380-6. PMID: 10384139.

Costa PR, Acencio ML, Lemke N. Cooperative RNA polymerase molecules behavior on a stochastic sequence-dependent model for transcription elongation. *PLoS One.* 2013;8(2):e57328. doi: 10.1371/journal.pone.0057328. Epub 2013 Feb 21. PMID: 23437369; PMCID: PMC3578854.

D'Amato RJ, Lentzsch S, Rogers MS. Pomalidomide is strongly antiangiogenic and teratogenic in relevant animal models. *Proc Natl Acad Sci U S A*. 2013 Dec 10;110(50):E4818. doi: 10.1073/pnas.1315875110. Epub 2013 Dec 3. PMID: 24302770; PMCID: PMC3864340.

D'Amato RJ, Loughnan MS, Flynn E, Folkman J. Thalidomide is an inhibitor of angiogenesis. *Proc Natl Acad Sci U S A*. 1994 Apr 26;91(9):4082-5. doi: 10.1073/pnas.91.9.4082. PMID: 7513432; PMCID: PMC43727.

D'Costa A, Shepherd IT. Zebrafish development and genetics: introducing undergraduates to developmental biology and genetics in a large introductory laboratory class. *Zebrafish.* 2009 Jun;6(2):169-77. doi: 10.1089/zeb.2008.0562. PMID: 19537943 PMCID: PMC2774836

Dauban L, Montagne R, Thierry A, Lazar-Stefanita L, Bastié N, Gadal O, Cournac A, Koszul R, Beckouët F. Regulation of Cohesin-Mediated Chromosome Folding by Eco1 and Other Partners. *Mol Cell*. 2020 Mar 19;77(6):1279-1293.e4. doi: 10.1016/j.molcel.2020.01.019. Epub 2020 Feb 6. PMID: 32032532.

Deardorff MA, Kaur M, Yaeger D, Rampuria A, Korolev S, Pie J, Gil-Rodríguez C, Arnedo M, Loeys B, Kline AD, Wilson M, Lillquist K, Siu V, Ramos FJ, Musio A, Jackson LS, Dorsett D, Krantz ID. Mutations in cohesin complex members SMC3 and SMC1A cause a mild variant of Cornelia de Lange syndrome with predominant mental retardation. *Am J Hum Genet*. 2007 Mar;80(3):485-94. doi: 10.1086/511888. Epub 2007 Jan 17. PMID: 17273969; PMCID: PMC1821101.

Deardorff MA, Wilde JJ, Albrecht M, Dickinson E, Tennstedt S, Braunholz D, Mönnich M, Yan Y, Xu W, Gil-Rodríguez MC, Clark D, Hakonarson H, Halbach S, Michelis LD, Rampuria A, Rossier E, Spranger S, Van Maldergem L, Lynch SA, Gillessen-Kaesbach G, Lüdecke HJ, Ramsay RG, McKay MJ, Krantz ID, Xu H, Horsfield JA, Kaiser FJ. RAD21 mutations cause a human cohesinopathy. *Am J*

Hum Genet. 2012 Jun 8;90(6):1014-27. doi: 10.1016/j.ajhg.2012.04.019. Epub 2012 May 24. PMID: 22633399; PMCID: PMC3370273.

Degner SC, Verma-Gaur J, Wong TP, Bossen C, Iverson GM, Torkamani A, Vettermann C, Lin YC, Ju Z, Schulz D, Murre CS, Birshtein BK, Schork NJ, Schlissel MS, Riblet R, Murre C, Feeney AJ. CCCTC-binding factor (CTCF) and cohesin influence the genomic architecture of the Igh locus and antisense transcription in pro-B cells. *Proc Natl Acad Sci U S A.* 2011 Jun 7;108(23):9566-71. doi: 10.1073/pnas.1019391108. Epub 2011 May 23. PMID: 21606361; PMCID: PMC3111298.

Dorsett D, Merkenschlager M. Cohesin at active genes: a unifying theme for cohesin and gene expression from model organisms to humans. *Curr Opin Cell Biol*. 2013 Jun;25(3):327-33. doi: 10.1016/j.ceb.2013.02.003. Epub 2013 Mar 1. PMID: 23465542; PMCID: PMC3691354.

Dorsett D. Gene regulation: the cohesin ring connects developmental highways. *Curr Biol*. 2010 Oct 26;20(20):R886-8. doi: 10.1016/j.cub.2010.09.036. PMID: 20971431.

Fang S, Weissman AM. A field guide to ubiquitylation. *Cell Mol Life Sci*. 2004 Jul;61(13):1546-61. doi: 10.1007/s00018-004-4129-5. PMID: 15224180.

Gandhi AK, Kang J, Havens CG, Conklin T, Ning Y, Wu L, Ito T, Ando H, Waldman MF, Thakurta A, Klippel A, Handa H, Daniel TO, Schafer PH, Chopra R. Immunomodulatory agents lenalidomide and pomalidomide co-stimulate T cells by inducing degradation of T cell repressors Ikaros and Aiolos via modulation of the E3 ubiquitin ligase complex CRL4(CRBN.). *Br J Haematol*. 2014

Mar;164(6):811-21. doi: 10.1111/bjh.12708. Epub 2013 Dec 13. PMID: 24328678; PMCID: PMC4232904.

Ghiselli G. SMC3 knockdown triggers genomic instability and p53-dependent apoptosis in human and zebrafish cells. *Mol Cancer.* 2006 Nov 2;5:52. doi: 10.1186/1476-4598-5-52. PMID: 17081288; PMCID: PMC1636066.

Gillis LA, McCallum J, Kaur M, DeScipio C, Yaeger D, Mariani A, Kline AD, Li HH, Devoto M, Jackson LG, Krantz ID. NIPBL mutational analysis in 120 individuals with Cornelia de Lange syndrome and evaluation of genotype-phenotype correlations. *Am J Hum Genet*. 2004 Oct;75(4):610-23. doi: 10.1086/424698. Epub 2004 Aug 18. PMID: 15318302; PMCID: PMC1182048.

Gomes JDA, Kowalski TW, Fraga LR, Macedo GS, Sanseverino MTV, Schuler-Faccini L, Vianna FSL. The role of ESCO2, SALL4 and TBX5 genes in the susceptibility to thalidomide teratogenesis. *Sci Rep*. 2019 Aug 6;9(1):11413. doi: 10.1038/s41598-019-47739-8. PMID: 31388035; PMCID: PMC6684595.

Gordillo M, Vega H, Trainer AH, Hou F, Sakai N, Luque R, Kayserili H, Basaran S, Skovby F, Hennekam RC, Uzielli ML, Schnur RE, Manouvrier S, Chang S, Blair E, Hurst JA, Forzano F, Meins M, Simola KO, Raas-Rothschild A, Schultz RA, McDaniel LD, Ozono K, Inui K, Zou H, Jabs EW. The molecular mechanism underlying Roberts syndrome involves loss of ESCO2 acetyltransferase activity. *Hum Mol Genet*. 2008 Jul 15;17(14):2172-80. doi: 10.1093/hmg/ddn116. PMID: 18411254

Guacci V, Koshland D, Strunnikov A. A direct link between sister chromatid cohesion and chromosome condensation revealed through the analysis of MCD1 in S.

cerevisiae. *Cell*. 1997 Oct 3;91(1):47-57. doi: 10.1016/s0092-8674(01)80008-8. PMID: 9335334; PMCID: PMC2670185.

Guo Y, Monahan K, Wu H, Gertz J, Varley KE, Li W, Myers RM, Maniatis T, Wu Q. CTCF/cohesin-mediated DNA looping is required for protocadherin α promoter choice. *Proc Natl Acad Sci U S A*. 2012 Dec 18;109(51):21081-6. doi: 10.1073/pnas.1219280110. Epub 2012 Nov 30. PMID: 23204437; PMCID: PMC3529044.

Gupta D, Treon SP, Shima Y, Hideshima T, Podar K, Tai YT, Lin B, Lentzsch S, Davies FE, Chauhan D, Schlossman RL, Richardson P, Ralph P, Wu L, Payvandi F, Muller G, Stirling DI, Anderson KC. Adherence of multiple myeloma cells to bone marrow stromal cells upregulates vascular endothelial growth factor secretion: therapeutic applications. *Leukemia*. 2001 Dec;15(12):1950-61. doi: 10.1038/sj.leu.2402295. PMID: 11753617.

Hadjur S, Williams LM, Ryan NK, Cobb BS, Sexton T, Fraser P, Fisher AG, Merkenschlager M. Cohesins form chromosomal cis-interactions at the developmentally regulated IFNG locus. *Nature*. 2009 Jul 16;460(7253):410-3. doi: 10.1038/nature08079. Epub 2009 May 20. PMID: 19458616; PMCID: PMC2869028.

Heintel D, Rocci A, Ludwig H, Bolomsky A, Caltagirone S, Schreder M, Pfeifer S, Gisslinger H, Zojer N, Jäger U, Palumbo A. High expression of cereblon (CRBN) is associated with improved clinical response in patients with multiple myeloma treated with lenalidomide and dexamethasone. *Br J Haematol*. 2013 Jun;161(5):695-700. doi: 10.1111/bjh.12338. Epub 2013 Apr 9. PMID: 23565715.

Higa LA, Banks D, Wu M, Kobayashi R, Sun H, Zhang H. L2DTL/CDT2 interacts with the CUL4/DDB1 complex and PCNA and regulates CDT1 proteolysis in response to DNA damage. Cell Cycle. 2006 Aug;5(15):1675-80. doi: 10.4161/cc.5.15.3149. Epub 2006 Aug 1. PMID: 16861906.

Horsfield JA, Anagnostou SH, Hu JK, Cho KH, Geisler R, Lieschke G, Crosier KE, Crosier PS. Cohesin-dependent regulation of Runx genes. *Development*. 2007 Jul;134(14):2639-49. doi: 10.1242/dev.002485. Epub 2007 Jun 13. PMID: 17567667.

Horsfield JA, Print CG, Mönnich M. Diverse developmental disorders from the one ring: distinct molecular pathways underlie the cohesinopathies. *Front Genet.* 2012 Sep 12;3:171. doi: 10.3389/fgene.2012.00171. PMID: 22988450; PMCID: PMC3439829.

Hou C, Dale R, Dean A. Cell type specificity of chromatin organization mediated by CTCF and cohesin. *Proc Natl Acad Sci U S A*. 2010 Feb 23;107(8):3651-6. doi: 10.1073/pnas.0912087107. Epub 2010 Feb 2. PMID: 20133600; PMCID: PMC2840441.

Hou F, Zou H. Two human orthologues of Eco1/Ctf7 acetyltransferases are both required for proper sister-chromatid cohesion. *Mol Biol* Cell. 2005 Aug;16(8):3908-18. doi: 10.1091/mbc.e04-12-1063. Epub 2005 Jun 15. PMID: 15958495; PMCID: PMC1182326.

Howe K, Clark MD, Torroja CF, Torrance J, Berthelot C, Muffato M, Collins JE, Humphray S, McLaren K, Matthews L, McLaren S, Sealy I, Caccamo M, Churcher C, Scott C, Barrett JC, Koch R, Rauch GJ, White S, Chow W, Kilian B,

Quintais LT, Guerra-Assunção JA, Zhou Y, Gu Y, Yen J, Vogel JH, Eyre T, Redmond S, Banerjee R, Chi J, Fu B, Langley E, Maguire SF, Laird GK, Lloyd D, Kenyon E, Donaldson S, Sehra H, Almeida-King J, Loveland J, Trevanion S, Jones M, Quail M, Willey D, Hunt A, Burton J, Sims S, McLay K, Plumb B, Davis J, Clee C, Oliver K, Clark R, Riddle C, Elliot D, Threadgold G, Harden G, Ware D, Begum S, Mortimore B, Kerry G, Heath P, Phillimore B, Tracey A, Corby N, Dunn M, Johnson C, Wood J, Clark S, Pelan S, Griffiths G, Smith M, Glithero R, Howden P, Barker N, Lloyd C, Stevens C, Harley J, Holt K, Panagiotidis G, Lovell J, Beasley H, Henderson C, Gordon D, Auger K, Wright D, Collins J, Raisen C, Dyer L, Leung K, Robertson L, Ambridge K, Leongamornlert D, McGuire S, Gilderthorp R, Griffiths C, Manthravadi D, Nichol S, Barker G, Whitehead S, Kay M, Brown J, Murnane C, Gray E, Humphries M, Sycamore N, Barker D, Saunders D, Wallis J, Babbage A, Hammond S, Mashreghi-Mohammadi M, Barr L, Martin S, Wray P, Ellington A, Matthews N, Ellwood M, Woodmansey R, Clark G, Cooper J, Tromans A, Grafham D, Skuce C, Pandian R, Andrews R, Harrison E, Kimberley A, Garnett J, Fosker N, Hall R, Garner P, Kelly D, Bird C, Palmer S, Gehring I, Berger A, Dooley CM, Ersan-Ürün Z, Eser C, Geiger H, Geisler M, Karotki L, Kirn A, Konantz J, Konantz M, Oberländer M, Rudolph-Geiger S, Teucke M, Lanz C, Raddatz G, Osoegawa K, Zhu B, Rapp A, Widaa S, Langford C, Yang F, Schuster SC, Carter NP, Harrow J, Ning Z, Herrero J, Searle SM, Enright A, Geisler R, Plasterk RH, Lee C, Westerfield M, de Jong PJ, Zon LI, Postlethwait JH, Nüsslein-Volhard C, Hubbard TJ, Roest Crollius H, Rogers J, Stemple DL. The

zebrafish reference genome sequence and its relationship to the human genome. *Nature*. 2013 Apr 25;496(7446):498-503. doi: 10.1038/nature12111. Epub 2013 Apr 17. Erratum in: Nature. 2014 Jan 9;505(7482):248. Cooper, James [corrected to Cooper, James D]; Eliott, David [corrected to Elliot, David]; Mortimer, Beverly [corrected to Mortimore, Beverley]; Begum, Sharmin [added]; Lloyd, Christine [added]; Lanz, Christa [added]; Raddatz, Günter [added]; Schuster, Ste. PMID: 23594743; PMCID: PMC3703927.

Hua Z, Vierstra RD. The cullin-RING ubiquitin-protein ligases. *Annu Rev Plant Biol*. 2011;62:299-334. doi: 10.1146/annurev-arplant-042809-112256. PMID: 21370976

Hwang WY, Fu Y, Reyon D, Maeder ML, Tsai SQ, Sander JD, Peterson RT, Yeh JR, Joung JK. Efficient genome editing in zebrafish using a CRISPR-Cas system. *Nat Biotechnol.* 2013 Mar;31(3):227-9. doi: 10.1038/nbt.2501. Epub 2013 Jan 29. PMID: 23360964; PMCID: PMC3686313.

Ito T, Ando H, Handa H. Teratogenic effects of thalidomide: molecular mechanisms. *Cell Mol Life Sci*. 2011 May;68(9):1569-79. doi: 10.1007/s00018-010-0619-9. Epub 2011 Jan 5. PMID: 21207098.

Ito T, Ando H, Suzuki T, Ogura T, Hotta K, Imamura Y, Yamaguchi Y, Handa H. Identification of a primary target of thalidomide teratogenicity. *Science*. 2010 Mar;327(5971: 1345-50. doi: 10.1126/science.1177319. PMID: 20223979.

Ivanov D, Schleiffer A, Eisenhaber F, Mechtler K, Haering CH, Nasmyth K. Eco1 is a novel acetyltransferase that can acetylate proteins involved in cohesion. *Curr*

Biol. 2002 Feb 19;12(4):323-8. doi: 10.1016/s0960-9822(02)00681-4. PMID: 11864574

Jackson S, Xiong Y. CRL4s: the CUL4-RING E3 ubiquitin ligases. *Trends Biochem Sci.* 2009 Nov;34(11):562-70. doi: 10.1016/j.tibs.2009.07.002. Epub 2009 Oct 7. PMID: 19818632; PMCID: PMC2783741.

Jeppsson K, Carlborg KK, Nakato R, Berta DG, Lilienthal I, Kanno T, Lindqvist A, Brink MC, Dantuma NP, Katou Y, Shirahige K, Sjögren C. The chromosomal association of the Smc5/6 complex depends on cohesion and predicts the level of sister chromatid entanglement. *PLoS Genet*. 2014 Oct 16;10(10):e1004680. doi: 10.1371/journal.pgen.1004680. PMID: 25329383; PMCID: PMC4199498.

Jiang B, Zhao W, Yuan J, Qian Y, Sun W, Zou Y, Guo C, Chen B, Shao C, Gong Y. Lack of Cul4b, an E3 ubiquitin ligase component, leads to embryonic lethality and abnormal placental development. *PLoS One*. 2012;7(5):e37070. doi: 10.1371/journal.pone.0037070. Epub 2012 May 14. PMID: 22606329; PMCID: PMC3351389.

Kagey MH, Newman JJ, Bilodeau S, et al. Mediator and cohesin connect gene expression and chromatin architecture [published correction appears in *Nature*. 2011 Apr 14;472(7342):247]. *Nature*. 2010;467(7314):430-435. doi:10.1038/nature09380

Kakui, Y., and Uhlmann, F. SMC complexes orchestrate the mitotic chromatin interaction landscape. *Curr. Genet*. 2018. 64 (2), 335–339. doi:10.1007/s00294-017-0755-y

Kim, Y., and Yu, H. Shaping of the 3D genome by the ATPase machine cohesin. *Exp. Mol. Med*. 2020. 52 (12), 1891–1897. doi:10.1038/s12276-020-00526-2

Kimmel CB, Ballard WW, Kimmel SR, Ullmann B, Schilling TF. Stage of Embryonic Development of the Zebrafish. *Dev Dyn*. 1995 Jul;203(3):253-310. doi: 10.1002/aja.1002030302. PMID: 8589427

Krantz ID, McCallum J, DeScipio C, Kaur M, Gillis LA, Yaeger D, Jukofsky L, Wasserman N, Bottani A, Morris CA, Nowaczyk MJ, Toriello H, Bamshad MJ, Carey JC, Rappaport E, Kawauchi S, Lander AD, Calof AL, Li HH, Devoto M, Jackson LG. Cornelia de Lange syndrome is caused by mutations in NIPBL, the human homolog of Drosophila melanogaster Nipped-B. *Nat Genet.* 2004 Jun;36(6):631-5. doi: 10.1038/ng1364. Epub 2004 May 16. PMID: 15146186; PMCID: PMC4902017.

Langley AR, Smith JC, Stemple DL, Harvey SA. New insights into the maternal to zygotic transition. *Development.* 2014 Oct;141(20):3834-41. doi: 10.1242/dev.102368. PMID: 25294937.

Lederman L. Pomalyst (Pomalidomide): A New Third-Generation Immunomodulatory Drug for Relapsed and/or Refractory Multiple Myeloma. *Am Health Drug Benefits.* 2014. 7:139-41.

Lee J, Zhou P. DCAFs, the missing link of the CUL4-DDB1 ubiquitin ligase. *Mol Cell*. 2007 Jun 22;26(6):775-80. doi: 10.1016/j.molcel.2007.06.001. PMID: 17588513.

Leem YE, Choi HK, Jung SY, Kim BJ, Lee KY, Yoon K, Qin J, Kang JS, Kim ST. Esco2 promotes neuronal differentiation by repressing Notch signaling. *Cell Signal.* 2011 Nov;23(11):1876-84. doi: 10.1016/j.cellsig.2011.07.006. Epub 2011 Jul 14. PMID: 21777673.

Leung-Pineda V, Huh J, Piwnica-Worms H. DDB1 targets Chk1 to the Cul4 E3 ligase complex in normal cycling cells and in cells experiencing replication stress. *Cancer Res.* 2009 Mar 15;69(6):2630-7. doi: 10.1158/0008-5472.CAN-08-3382. Epub 2009 Mar 10. PMID: 19276361; PMCID: PMC2776040.

Li X, Lu D, He F, Zhou H, Liu Q, Wang Y, Shao C, Gong Y. Cullin 4B protein ubiquitin ligase targets peroxiredoxin III for degradation. *J Biol Chem*. 2011 Sep 16;286(37):32344-54. doi: 10.1074/jbc.M111.249003. Epub 2011 Jul 27. PMID: 21795677; PMCID: PMC3173229.

Liu L, Yin Y, Li Y, Prevedel L, Lacy EH, Ma L, Zhou P. Essential role of the CUL4B ubiquitin ligase in extra-embryonic tissue development during mouse embryogenesis. *Cell Res.* 2012 Aug;22(8):1258-69. doi: 10.1038/cr.2012.48. Epub 2012 Mar 27. PMID: 22453236; PMCID: PMC3411166.

Lopez-Girona A, Mendy D, Ito T, Miller K, Gandhi AK, Kang J, Karasawa S, Carmel G, Jackson P, Abbasian M, Mahmoudi A, Cathers B, Rychak E, Gaidarova S, Chen R, Schafer PH, Handa H, Daniel TO, Evans JF, Chopra R. Cereblon is a direct protein target for immunomodulatory and antiproliferative activities of lenalidomide and pomalidomide. *Leukemia.* 2012 Nov;26(11):2326-35. doi: 10.1038/leu.2012.119. Epub 2012 May 3. Erratum in: Leukemia. 2012 Nov;26(11):2445. PMID: 22552008; PMCID: PMC3496085.

Majumder P, Boss JM. Cohesin regulates MHC class II genes through interactions with MHC class II insulators. *J Immunol*. 2011 Oct 15;187(8):4236-44. doi: 10.4049/jimmunol.1100688. Epub 2011 Sep 12. PMID: 21911605; PMCID: PMC3186872.

Marston AL. Chromosome segregation in budding yeast: sister chromatid cohesion and related mechanisms. *Genetics*. 2014 Jan;196(1):31-63. doi: 10.1534/genetics.112.145144. PMID: 24395824; PMCID: PMC3872193.

McCall CM, Miliani de Marval PL, Chastain PD 2nd, Jackson SC, He YJ, Kotake Y, Cook JG, Xiong Y. Human immunodeficiency virus type 1 Vpr-binding protein VprBP, a WD40 protein associated with the DDB1-CUL4 E3 ubiquitin ligase, is essential for DNA replication and embryonic development. *Mol Cell Biol*. 2008 Sep;28(18):5621-33. doi: 10.1128/MCB.00232-08. Epub 2008 Jul 7. PMID: 18606781; PMCID: PMC2546929.

McKay MJ, Craig J, Kalitsis P, Kozlov S, Verschoor S, Chen P, et al. A Roberts Syndrome Individual With Differential Genotoxin Sensitivity and a DNA Damage Response Defect. *Int J Radiat Oncol Biol Phys*. 2019;1–3 (5):1194–202.

Mehta GD, Kumar R, Srivastava S, Ghosh SK. Cohesin: functions beyond sister chromatid cohesion. *FEBS Lett*. 2013 Aug 2;587(15):2299-312. doi: 10.1016/j.febslet.2013.06.035. Epub 2013 Jul 4. PMID: 23831059.

Meier M, Grant J, Dowdle A, Thomas A, Gerton J, Collas P, O'Sullivan JM, Horsfield JA. Cohesin facilitates zygotic genome activation in zebrafish. *Development*. 2018 Jan 3;145(1):dev156521. doi: 10.1242/dev.156521. PMID: 29158440.

Michaelis C, Ciosk R, Nasmyth K. Cohesins: chromosomal proteins that prevent premature separation of sister chromatids. *Cell*. 1997 Oct 3;91(1):35-45. doi: 10.1016/s0092-8674(01)80007-6. PMID: 9335333.

Minamino M, Tei S, Negishi L, Kanemaki MT, Yoshimura A, Sutani T, Bando M, Shirahige K. Temporal Regulation of ESCO2 Degradation by the MCM Complex,

the CUL4-DDB1-VPRBP Complex, and the Anaphase-Promoting Complex. *Curr Biol.* 2018 Aug 20;28(16):2665-2672.e5. doi: 10.1016/j.cub.2018.06.037. Epub 2018 Aug 9. PMID: 30100344.

Mishiro T, Ishihara K, Hino S, Tsutsumi S, Aburatani H, Shirahige K, Kinoshita Y, Nakao M. Architectural roles of multiple chromatin insulators at the human apolipoprotein gene cluster. *EMBO J*. 2009 May 6;28(9):1234-45. doi: 10.1038/emboj.2009.81. Epub 2009 Mar 26. PMID: 19322193; PMCID: PMC2683055.

Monnich M, Kuriger Z, Print CG, Horsfield JA. A zebrafish model of Roberts syndrome reveals that Esco2 depletion interferes with development by disrupting the cell cycle. *PLoS One*. 2011;6(5):e20051. doi: 10.1371/journal.pone.0020051. Epub 2011 May 26. PMID: 21637801; PMCID: PMC3102698.

Morita, A., Nakahira, K., Hasegawa, T., Uchida, K., Taniguchi, Y., Takeda, S., Toyoda, A., Sakaki, Y., Shimada, A., Takeda, H., et al. 2012. Establishment and characterization of Roberts syndrome and SC phocomelia model medaka (Oryzias latipes). *Dev Growth Differ*. 2012 Jun;54(5):588-604. doi: 10.1111/j.1440-169X.2012.01362.x. PMID: 22694322

Mujagic H, Chabner BA, Mujagic Z. Mechanism of action and potential therapeutic use of thalidomide. *Croat Med J*. 2002 Jun;43(3):274-85. PMID: 12035132

Muller GW, Chen R, Huang SY, Corral LG, Wong LM, Patterson RT, Chen Y, Kaplan G, Stirling DI. Amino-substituted thalidomide analogs: potent inhibitors of TNF-alpha production. *Bioorg Med Chem Lett*. 1999 Jun 7;9(11):1625-30. doi: 10.1016/s0960-894x(99)00250-4. PMID: 10386948.

Muller GW, Corral LG, Shire MG, Wang H, Moreira A, Kaplan G, Stirling DI. Structural modifications of thalidomide produce analogs with enhanced tumor necrosis factor inhibitory activity. *J Med Chem*. 1996 Aug 16;39(17):3238-40. doi: 10.1021/jm9603328. PMID: 8765505.

Murugan R, Kreiman G. Theory on the coupled stochastic dynamics of transcription and splice-site recognition. *PLoS Comput Biol*. 2012;8(11):e1002747. doi: 10.1371/journal.pcbi.1002747. Epub 2012 Nov 1. PMID: 23133354; PMCID: PMC3486868.

Musio A, Selicorni A, Focarelli ML, Gervasini C, Milani D, Russo S, Vezzoni P, Larizza L. X-linked Cornelia de Lange syndrome owing to SMC1L1 mutations. *Nat Genet.* 2006 May;38(5):528-30. Epub 2006 Apr 9. DOI: 10.1038/ng1779. PMID: 16604071.

Muto A, Calof AL, Lander AD, Schilling TF. Multifactorial origins of heart and gut defects in nipbl-deficient zebrafish, a model of Cornelia de Lange Syndrome. *PLoS Biol*. 2011 Oct;9(10):e1001181. doi: 10.1371/journal.pbio.1001181. Epub 2011 Oct 25. PMID: 22039349; PMCID: PMC3201921.

Nasevicius A, Ekker SC. Effective targeted gene 'knockdown' in zebrafish. *Nat Genet.* 2000 Oct;26(2):216-20. doi: 10.1038/79951. PMID: 11017081.

Nativio R, Sparago A, Ito Y, Weksberg R, Riccio A, Murrell A. Disruption of genomic neighbourhood at the imprinted IGF2-H19 locus in Beckwith-Wiedemann syndrome and Silver-Russell syndrome. *Hum Mol Genet*. 2011 Apr 1;20(7):1363-74. doi: 10.1093/hmg/ddr018. Epub 2011 Jan 31. PMID: 21282187; PMCID: PMC3049359.

Nativio R, Wendt KS, Ito Y, Huddleston JE, Uribe-Lewis S, Woodfine K, Krueger C, Reik W, Peters JM, Murrell A. Cohesin is required for higher-order chromatin conformation at the imprinted IGF2-H19 locus. *PLoS Genet*. 2009 Nov;5(11):e1000739. doi: 10.1371/journal.pgen.1000739. Epub 2009 Nov 26. PMID: 19956766; PMCID: PMC2776306.

Neuert G, Munsky B, Tan RZ, Teytelman L, Khammash M, van Oudenaarden A. Systematic identification of signal-activated stochastic gene regulation. *Science*. 2013 Feb 1;339(6119):584-7. doi: 10.1126/science.1231456. PMID: 23372015; PMCID: PMC3751578.

Okpala BC, Echendu ST, Ikechebelu JI, Eleje GU, Joe-Ikechebelu NN, Nwajiaku LA, Nwachukwu CE, Igbodike EP, Nnoruka MC, Okpala AN, Ofojebe CJ, Umeononihu OS. Roberts syndrome with tetraphocomelia: A case report and literature review. *SAGE Open Med Case* Rep. 2022 Apr 21;10:2050313X221094077. doi: 10.1177/2050313X221094077. PMID: 35495290; PMCID: PMC9039428.

Onn, I., Heidinger-Pauli, J. M., Guacci, V., Unal, E., and Koshland, D. E. Sister chromatid cohesion: a simple concept with a complex reality. *Annu. Rev. Cell Dev. Biol*. 2008. 24, 105–129. doi:10.1146/annurev.cellbio.24.110707.175350

Opitz JM. The Brachmann-de Lange syndrome. Am J Med Genet. 1985 Sep;22(1):89-102. doi: 10.1002/ajmg.1320220110. PMID: 3901753.

Ou CY, Lin YF, Chen YJ, Chien CT. Distinct protein degradation mechanisms mediated by Cul1 and Cul3 controlling Ci stability in Drosophila eye development. *Genes*

Dev. 2002 Sep 15;16(18):2403-14. doi: 10.1101/gad.1011402. PMID: 12231629; PMCID: PMC187440.

Parelho V, Hadjur S, Spivakov M, Leleu M, Sauer S, Gregson HC, Jarmuz A, Canzonetta C, Webster Z, Nesterova T, Cobb BS, Yokomori K, Dillon N, Aragon L, Fisher AG, Merkenschlager M. Cohesins functionally associate with CTCF on mammalian chromosome arms. *Cell.* 2008 Feb 8;132(3):422-33. doi: 10.1016/j.cell.2008.01.011. Epub 2008 Jan 31. PMID: 18237772.

Percival SM, Parant JM. Observing Mitotic Division and Dynamics in a Live Zebrafish Embryo. *J Vis Exp.* 2016 Jul 15;(113):10.3791/54218. doi: 10.3791/54218. PMID: 27501381; PMCID: PMC6082026.

Percival SM, Thomas HR, Amsterdam A, Carroll AJ, Lees JA, Yost HJ, Parant JM. Variations in dysfunction of sister chromatid cohesion in esco2 mutant zebrafish reflect the phenotypic diversity of Roberts syndrome. *Dis Model Mech*. 2015 Aug 1;8(8):941-55. doi: 10.1242/dmm.019059. Epub 2015 Jun 4. PMID: 26044958; PMCID: PMC4527282.

Petroski M, Deshaies R. Function, and regulation of cullin–RING ubiquitin ligases. *Nat Rev Mol Cell Biol* 6, 9–20 (2005). https://doi.org/10.1038/nrm1547. PMID: 15688063

Putnam, Christopher D, and Richard D Kolodner. Pathways and Mechanisms That Prevent Genome. *Genetics.* 2017. 206: 1187–1225.

Rahman S, Jones MJ, Jallepalli PV. Cohesin recruits the Esco1 acetyltransferase genome wide to repress transcription and promote cohesion in somatic cells. *Proc Natl*

Acad Sci U S A. 2015 Sep 8;112(36):11270-5. doi: 10.1073/pnas.1505323112. Epub 2015 Aug 24. PMID: 26305936; PMCID: PMC4568707.

Ren Q, Yang H, Gao B, Zhang Z. Global transcriptional analysis of yeast cell death induced by mutation of sister chromatid cohesin. *Comp Funct Genomics*. 2008;2008:634283. pmid:18551189

Ren Q, Yang H, Rosinski M, Conrad MN, Dresser ME, Guacci V, et al. Mutation of the cohesin related gene PDS5 causes cell death with predominant apoptotic features in *Saccharomyces cerevisiae* during early meiosis. *Mutat Res*. 2005;570 (2):163–73. pmid:15708575

Rhodes JM, Bentley FK, Print CG, Dorsett D, Misulovin Z, Dickinson EJ, Crosier KE, Crosier PS, Horsfield JA. Positive regulation of c-Myc by cohesin is direct, and evolutionarily conserved. *Dev Biol*. 2010 Aug 15;344(2):637-49. doi: 10.1016/j.ydbio.2010.05.493. Epub 2010 May 27. PMID: 20553708; PMCID: PMC2941799.

Rolef Ben-Shahar T, Heeger S, Lehane C, East P, Flynn H, Skehel M, Uhlmann F. Eco1-dependent cohesin acetylation during establishment of sister chromatid cohesion. *Science*. 2008 Jul 25;321(5888):563-6. doi: 10.1126/science.1157774. PMID: 18653893.

Rollins RA, Korom M, Aulner N, Martens A, Dorsett D. Drosophila nipped-B protein supports sister chromatid cohesion and opposes the stromalin/Scc3 cohesion factor to facilitate long-range activation of the cut gene. *Mol Cell Biol*. 2004 Apr;24(8):3100-11. doi: 10.1128/mcb.24.8.3100-3111.2004. PMID: 15060134; PMCID: PMC381657.

Rollins RA, Morcillo P, Dorsett D. Nipped-B, a Drosophila homologue of chromosomal adherins, participates in activation by remote enhancers in the cut and Ultrabithorax genes. *Genetics*. 1999 Jun;152(2):577-93. PMID: 10353901; PMCID: PMC1460629.

Roodbarkelari F, Bramsiepe J, Weinl C, Marquardt S, Novák B, Jakoby MJ, Lechner E, Genschik P, Schnittger A. Cullin 4-ring finger-ligase plays a key role in the control of endoreplication cycles in Arabidopsis trichomes. *Proc Natl Acad Sci U S A.* 2010 Aug 24;107(34):15275-80. doi: 10.1073/pnas.1006941107. Epub 2010 Aug 9. PMID: 20696906; PMCID: PMC2930562.

Rubio ED, Reiss DJ, Welcsh PL, Disteche CM, Filippova GN, Baliga NS, Aebersold R, Ranish JA, Krumm A. CTCF physically links cohesin to chromatin. *Proc Natl Acad Sci U S A*. 2008 Jun 17;105(24):8309-14. doi: 10.1073/pnas.0801273105. Epub 2008 Jun 11. PMID: 18550811; PMCID: PMC2448833.

Sampaio EP, Sarno EN, Galilly R, Cohn ZA, Kaplan G. Thalidomide selectively inhibits tumor necrosis factor alpha production by stimulated human monocytes. *J Exp Med*. 1991 Mar 1;173(3):699-703. doi: 10.1084/jem.173.3.699. PMID: 1997652; PMCID: PMC2118820.

Schüle B, Oviedo A, Johnston K, Pai S, Francke U. Inactivating mutations in ESCO2 cause SC phocomelia and Roberts syndrome: no phenotype-genotype correlation. *Am J Hum Genet*. 2005 Dec;77(6):1117-28. doi: 10.1086/498695. Epub 2005 Oct 31. PMID: 16380922; PMCID: PMC1285169.

Seitan VC, Banks P, Laval S, Majid NA, Dorsett D, Rana A, Smith J, Bateman A, Krpic S, Hostert A, Rollins RA, Erdjument-Bromage H, Tempst P, Benard CY, Hekimi

S, Newbury SF, Strachan T. Metazoan Scc4 homologs link sister chromatid cohesion to cell and axon migration guidance. Version 2. *PLoS Biol*. 2006 Jul;4(8):e242. doi: 10.1371/journal.pbio.0040242. PMID: 16802858; PMCID: PMC1484498.

Seruggia D, Montoliu L. The new CRISPR-Cas system: RNA-guided genome engineering to efficiently produce any desired genetic alteration in animals. *Transgenic Res*. 2014 Oct;23(5):707-16. doi: 10.1007/s11248-014-9823-y. Epub 2014 Aug 6. PMID: 25092533.

Sheskin J. Thalidomide in the Treatment of Lepra Reactions. *Clin Pharmacol Ther*. 1965 May-Jun;6:303-6. doi: 10.1002/cpt196563303. PMID: 14296027.

Shortt J, Hsu AK, Johnstone RW. Thalidomide-analogue biology: immunological, molecular and epigenetic targets in cancer therapy. Oncogene. 2013 Sep 5;32(36):4191-202. doi: 10.1038/onc.2012.599. Epub 2013 Jan 14. PMID: 23318436.

Skibbens RV, Colquhoun JM, Green MJ, Molnar CA, Sin DN, Sullivan BJ, Tanzosh EE. Cohesinopathies of a feather flock together. *PLoS Genet*. 2013;9(12):e1004036. doi: 10.1371/journal.pgen.1004036. Epub 2013 Dec 19. PMID: 24367282; PMCID: PMC3868590.

Skibbens RV, Corson LB, Koshland D, Hieter P. Ctf7p is essential for sister chromatid cohesion and links mitotic chromosome structure to the DNA replication machinery. *Genes Dev*. 1999 Feb 1;13(3):307-19. doi: 10.1101/gad.13.3.307. PMID: 9990855; PMCID: PMC316428.

Skibbens RV. Establishment of sister chromatid cohesion. *Curr Biol*. 2009 Dec 29;19(24):R1126-32. doi: 10.1016/j.cub.2009.10.067. PMID: 20064425; PMCID: PMC4867117.

Skibbens RV. Of Rings and Rods: Regulating Cohesin Entrapment of DNA to Generate Intra- and Intermolecular Tethers. *PLoS Genet*. 2016 Oct 27;12(10):e1006337. doi: 10.1371/journal.pgen.1006337. Erratum in: PLoS Genet. 2016 Dec 1;12 (12):e1006478. PMID: 27788133; PMCID: PMC5082857.

Smithells RW, Newman CG. Recognition of thalidomide defects. *J Med Genet*. 1992 Oct;29(10):716-23. doi: 10.1136/jmg.29.10.716. PMID: 1433232; PMCID: PMC1016130.

Ström, Lena, Charlotte Karlsson, Hanna Betts Lindroos, Sara Wedahl, Yuki Katou, Katsuhiko Shirahige, and Camilla Sjögren. Postreplicative Formation of Cohesion Is Required for Repair and Induced by a Single DNA Break. 2007. *Science* 317: 242–45.

Ström, Lena, Hanna Betts Lindroos, Katsuhiko Shirahige, and Camilla Sjogren. Postreplicative Recruitment of Cohesin to Double-Strand Breaks Is Required for DNA Repair. 2004. *Mol. Cell* 16: 1003–15.

Sun H, Zhang J, Xin S, Jiang M, Zhang J, Li Z, Cao Q, Lou H. Cul4-Ddb1 ubiquitin ligases facilitate DNA replication-coupled sister chromatid cohesion through regulation of cohesin acetyltransferase Esco2. *PLoS Genet*. 2019 Feb 19;15(2):e1007685. doi: 10.1371/journal.pgen.1007685. PMID: 30779731; PMCID: PMC6396947.

Tanaka, T., Fuchs, J., Loidl, J., and Nasmyth, K. Cohesin ensures bipolar attachment of microtubules to sister centromeres and resists their precocious separation. *Nat. Cell Biol.* 2000. 2 (8), 492–499. doi:10.1038/35019529

Tarpey PS, Raymond FL, O'Meara S, Edkins S, Teague J, Butler A, Dicks E, Stevens C, Tofts C, Avis T, Barthorpe S, Buck G, Cole J, Gray K, Halliday K, Harrison R, Hills K, Jenkinson A, Jones D, Menzies A, Mironenko T, Perry J, Raine K, Richardson D, Shepherd R, Small A, Varian J, West S, Widaa S, Mallya U, Moon J, Luo Y, Holder S, Smithson SF, Hurst JA, Clayton-Smith J, Kerr B, Boyle J, Shaw M, Vandeleur L, Rodriguez J, Slaugh R, Easton DF, Wooster R, Bobrow M, Srivastava AK, Stevenson RE, Schwartz CE, Turner G, Gecz J, Futreal PA, Stratton MR, Partington M. Mutations in CUL4B, which encodes a ubiquitin E3 ligase subunit, cause an X-linked mental retardation syndrome associated with aggressive outbursts, seizures, relative macrocephaly, central obesity, hypogonadism, pes cavus, and tremor. *Am J Hum Genet*. 2007 Feb;80(2):345-52. doi: 10.1086/511134. Epub 2007 Jan 4. PMID: 17236139; PMCID: PMC1785336.

Therapontos C, Erskine L, Gardner ER, Figg WD, Vargesson N. Thalidomide induces limb defects by preventing angiogenic outgrowth during early limb formation. *Proc Natl Acad Sci U S* A. 2009 May 26;106(21):8573-8. doi: 10.1073/pnas.0901505106. Epub 2009 May 11. PMID: 19433787; PMCID: PMC2688998.

Tokunaga E, Yamamoto T, Ito E, Shibata N. Understanding the Thalidomide Chirality in Biological Processes by the Self-disproportionation of Enantiomers. *Sci Rep*.

2018 Nov 20;8(1):17131. doi: 10.1038/s41598-018-35457-6. PMID: 30459439; PMCID: PMC6244226.

Tomkins D, Hunter A, Roberts M. Cytogenetic findings in Roberts-SC phocomelia syndrome (s). *Am J Med Genet*. 1979;4(1):17-26. doi: 10.1002/ajmg.1320040104. PMID: 495649

Tomkins DJ, Sisken JE. Abnormalities in the cell-division cycle in Roberts syndrome fibroblasts: a cellular basis for the phenotypic characteristics? *Am J Hum Genet*. 1984 Nov;36(6):1332-40. PMID: 6517054; PMCID: PMC1684655.

Tonkin ET, Wang TJ, Lisgo S, Bamshad MJ, Strachan T. NIPBL, encoding a homolog of fungal Scc2-type sister chromatid cohesion proteins and fly Nipped-B, is mutated in Cornelia de Lange syndrome. *Nat Genet*. 2004 Jun;36(6):636-41. Epub 2004 May 16. doi: 10.1038/ng1363 PMID: 15146185

Tóth A, Ciosk R, Uhlmann F, Galova M, Schleiffer A, Nasmyth K. Yeast cohesin complex requires a conserved protein, Eco1p(Ctf7), to establish cohesion between sister chromatids during DNA replication. *Genes Dev*. 1999 Feb 1;13(3):320-33. doi: 10.1101/gad.13.3.320. PMID: 9990856; PMCID: PMC316435.

Tramontana JM, Utaipat U, Molloy A, Akarasewi P, Burroughs M, Makonkawkeyoon S, Johnson B, Klausner JD, Rom W, Kaplan G. Thalidomide treatment reduces tumor necrosis factor alpha production and enhances weight gain in patients with pulmonary tuberculosis. *Mol Med*. 1995 May;1(4):384-97. doi: 10.1007/BF03401576 PMID: 8521296; PMCID: PMC2229989.

Ünal E, Heidinger-Pauli JM, Kim W, Guacci V, Onn I, Gygi SP, et al. A Molecular Determinant for the Establishment of Sister Chromatid Cohesion. *Science*. 2008;321:566.

Ünal, Elcin, Ayelet Arbel-eden, Ulrike Sattler, Robert Shroff, Michael Lichten, James EHaber, and Douglas Koshland. DNA Damage Response Pathway Uses Histone Modification to Assemble a Double-Strand Break-Specific Cohesin Domain. *Mol. Cell. 2004* 16: 991–1002.

Van Den Berg DJ, Franckle U. Roberts syndrome: a review of 100 cases and a new rating system for severity. *Am J Med Genet*. 1993 Nov 15;47(7):1104-23. doi: 10.1002/ajmg.1320470735. PMID: 8291532

Vargesson N. Thalidomide-induced teratogenesis: history and mechanisms. Birth Defects *Res C Embryo Today*. 2015 Jun;105(2):140-56. doi: 10.1002/bdrc.21096. Epub 2015 Jun 4. PMID: 26043938; PMCID: PMC4737249.

Vega H, Waisfisz Q, Gordillo M, Sakai N, Yanagihara I, Yamada M, van Gosliga D, Kayserili H, Xu C, Ozono K, Jabs EW, Inui K, Joenje H. Roberts syndrome is caused by mutations in ESCO2, a human homolog of yeast ECO1 that is essential for the establishment of sister chromatid cohesion. *Nat Genet*. 2005 May;37(5):468-70. Epub 2005 Apr 10. doi: 10.1038/ng1548. PMID: 15821733

Waning DL, Li B, Jia N, Naaldijk Y, Goebel WS, HogenEsch H, Chun KT. Cul4A is required for hematopoietic cell viability and its deficiency leads to apoptosis. *Blood*. 2008 Jul 15;112(2):320-9. doi: 10.1182/blood-2007-11-126300. Epub 2008 Mar 13. PMID: 18339895; PMCID: PMC2442743.

Wendt KS, Peters JM. How cohesin and CTCF cooperate in regulating gene expression. *Chromosome Res*. 2009;17(2):201-14. doi: 10.1007/s10577-008-9017-7. Epub 2009 Mar 24. PMID: 19308701.

Xu B, Gogol M, Gaudenz K, Gerton JL. Improved transcription and translation with L-leucine stimulation of mTORC1 in Roberts syndrome. *BMC Genomics*. 2016 Jan 5;17:25. doi: 10.1186/s12864-015-2354-y. PMID: 26729373; PMCID: PMC4700579.

Xu B, Lee KK, Zhang L, Gerton JL. Stimulation of mTORC1 with L-leucine Rescues Defects Associated with Roberts Syndrome. *PLoS Genet*. 2013;9 (10):e1003857. pmid:24098154

Xu B, Lee KK, Zhang L, Gerton JL. Stimulation of mTORC1 with L-leucine rescues defects associated with Roberts syndrome. *PLoS Genet*. 2013;9(10):e1003857. doi: 10.1371/journal.pgen.1003857. Epub 2013 Oct 3. PMID: 24098154; PMCID: PMC3789817.

Yabu T, Tomimoto H, Taguchi Y, Yamaoka S, Igarashi Y, Okazaki T. Thalidomide-induced antiangiogenic action is mediated by ceramide through depletion of VEGF receptors, and is antagonized by sphingosine-1-phosphate. *Blood* 2005; 106: 125–134. doi: 10.1182/blood-2004-09-3679.

Yu C, Ji SY, Sha QQ, Sun QY, Fan HY. CRL4-DCAF1 ubiquitin E3 ligase directs protein phosphatase 2A degradation to control oocyte meiotic maturation. *Nat Commun*. 2015 Aug 18;6:8017. doi: 10.1038/ncomms9017. PMID: 26281983; PMCID: PMC4557334.

Yuan B, Pehlivan D, Karaca E, Patel N, Charng WL, Gambin T, Gonzaga-Jauregui C, Sutton VR, Yesil G, Bozdogan ST, Tos T, Koparir A, Koparir E, Beck CR, Gu S, Aslan H, Yuregir OO, Al Rubeaan K, Alnaqeb D, Alshammari MJ, Bayram Y, Atik MM, Aydin H, Geckinli BB, Seven M, Ulucan H, Fenercioglu E, Ozen M, Jhangiani S, Muzny DM, Boerwinkle E, Tuysuz B, Alkuraya FS, Gibbs RA, Lupski JR. Global transcriptional disturbances underlie Cornelia de Lange syndrome and related phenotypes. *J Clin Invest*. 2015 Feb;125(2):636-51. doi: 10.1172/JCI77435. Epub 2015 Jan 9. PMID: 25574841; PMCID: PMC4319410.

Zakari M, Yuen K, Gerton JL. Etiology and pathogenesis of the cohesinopathies. *Wiley Interdiscip Rev Dev Biol.* 2015 Sep-Oct;4(5):489-504. doi: 10.1002/wdev.190. Epub 2015 Apr 7. PMID: 25847322; PMCID: PMC6680315.

Zhang J, Shi X, Li Y, Kim BJ, Jia J, Huang Z, Yang T, Fu X, Jung SY, Wang Y, Zhang P, Kim ST, Pan X, Qin J. Acetylation of Smc3 by Eco1 is required for S phase sister chromatid cohesion in both human and yeast. *Mol Cell*. 2008 Jul 11;31(1):143-51. doi: 10.1016/j.molcel.2008.06.006. PMID: 18614053.

Zhou J, Yang X, Jin X, Jia Z, Lu H, Qi Z. Long-term survival after corrective surgeries in two patients with severe deformities due to Roberts syndrome: A Case report and review of the literature. *Exp Ther Med*. 2018 Feb;15(2):1702-1711. doi: 10.3892/etm.2017.5592. Epub 2017 Dec 5. PMID: 29434756; PMCID: PMC5776516.

Zhu YX, Braggio E, Shi CX, Bruins LA, Schmidt JE, Van Wier S, Chang XB, Bjorklund CC, Fonseca R, Bergsagel PL, Orlowski RZ, Stewart AK. Cereblon expression is required for the antimyeloma activity of lenalidomide and pomalidomide. *Blood*.

2011 Nov 3;118(18):4771-9. doi: 10.1182/blood-2011-05-356063. Epub 2011 Aug 22. PMID: 21860026; PMCID: PMC3208291.

Zimmerman ES, Schulman BA, Zheng N. Structural assembly of cullin-RING ubiquitin ligase complexes. *Curr Opin Struct Biol*. 2010 Dec;20(6):714-21. doi: 10.1016/j.sbi.2010.08.010. Epub 2010 Sep 27. PMID: 20880695. PMCID: PMC3070871.

CHAPTER 2:

ESCO2 AND COHESIN REGULATE CRL4 UBIQUITIN LIGASE DDB1 EXPRESSION AND THALIDOMIDE TERATOGENICITY

2.1 Abstract

Cornelia de Lange syndrome (CdLS) and Roberts syndrome (RBS) are severe developmental maladies that arise from mutation of cohesin (including SMC3, CdLS) and ESCO2 (RBS). Though ESCO2 activates cohesin, CdLS and RBS etiologies are currently considered non-synonymous and for which pharmacological treatments are unavailable. Here, we identify a unifying mechanism that integrates these genetic maladies to pharmacologically-induced teratogenicity via thalidomide. Our results reveal that Esco2 and cohesin co-regulate the transcription of a component of CRL4 ubiquitin ligase through which thalidomide exerts teratogenic effects. These findings are the first to link RBS and CdLS to thalidomide teratogenicity and offer new insights into treatments.

2.2 Introduction

Thalidomide was an over-the-counter drug used to relieve morning sickness during pregnancy, among other uses in the late 1950s, which lead to a suite of birth defects that include phocomelia, organ malformation, craniofacial abnormalities, and intellectual disabilities (Smithells and Newman, 1992). These teratogenic effects result from inhibition of Cullin4 Ring Ligase (CRL4), the most common E3 ubiquitin ligase in eukaryotes and which contains Cullin4 (CUL4), DNA Damage Binding Protein 1 (DDB1), and DDB1-CUL4-Associated Factor (DCAF) Cereblon (CRBN) (Petroski and Deshaies, 2005; Ito et al., 2010). Inhibition of CRL4 function is solely responsible for thalidomide teratogenicity: 1) development proceeds normally upon thalidomide exposure in zebrafish embryos expressing thalidomide-resistant CRL4 and 2) mutation of CRL4 subunits are sufficient to produce embryonic damage and intellectual disabilities (Asatsuma-Okumura et al., 2019). Roberts syndrome (RBS) and Cornelia de Lange syndrome (CdLS) are severe genetic maladies in which manifestations highly resemble those observed in thalidomide babies (Cheng et al., 1971; Banerji et al., 2017a). RBS arises through mutation of ESCO2 while CdLS arises through mutation of cohesin subunits (including SMC1, SMC3, and RAD21) and regulators (NIPBL and HDAC) (Banerji et al., 2017a). ESCO2 acetylates SMC3 to activate cohesin. Despite the direct link between ESCO2 and SMC3, CdLS and RBS etiologies are currently considered non-synonymous and for which pharmacological access is largely unavailable.

Here, we document that Smc3 and Esco2 knockdowns (KDs) in zebrafish embryos provide robust models for CdLS and RBS and identify a unifying

mechanism that integrates these genetic maladies to the pharmacologically-induced teratogenicity produced by thalidomide. Our results reveal that Esco2 and cohesin co-regulate *ddb1* transcription, which is a key component of CRL4 ubiquitin ligase through which thalidomide exerts teratogenic effects. Importantly, Ddb1 KD embryo phenotypes overlap with Smc3 KD and Esco2 KD embryos and exogenous *ddb1* expression rescues developmental defects that otherwise arise in Smc3 KD embryos. These findings are the first to directly link both RBS and CdLS to thalidomide teratogenicity and transform current notions of cohesinopathies.

2.3 Materials and Methods

Zebrafish (Danio rerio) strain C32 was used. This study was performed in accordance with the recommendations in the Guide for the Care and Use of Laboratory Animals of the National Institutes of Health. These protocols were approved by Lehigh's Institutional Animal Care and Use Committee (IACUC) (Protocol 187). Lehigh University's Animal Welfare Assurance Number is A-3877-01.

Morpholino (MO) Injections

MO purchased from GeneTools, LLC (Philomath, OR) were dissolved in sterile dH_2O, for a 1mM concentration (sequences available upon request). These were heated to 65°C for 15 minutes prior to use. Full MO concentration resulted in embryo lethality, thus smc3 MO was diluted in 1X phenol red to a concentration of 0.5mM to allow for embryo comparisons at 72 hours post fertilization (hpf), and esco2 MO was diluted in 1X phenol red to a concentration of 0.25mM. A standard control (SC) MO

with no target sequence in zebrafish was used as control. Microinjections were performed at the 1-cell stage using the Narishige IM 300 Microinjector and Nikon SMZ 800 for visualization. Zygotes were sorted for viability and fertilized embryos were kept in egg water and Ampicillin solution at 28°C. Embryos were dechorionated using pronase if needed, then harvested for lysate or cDNA preparations or fixed in 4% paraformaldehyde (PFA), and kept at 4°C overnight for phenotype analysis. Embryos were stored in 100% methanol at -20°C for long term use after fixing.

Thalidomide Treatments

As adapted from Ito et al. 2010 (3), a stock 400mM solution of thalidomide dissolved in DMSO was made in order to keep the final DMSO concentration under 0.1%. The 400 mM stock solution was diluted in E3 medium prewarmed at 65ºC and mixed for 1 or 2 min to make 200µM, 400µM and 800µM final concentrations. Zebrafish embryos were manually dechorionated prior to thalidomide treatment by use of forceps. After chorion removal, embryos were immediately transferred to E3 medium containing thalidomide or DMSO only control and further incubated at 28ºC until the 72 hpf timepoint was reached. E3 medium was replaced with freshly prepared medium every 12 hours. Embryos were fixed in 4% PFA and kept at 4°C overnight for phenotypes analysis. Embryos were stored in 100% methanol at -20°C for long term use after fixing.

Embryo Lysates and Immunoblotting

MO injected embryo lysates were made at 24 hpf for Esco2, Smc3 and SC. Protocol was adapted from Schabel et al., 2019. In short, embryos were dechorinated with pronase then washed in E3 egg water. Individual embryos were placed in 1.5mL

centrifuge tubes and all excess egg water was removed. 500µl of heptane were added then immediately after 500µl of cold methanol were added and sample was fixed for 5 mins. Embryo was washed two times with 500µl of cold methanol then 2 times with 100µl of Embryo Buffer (EB). Embryos were homogenized in 20µl of EB. Three single embryo lysate preps were pulled to create one biological replicate. Lysates were stored at -80°C, 5X SDS Loading buffer was added and samples were boiled before use. A primary antibody specifically for zebrafish was used to detect Esco2 (1:1000, GenScript) (Banerji et al., 2016). Alexa 546 anti-rabbit (1:1000, Invitrogen) was used to detect Esco2 primary antibody. A primary antibody specifically for zebrafish was used to detect Smc3 (1:1000, Santa Cruz Biotechnology, sc-8198). Alexa 568 anti-goat (1:1000, Invitrogen) was used to detect Smc3 primary antibody. An antibody for human Ddb1 protein sharing 97% homology to zebrafish Ddb1 was used to detect Ddb1 (1:500, Abcam, ab124672). Alexa 488 anti-rabbit (1:1000, Invitrogen). Mouse anti-α-tubulin (1:1000, Sigma-Aldrich, T9026) was used as a loading control. Alexa 647 anti-mouse (1:1000, Invitrogen) was used to detect the tubulin primary antibody. For measurement of band intensities, ImageJ software (https://imagej.nih. gov/ij/) was used. Relative pixel densities of gel bands were measured using the gel analysis tool in ImageJ software as previously described in Bhadra and Iovine, 2015. Tubulin was used as a loading control and thus the relative expression calculations were based on the ratio of Esco2 or Smc3 to Tubulin.

RT-PCR

For RT-PCR, total mRNA was extracted from around 15 embryos to make one biological replicate using Trizol reagent and the standard protocol. The resulting

mRNA pellet was resuspended in a solution of DEPC H2O and RNAse Inhibitor, then the concentration of RNA was recorded using the Thermo Scientific Nanodrop 2000. For making cDNA, 1 μg of total RNA was reverse transcribed with SuperScript III reverse transcriptase (Invitrogen) using oligo (dT) primers. The resulting cDNA was diluted 1:10 for RT-PCR. Control primers (F: 5'-CAGAAGCCCACGGCGGTGAA-3', R: 5'-CCTGAACAGCTCCATCACCGC-3') were used that expand a region within exon 2 of *ddb1* mRNA, unaffected by the MO. Target primers (F: 5'-CGGCCAAATACAACGCCTGC-3' R: 5'-CTGGAATGACCATCGATGCC-3') were used expanding from exon 3 – exon 5. PCR was set up for SC MO injected embryos and *ddb1* MO injected embryos. A 1% agarose gel was poured, and PCR products ran at 100V for ~ 1 hour.

mRNA Rescue

Full length mRNA encoding for *ddb1* was designed using the sequence from the ZFin database. The plasmid was stored at -20°C until used. Plasmid was diluted to a 1:10 concentration of 0.2μg/μl in sterile water. One Shot Max Efficiency DH5α cells were transformed with the plasmid using standard procedures. The Qiagen Mini-Prep kit was used to isolate plasmid DNA from the transformed bacteria. The plasmid DNA was then linearized by performing an AvrII digest. A transcription reaction was then performed using the Invitrogen mMessage mMachine kit. The concentration of the resulting mRNA was assessed using the Thermo Scientific Nanodrop 2000. This was also run on a formaldehyde gel and imaged using the BioRad Gel Doc. The mRNA was then diluted to concentrations of 25ng/μl and 100ng/μl in phenol red. Diluted mRNA was heated at 65°C for 5 minutes prior to injections into zebrafish

embryos at the 1-cell stage as previously described. The mRNA was also co-injected into embryos that had been injected with the smc3 and esco2-ATG start site blocker MOs. Both the mRNA injected embryos and co-injected rescue embryos were fixed at 72 hpf in 4% PFA overnight at 4°C and for phenotypes analysis. Embryos were stored in 100% methanol at -20°C for long term use after fixing.

qRT-PCR

For qRT-PCR, total mRNA was extracted from around 15 embryos to make one biological replicate using Trizol reagent and the standard protocol. The resulting mRNA pellet was resuspended in a solution of DEPC H2O and RNAse Inhibitor, then the concentration of RNA was recorded using the Thermo Scientific Nanodrop 2000. For making cDNA, 1 µg of total RNA was reverse transcribed with SuperScript III reverse transcriptase (Invitrogen) using oligo (dT) primers. The resulting cDNA was diluted 1:10 for qRT-PCR, using the Rotor-Gene 6000. cDNA was made on esco2-ATG MO injected embryos, smc3-ATG MO injected embryos and SC MO injected embryos. For each cDNA used, primers at a 10µM concentrations were used. Three primers were specific for components of the CRL4 E3 Ligase affected by thalidomide, Cul4a (F: 5'-GCGGAATATGGAGTGTGTATGA-3', R: 5'-TCCTGCTTTGGCGGATTT-3'), Crbn (F: 5'-CTTGTTCAGAGCGGATTGTAAAC-3', R: 5'-TGGCAGACTCGTGTCAAAG-3') and Ddb1 (F: 5'-GCACACTGCAGATTGATGAC-3', R: 5'-GACGACTCCACTAACACTACAG-3'). keratin4 primers (F: 5'-TCATCGACAAAGTGCGCTTC-3'; R: 5'-TCGATGTTGGAACGTGTGGT-3') were used as a housekeeping gene control. For each PCR tube, 7.5µl of Sybr Green,

3µl 10µM Primers , 3.5µl sterile H2O, and 1µl cDNA was added. Analyses of the samples were done using Rotor-Gene 6000 series software (Corbette Research) and the average cycle number (C_T) determined for each amplicon. Delta C_T (ΔC_T) between housekeeping gene and CRL4 genes were calculated to represent expression levels normalized to keratin values. $\Delta\Delta C_T$ values were calculated to represent the relative level of gene expression and the fold difference was determined using the $\Delta\Delta C_T$ method ($2^{-\Delta\Delta C_T}$) as previously described (Banerji et al., 2016; Ton and Iovine 2012).

Imaging Analysis of Embryos

Zebrafish embryos fixed at 72 hpf were mounted on double cavity slides using 3% methyl cellulose for embedding. Embryo phenotypes were observed using the Nikon SMZ 1500, 1X objective at room temperature and the Nikon Eclipse 80i Microscope, 10X and 20X objectives at room temperature. Microscopes were equipped with SPOT-RTKE digital camera (Diagnostic Instruments) and SPOT software (Diagnostic Instruments) for image acquisition. The images obtained were then used to quantify whole embryo length, eye diameter, and otolith phenotypes. Percent similarities were obtained for body and eye measurements for each treatment compared to wild-type (WT) un-treated embryos. First, percent difference was calculated by taking the change in value between treated/injected embryo and un-treated/un-injected WT embryos, divided by the average of the numbers, all multiplied by 100. Percent similarities were then obtained by subtracting percent difference from 100. Otolith phenotypes were observed and scored into four categories: normal otoliths, fused otoliths, small otoliths, and absent otoliths. Otolith

diameters were measured to distinguish between normal and small otoliths. Anterior and posterior otolith diameters were added; a sum less than 50μm was classified as small. Percent of embryos with each otolith phenotype were calculated by taking number of embryos in each category divided by total embryos analyzed.

Statistical Analysis

ANOVA tests were used to determine if there was a statistically significant difference in body size, and eye size between KDs and controls. Statistical analysis was performed using ordinary one-way ANOVA tests. Two-tailed paired t-tests were used to determine if there was a statistically significant difference in qRT-PCR analysis between KDs and controls. N values of at least 16 were used in every experiment. Only values giving $P < 0.05$ are reported.

2.4 Results

Conservation of phenotypes derived from Esco2 (RBS) and Smc3 (CdLS) KDs, and Thalidomide exposure, in zebrafish embryos.

Esco2 acetyltransferase activates cohesin through acetylation of the cohesin subunit Smc3 (Rolef Ben-Shahar et al., 2008; Zhang et al., 2008; Ünal et al., 2008). The prevailing models of RBS (mutated ESCO2) and CdLS (mutated cohesin, including SMC3, and cohesin regulators), however, are quite different. Based on the initial discovery that Ctf7/Eco1 (herein Eco1, the homolog of human ESCO2) is critical for chromosome segregation (Skibbens et al., 1999; Tóth et al., 1999; Hou and Zou, 2005), and that mutations in ESCO2 lead to increase mitotic failure and apoptosis (Mönnich et al., 2011; Morita et al., 2012; Percival et al., 2015; Percival

and Parant, 2016; Banerji et al., 2017a), the prevailing model for RBS is based on mitotic failure that leads to proliferative stem cell loss (Percival and Parant, 2016, Zakari et al., 2015). In contrast, CdLS cells typically do not exhibit increased mitotic failure or apoptosis, even though CdLS arises due to cohesin pathway gene mutations (Banerji et al., 2017a; Dorsett and Krantz, 2009). NIPBL (homolog of drosophila Nipped-B and yeast Scc2) mutation produces the highest incidence of CdLS and early studies documented that NIPBL plays a critical role in transcription regulation (Rollins et al., 1999; Rollins et al., 2004). This and other findings led to the prevailing model of CdLS as one of transcription dysregulation (Dorsett and Krantz, 2009; Banerji et al., 2017a). The phenotypic similarities between both RBS and CdLS genetic maladies, and the pharmacologically-induced birth defects that result from in utero exposure to thalidomide, however, made it important to test whether all three are directly linked.

To address the role of Esco2 and cohesins in developing zebrafish embryos, we used previously well-characterized esco2 and smc3-targetting morpholinos (MOs) (Mönnich et al., 2011; Banerji et al., 2016; Banerji et al., 2017b). Targeted protein KDs of Esco2 and Smc3 were independently validated in the current study as well by Western blot of lysates obtained from MO-injected embryos, compared to lysates from standard control (SC) MO injected embryos. A significant reduction of Esco2 and Smc3 protein levels in 24 hpf embryos were obtained with esco2-ATG MO and smc3-ATG MO respectively (Supplemental Figure 2.1A, B). These findings extend the previously validated target specificity and KD efficacy of both MOs (Mönnich et al., 2011; Banerji et al., 2016; Banerji et al., 2017b).

We next assessed the effect of Esco2 KD and Smc3 in developing zebrafish embryos compared to the SC-MO that does not recognize target genes in zebrafish. MO injections were performed at the 1-cell stage and embryo phenotypes were assessed at 72 hours post fertilization (hpf). esco2 MO injected embryos exhibited defects that include shorter body length (Figure 2.1A, B), smaller eye size (Figure 2.1A, C) and abnormal otolith development (Figure 2.1A, D), compared to SC MO injected embryos. These phenotypes are consistent with the short stature phenotypes, and vision and hearing losses observed in RBS patients. Note that these phenotypes are also consistent with those previously observed in embryos injected with esco2-directed MOs and by esco2 mutations in zebrafish (Mönnich et al., 2011; Percival et al., 2015; Xu et al., 2013). Compared to control embryos, smc3 MO injected embryos also exhibited smaller body size (Figure 2.1A, B), reduced eye size (Figure 2.1A, C), and a notable absence of otoliths within the otic vesicle (Figure 2.1A, D), consistent with analogous phenotypes present in CdLS patients. Critically, the phenotypes obtained by smc3-directed MO are consistent with transgenic zebrafish lines deficient for rad21 or smc1a cohesin subunits and also embryos injected with rad21-directed MOs or smc3-directed MOs (Muto et al., 2011; Ghiselli et al., 2006; Horsfield et al., 2007; Schuster et al., 2015l Cukrov et al., 2018). In combination, these results document that both Esco2 and cohesin are critical for proper craniofacial and body development in zebrafish embryos and that MO-based strategies provide for robust zebrafish models of RBS and CdLS phenotypes.

Thalidomide is a well-established teratogen that elicits developmental defects also observed in RBS individuals (1). We thus exposed wild-type (WT) zebrafish embryos

to 200μM, 400μM and 800μM concentrations of thalidomide, compared to DMSO treated control embryos (Figure 2.2A). Significantly reduced body length was observed after treatment with 400μM and 800μM concentrations of thalidomide (Figure 2.2A, B). Eye size was significantly reduced at all concentrations of thalidomide (Figure 2.2A, C). Abnormalities in otolith development increased in a dose-dependent manner (Figure 2.2A, D). These findings are consistent with thalidomide-dependent developmental defects (Smithells and Newman, 1992; Ito et al., 2010). Importantly, the phenotypic overlap obtained from thalidomide treatment, and both in Esco2 KD and Smc3 KD embryos, spurred efforts to ascertain the extent to which these pharmacological and genetic maladies are linked.

Smc3 and Esco2 regulate expression of the CRL4 ligase gene *ddb1*

Thalidomide teratogenicity results from inhibition of CRL4 ubiquitin ligase function (Ito et al., 2010). Given the prevailing model that CdLS arises from transcription dysregulation (Dorsett and Krantz, 2009; Rollins et al., 1999; Rollins et al., 2004; Banerji et al., 2017a), we tested Smc3 KD embryos for transcriptional deregulation of *cul4a*, *ddb1*, and *crbn* genes, each of which encodes a key component of CRL4 ligase. cDNA obtained from smc3-ATG MO injected embryos were assessed by qRT-PCR at 24 hpf and compared to cDNA obtained from SC MO injected embryos. Fold changes in gene expression were calculated using Keratin as a housekeeping gene control. Neither *crbn* nor *cul4a* exhibited significant differences in gene expression. In contrast, *ddb1* was significantly reduced in Smc3 KD embryos (Supplemental Figure 2.2A). The prevailing model of RBS, based on mitotic failure and stem cell apoptosis (Mönnich et al., 2012; Morita et al., 2012; Percival et al.,

2015; Percival and Parant, 2016; Zakari et al., 2015), excludes a role for transcription dysregulation. Regardless, *ddb1* expression was significantly downregulated in embryos injected with esco2-ATG MO at 24 hpf (i.e. cul4a and crbn were not significantly deregulated (Supplemental Figure 2.2A), similar to Smc3 KD embryos. These results provide compelling evidence for an emerging transcription dysregulation-based model of RBS (Banerji et al., 2016, Banerji et al., 2017a, Banerji et al., 2017b) and link, for the first time, Esco2 and cohesin pathways to CRL4 regulation and thalidomide teratogenicity.

Exogenous *ddb1* rescues severe growth defects associated with Smc3 KD

If our finding that CRL4 is regulated by cohesin-dependent expression of *ddb1* is correct, consistent with the transcriptional model of CdLS etiology, then it should be possible to rescue Smc3 KD phenotypes by endogenous expression of *ddb1*. To test this hypothesis, embryos were injected with smc3-ATG MO, immediately followed by injection with *ddb1* mRNA (100ng/µl). When smc3-ATG MO injection was immediately followed by *ddb1* mRNA injection, developmental defects otherwise present in singly-injected smc3-ATG MO embryos were significantly ameliorated. For instance, both body and eye growth defects were significantly rescued by *ddb1* mRNA expression (Figure 2.3A, B, C), and 70% of dual-injected embryos exhibited a normal otolith phenotype, compared to 0% normal phenotypes with smc3 MO injection alone (Figure 2.3A, D). Reduced levels (25ng/µl) of *ddb1* mRNA led to a partial rescue of Smc3 KD eye and otolith phenotypes, revealing a dose-dependent response (Supplemental Figure 2.3A, B, C, D). In comparison, control embryos injected with *ddb1* mRNA alone produced embryo development indistinguishable

from un-injected WT embryos (Supplemental Figure 2.2B). Our findings that exogenous *ddb1* expression rescues developmental defects that arise in Smc3 KD embryos provide critical support for a model in which cohesins perform a transcriptional role upstream of CRL4 which, when abrogated, result in thalidomide-like teratogenicity.

Exacerbation of Esco2 KD phenotypes by exogenous *ddb1* reveals a feedback loop that is critical for development

Recent evidence revealed that CRL4 targets, and thus promotes, Esco2 degradation (Minamino et al., 2018; Sun et al., 2019). These findings suggest that, instead of rescuing phenotypes, elevated Ddb1 levels might instead exacerbate developmental defects in Esco2 KD zebrafish embryos. To test this possibility, embryos were injected with esco2-ATG MO, immediately followed by injection with *ddb1* mRNA (100ng/µl). Indeed, as opposed to rescuing esco2-ATG MO phenotypes, *ddb1* mRNA injection exacerbated the embryonic developmental defects. Body length and eye size were significantly decreased in the dual-injected embryos, compared to Esco2 KD alone embryos (Figure 2.4A, B, C). Otoliths, if formed, were increasingly abnormal with a major fraction of embryos devoid of otoliths (Figure 2.4A, D). Reduced levels (25ng/µl) of *ddb1* mRNA co-injected with esco2 MO, caused similar defects in body and otolith phenotypes compared to MO-only injected embryos, also revealing a dose-dependent response (Supplemental Figure 2.4A, B, C, D). While we cannot rule out the possibility that Esco2 and Ddb1 impact development via different or more complex mechanisms, we favor a model in which *ddb1* mRNA injection counteracts the reduction of Ddb1, caused by esco2-ATG MO,

and elevates CRL4 activity. In turn, CRL4 upregulation further decreases Esco2 levels and exacerbates Esco2 KD embryonic developmental defects. It is important to note, that the experiments that showed negative regulation of Esco2 by Ddb1 were performed using synchronous culture cells (Minamino et al., 2018; Sun et al., 2019). Not surprisingly, we were not able to detect a significant reduction in Esco2 levels in unsynchronized embryos co-injected with esco2-ATG MO and *ddb1* mRNA (data not shown). Future studies will be required to assess the possibility of this novel feedback loop through which Esco2 is regulated.

Ddb1 KD embryos recapitulate phenotypes observed in cohesinopathy and thalidomide zebrafish models

Our model linking RBS and CdLS to thalidomide teratogenicity predicts that Ddb1 KD embryos should recapitulate the developmental phenotypes obtained by Esco2 KD and Smc3 KD. To validate *ddb1*-directed MO efficacy, we first injected zebrafish embryos with either SC MO or *ddb1* MO (Supplemental Figure 2.5A) at the 1-cell stage and then harvested embryos at 24hpf to obtain RNA. RNA was converted to cDNA to confirm the splice blocking effect of the *ddb1* MO (Supplemental Figure 2.5A). In parallel, protein lysates of *ddb1* MO injected embryos, injected with 2 different MO concentrations (0.25mM and 0.5mM), were analyzed by Western blots. The results document that Ddb1 levels are significantly reduced in *ddb1* MO injected embryos, compared to control embryos (Supplemental Figure 2.5 B, C).

To assess the effect of Ddb1 KD on development, we injected zebrafish embryos with *ddb1* MO, or SC MO, at the 1-cell stage and assessed embryos at 72hpf. Our results show that both body size and eye size were significantly reduced in *ddb1* MO

injected embryos, compared to SC MO injected embryos (Figure 2.5 A, B and C). Otolith formation was also abnormal in *ddb1* MO embryos, compared to SC MO injected embryos (Figure 2.5 A, D).

We next validated that *ddb1* MO phenotypes are due to appropriate targeting of *ddb1* mRNA and not off target effects. To test this, we performed double injections in which *ddb1*-SB MO was immediately followed by *ddb1* mRNA injection at the 1-cell stage. Embryo phenotypes were then assessed at 72hpf. A significant rescue of both body size and eye size were observed in co-injected embryos, compared to embryos injected solely with *ddb1* MO (Figure 2.5A, B, C). Otolith development also improved significantly in co-injected embryos, compared to embryos injected solely with *ddb1* MO. Importantly, the rescue in otolith development depended on the *ddb1* mRNA concentration, revealing a dose-dependent effect (Figure 2.5 A, D). The results that Ddb1 KD embryos recapitulate phenotypes observed upon Smc3 KD, Esco2 KD, and also thalidomide treatment support a unified pathway through which Ddb1 levels exist in a delicate balance that depend on Esco2 and cohesin pathways.

2.5 Discussion

Discovering a pharmacologically based mechanism through which cohesinopathies converge on CRL4 represents a major advancement in our understanding of human development. We note that cohesins redistribute to over 18,000 new loci during zebrafish development (Meier et al., 2018), suggesting that regulating CRL4 subunit expression is only one example of many regulatory circuits through which Esco2 and cohesin function. A second example is cx43, a gap junction

gene involved in skeletal development that is similarly under control of the Esco2-cohesin axis (Banerji et al., 2016; Banerji et al., 2017b). Mutations in CX43 cause oculodentodigital dysplasia (ODDD) in humans, and defects in bone segment regrowth in zebrafish (Banerji et al., 2017a; Paznekas et al., 2003). The extent to which Esco2 and cohesin regulate genes independent of one another remains an important issue in development. Our findings that RBS and CdLS phenotypes are impacted by exogenous Ddb1 levels suggest that the identification of CRL4 targets, downstream of Esco2 and cohesin, will profoundly impact both current models of birth defects and their treatment. Moreover, the discovery that Ddb1 overexpression exacerbates, rather than rescues, Esco2 KD phenotypes provides new opportunities for analyzing feedback mechanisms during development. Regardless, mitotic failure-based models of RBS require significant revision with a new emphasis on transcriptional dysregulation, similar to CdLS. Such a transformation could reveal potential new treatment options for RBS and CdLS individual. For instance, DDB1 and CRBN mutations result in elevated BK_{Ca} high conductance channel trafficking to the plasma membrane, increased ion conductivity, high neuronal excitation, and seizures (Jo et al., 2005; Liu et al., 2014; Sun et al., 2015). Paxilline, a BK_{Ca} channel blocker, reduces the incidence and severity of seizures that arise due to CRBN loss (Liu et al., 2014). CLR4 knock-out mice also exhibit learning and memory deficits, an effect attributed to reduced translation of hippocampal glutamatergic synapse proteins via AMPK hyperphosphorylation. Compound C (an AMPK inhibitor) treatment normalizes glutamatergic protein levels and rescues both learning and memory deficits in CRBN knockout mice (Bavley et al., 2018). The extent to which

RBS and CdLS patients may benefit from such strategies represents exciting possibilities. The novel link between CRL4 and RBS and CdLS reported here is likely to extend to numerous other transcriptional dysregulated-based developmental disorders, as well as cancers that are tightly correlated with cohesin mutations (Bose et al., 2012; Mannini and Musio, 2011). We look forward to future experiments that test the extent to which the molecular mechanisms revealed here provide for new strategies of treatment for a broad range of developmental maladies and cancers.

2.6 Figures and Tables

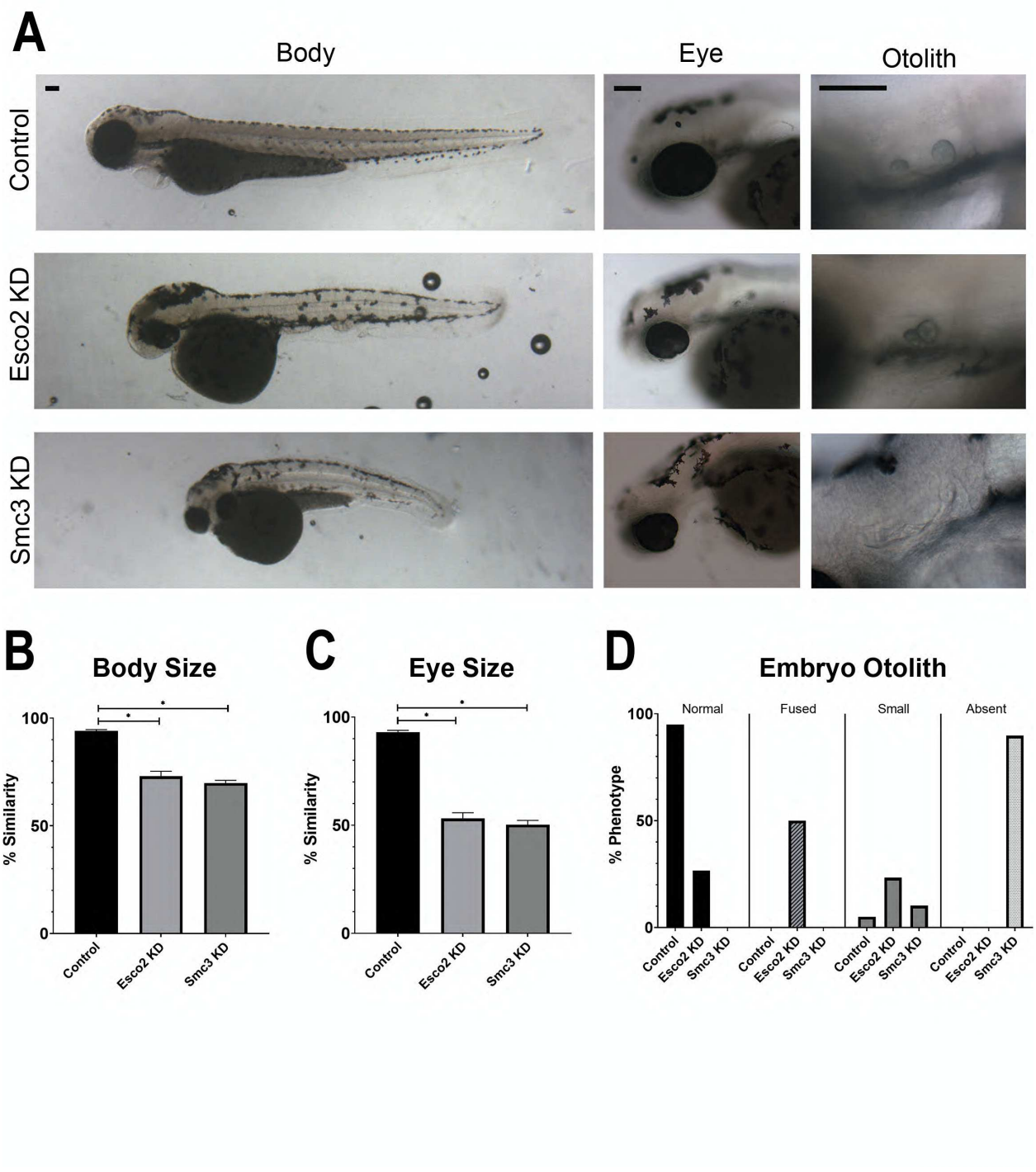

Figure. 2.1. Esco2 KD and Smc3 KD phenotypes include reduced body and eye size, and an increase in abnormal otolith development. (A) Representative images of control embryos (SC MO injected), Esco2 KD (esco2-ATG MO injected) and Smc3 KD (smc3-ATG MO injected) embryos. For all experiments 24-40 replicates were analyzed and at least 3 independent trials were performed. (B) Quantification of body size from MO injected embryos were compared to un-injected WT embryos to obtain percent similarity. Graph reveals significant reductions of body length in Esco2 KD and Smc3 KD compared to control embryos (error bars represent s.e.m., one-way ANOVA with Turkey's multiple comparison, *P<0.05). (C) Quantification of eye size from MO injected embryos were compared to un-injected WT embryos to obtain percent similarity. Graph reveals significant reductions of eye size in Esco2 KD and Smc3 KD compared to control embryos (error bars represent s.e.m., one-way ANOVA with Turkey's multiple comparison, *P<0.05). (D) Graph shows percent of normal, fused, small, or absent otolith phenotypes with MO treatments. Data reveals 95% of control embryo otoliths exhibit normal phenotype, while Esco2 KD and Smc3 KD embryos exhibited 27% and 0% normal otolith phenotypes, respectively. An increase in abnormal otolith phenotypes was observed with KD treatments with predominantly fused phenotypes in Esco2 KDs and absent phenotypes in Smc3 KDs. Scale bar: 100μm.

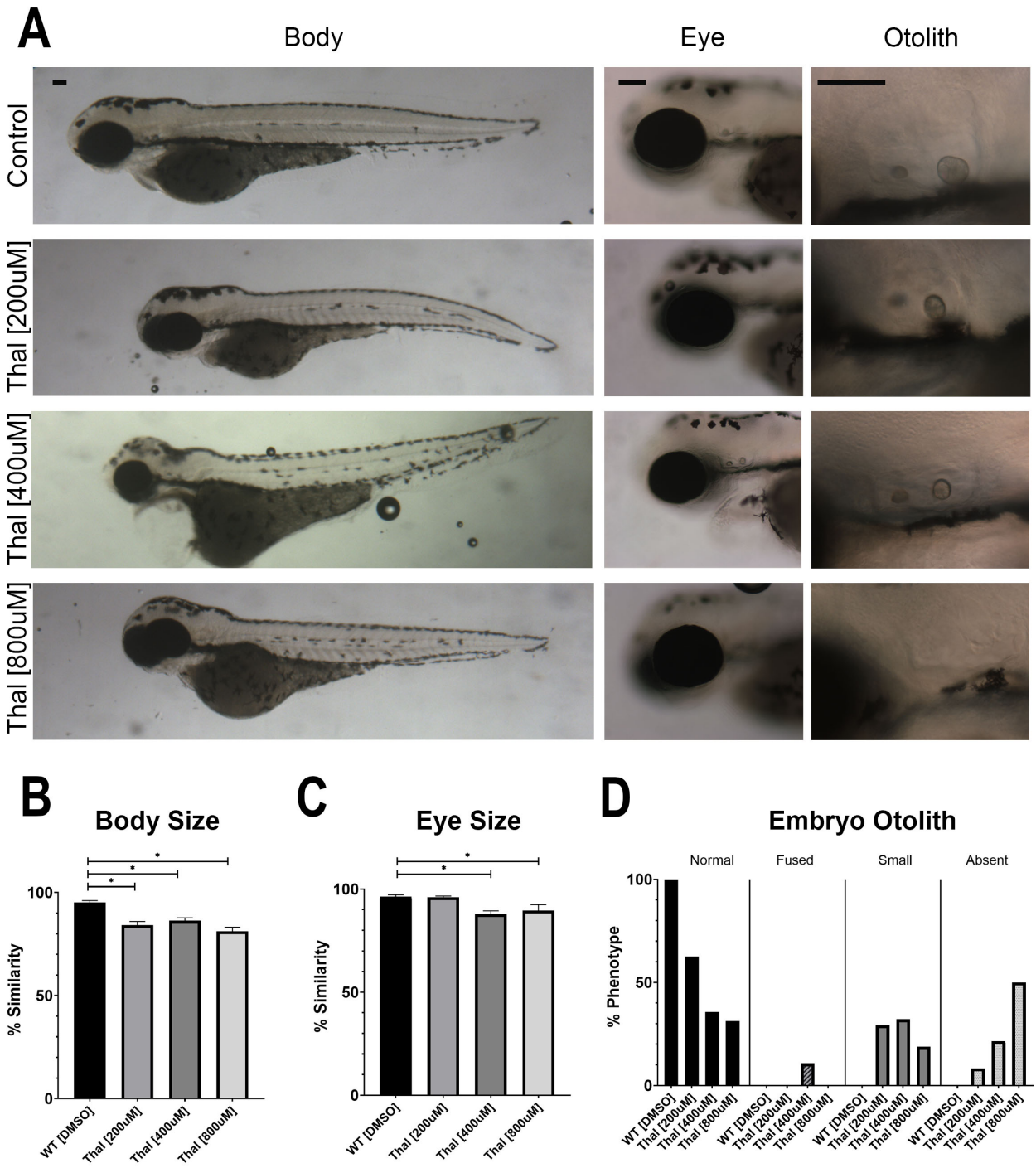
A
Body
Eye
Otolith
Control
Thal [200uM]
Thal [400uM]
Thal [800uM]
B
Body Size
% Similarity
100
50
0
WT [DMSO]
Thal [200uM]
Thal [400uM]
Thal [800uM]
C
Eye Size
% Similarity
100
50
0
WT [DMSO]
Thal [200uM]
Thal [400uM]
Thal [800uM]
D
Embryo Otolith
Normal
Fused
Small
Absent
% Phenotype
100
50
0
WT [DMSO]
Thal [200uM]
Thal [400uM]
Thal [800uM]

Figure 2.2. Phenotypes of thalidomide treated embryos overlap with Esco2 KD and Smc3 KD embryos. (A) Representative images of control embryos (WT treated with DMSO) and thalidomide (thal.) treatments (WT treated with 200μM, 400μM, and 800μM concentrations of thalidomide). For all experiments 16-28 replicates were analyzed and at least 3 independent trials were performed. (B) Quantification of body size after drug treatment were compared to un-treated WT embryos to obtain percent similarity. Bar graph reveals a significant reduction of body length with thal. treatments compared to DMSO treated controls (error bars represent s.e.m., one-way ANOVA with Turkey's multiple comparison, *P<0.05). (C) Quantification of eye size after drug treatment were compared to un-treated WT embryos to obtain percent similarity. Bar graph reveals a significant reduction of eye size with all thal. treatments compared to DMSO treated controls (error bars represent s.e.m., one-way ANOVA with Turkey's multiple comparison, *P<0.05). (D) Graph shows percent of normal, fused, small, or absent otolith phenotypes with drug treatments. Data reveals 100% of control embryo otoliths exhibit normal phenotype, while 200μM, 400μM, and 800μM thal. treatments had 31%, 36% and 63% normal otolith phenotypes, respectively. An increase in absent otolith phenotypes was observed with increasing concentrations of thalidomide. Scale bar: 100μm.

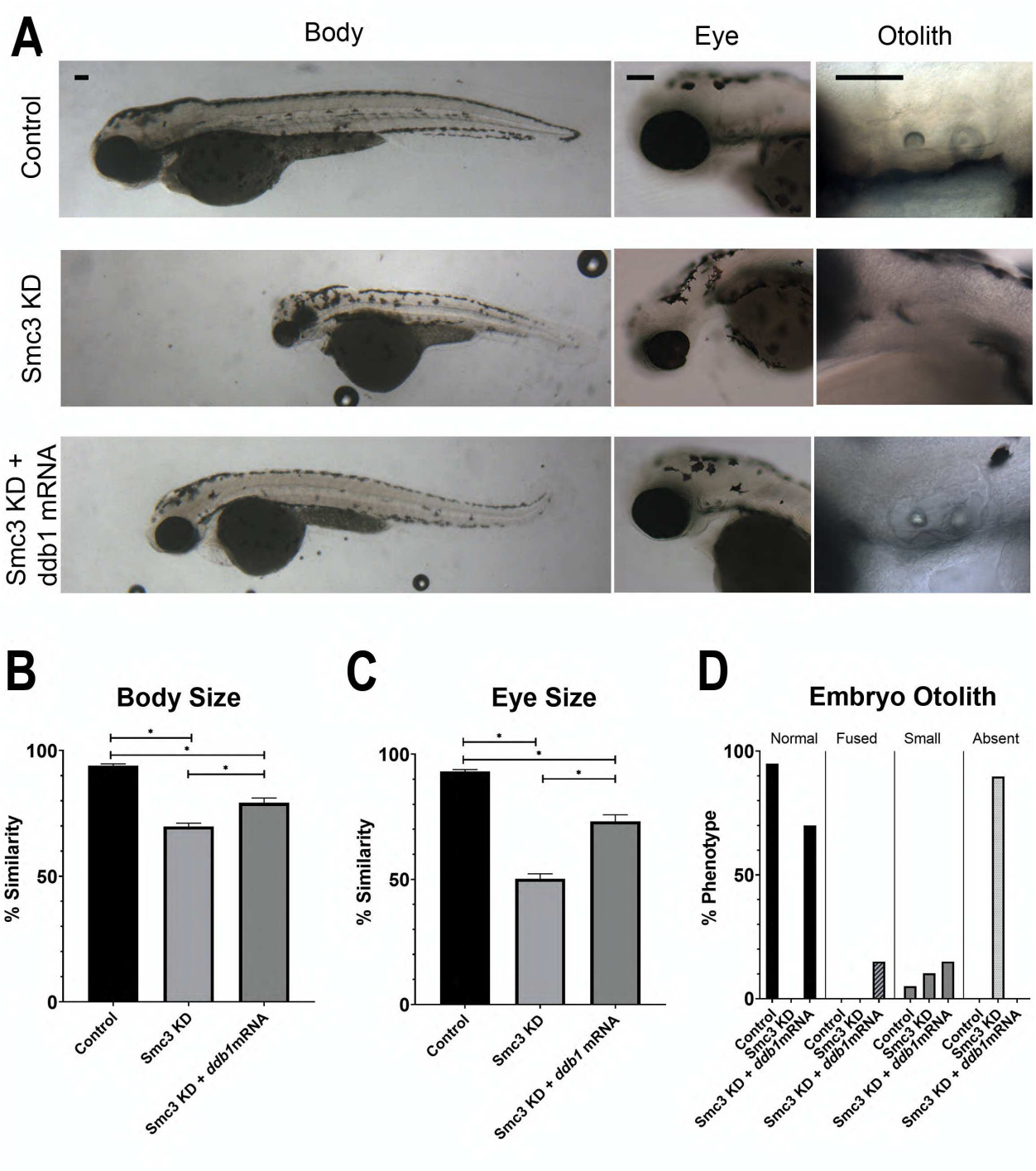
A
Body
Eye
Otolith
Control
Smc3 KD
Smc3 KD + ddb1 mRNA
B
Body Size
% Similarity
100
50
0
Control
Smc3 KD
Smc3 KD + ddb1mRNA
C
Eye Size
% Similarity
100
50
0
Control
Smc3 KD
Smc3 KD + ddb1 mRNA
D
Embryo Otolith
Normal
Fused
Small
Absent
% Phenotype
100
50
0
Control
Smc3 KD
Smc3 KD + ddb1mRNA

Figure 2.3. Exogenous *ddb1* overexpression rescues Smc3 KD phenotypes. (A) Representative images of control embryos (WT injected with *ddb1* mRNA), Smc3 KD (*smc3*-ATG MO injected) and Smc3 KD + *ddb1* mRNA (*smc3*-ATG MO co-injected with *ddb1* mRNA) embryos. For all experiments 26-40 replicates were analyzed and at least 3 independent trials were performed. (B) Quantification of body size from injected embryos were compared to un-injected WT embryos to obtain percent similarity. Bar graph reveals a significant rescue of body length in Smc3 KD + *ddb1* mRNA compared to Smc3 KD alone (error bars represent s.e.m., one-way ANOVA with Turkey's multiple comparison, *P<0.05). (C) Quantification of eye size from injected embryos were compared to un-injected WT embryos to obtain percent similarity. Bar graph reveals a significant rescue of eye size in Smc3 KD + *ddb1* mRNA compared to Smc3 KD alone (error bars represent s.e.m., one-way ANOVA with Turkey's multiple comparison, *P<0.05). (D) Graph shows percent of normal, fused, small, or absent otolith phenotypes with MO treatments. Data reveals 0% of Smc3 KD embryos exhibited normal otoliths, while 70% of Smc3 KD + *ddb1* mRNA embryo otoliths were rescued to normal levels. A decrease in absent otolith phenotypes was observed with *ddb1* mRNA co-injections compared to KD alone. Scale bar: 100μm.

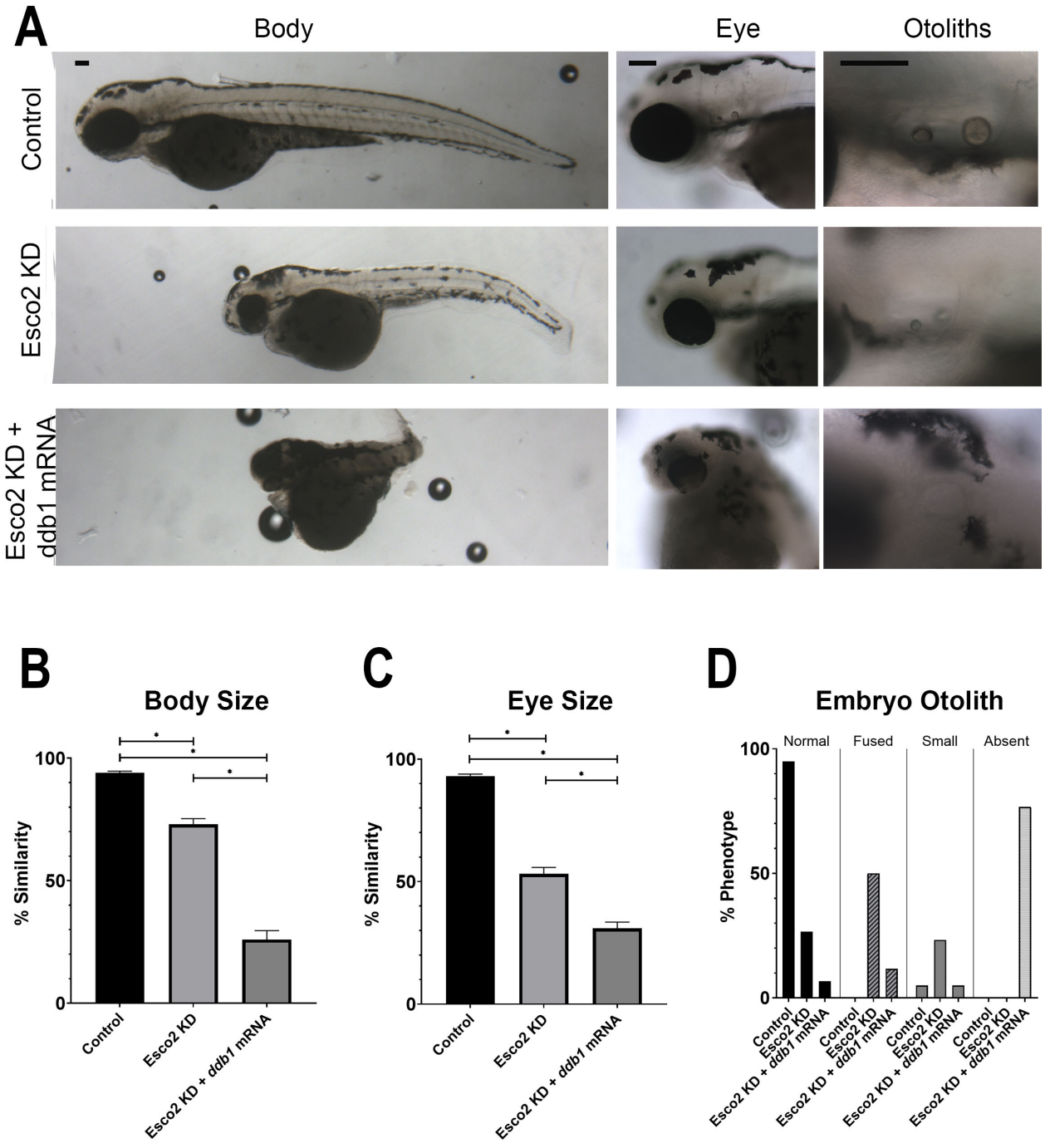

Figure 2.4. Exogenous *ddb1* overexpression exacerbates Esco2 KD phenotypes. (A) Representative images of control embryos (WT injected with *ddb1* mRNA), Esco2 KD (esco2-ATG MO injected) and Esco2 KD + *ddb1* mRNA (esco2-ATG MO co-injected with *ddb1* mRNA) embryos. For all experiments 29-38 replicates were analyzed and at

least 3 independent trials were performed. (B) Quantification of body size from injected embryos were compared to un-injected WT embryos to obtain percent similarity. Bar graph reveals a significant reduction of body length in Esco2 KD + *ddb1* mRNA compared to Esco2 KD alone (error bars represent s.e.m., one-way ANOVA with Turkey's multiple comparison, *P<0.05). (C) Quantification of eye size from injected embryos were compared to un-injected WT embryos to obtain percent similarity. Bar graph reveals a significant reduction of eye size in Esco2 KD + *ddb1* mRNA compared to Esco2 KD alone (error bars represent s.e.m., one-way ANOVA with Turkey's multiple comparison, *P<0.05). (D) Graph shows percent of normal, fused, small, or absent otolith phenotypes with MO treatments. Data reveals 27% of Esco2 KD embryos exhibited normal otoliths, while only 7% of Esco2 KD + *ddb1* mRNA embryo otoliths were normal with an absent phenotype largely observed. Scale bar: 100μm.

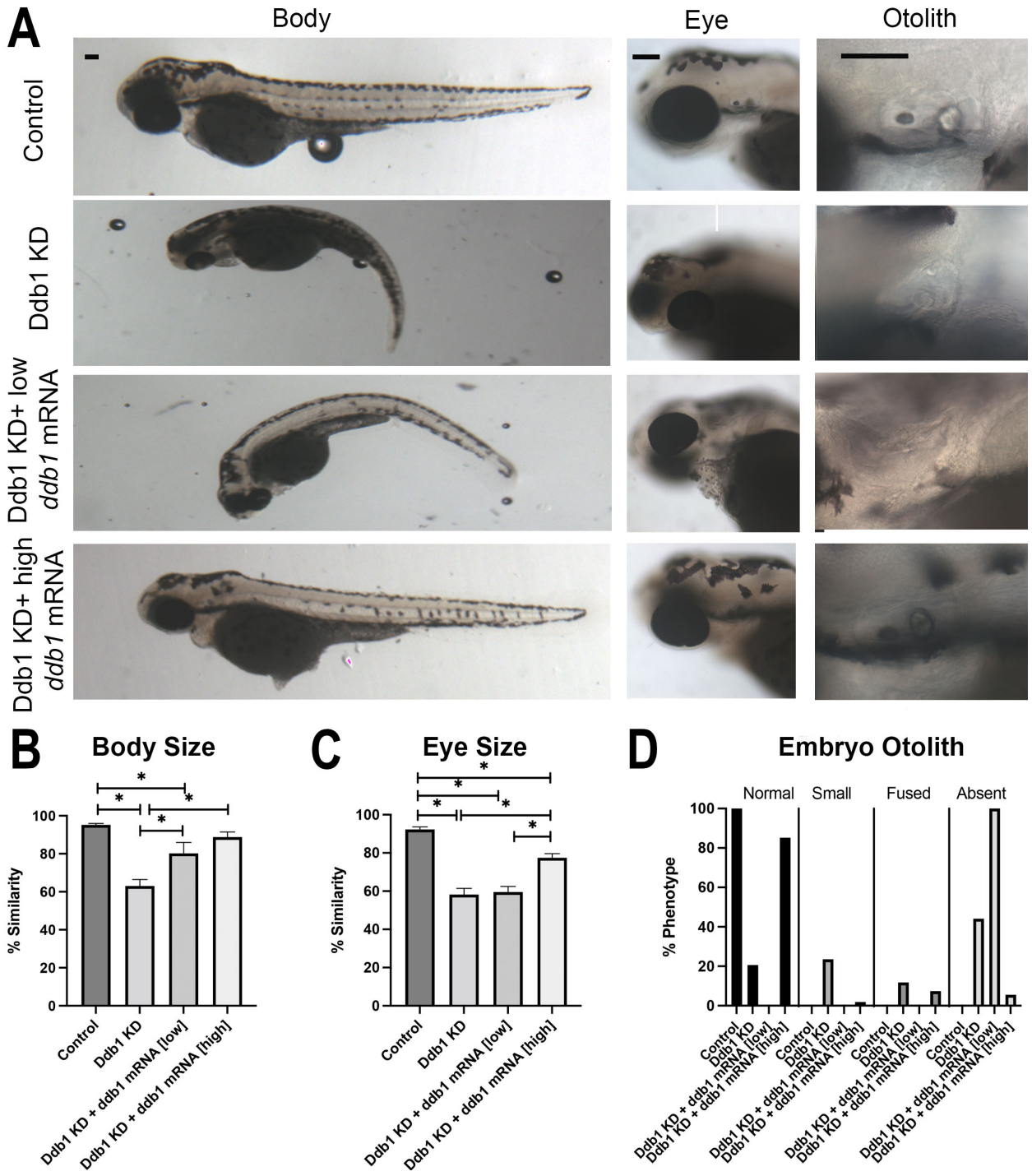

Figure 2.5. Ddb1 KD phenotypes overlap cohesinopathies and thalidomide teratogenicity phenotypes. (A) Representative images of control embryos (WT injected with *ddb1* mRNA), Ddb1 KD (*ddb1*-SB MO injected), Ddb1 KD + low *ddb1* mRNA

(*ddb1*-SB MO co-injected with 25ng/µl *ddb1* mRNA) and Ddb1 KD + high *ddb1* mRNA (*ddb1*-SB MO co-injected with 100ng/µl *ddb1* mRNA) embryos. For all experiments 24-60 replicates were analyzed and at least 3 independent trials were performed. (B) Quantification of body size from injected embryos were compared to un-injected WT embryos to obtain percent similarity. Bar graph reveals a significant reduction of body length in Ddb1 KD that is rescued by *ddb1* mRNA (error bars represent s.e.m., one-way ANOVA with Turkey's multiple comparison, *P<0.05). (C) Quantification of eye size from injected embryos were compared to un-injected WT embryos to obtain percent similarity. Bar graph reveals a significant reduction of eye size in Ddb1 KD that is partially rescued with *ddb1* mRNA (error bars represent s.e.m., one-way ANOVA with Turkey's multiple comparison, *P<0.05). (D) Graph shows percent of normal, fused, small, or absent otolith phenotypes with MO treatments. Data reveals 21% of Ddb1 KD embryos exhibited normal otoliths, while 85% of Ddb1 KD + high *ddb1* mRNA embryo otoliths were normal. Scale bars: 100µm

2.7 Supplementary Figures and Tables

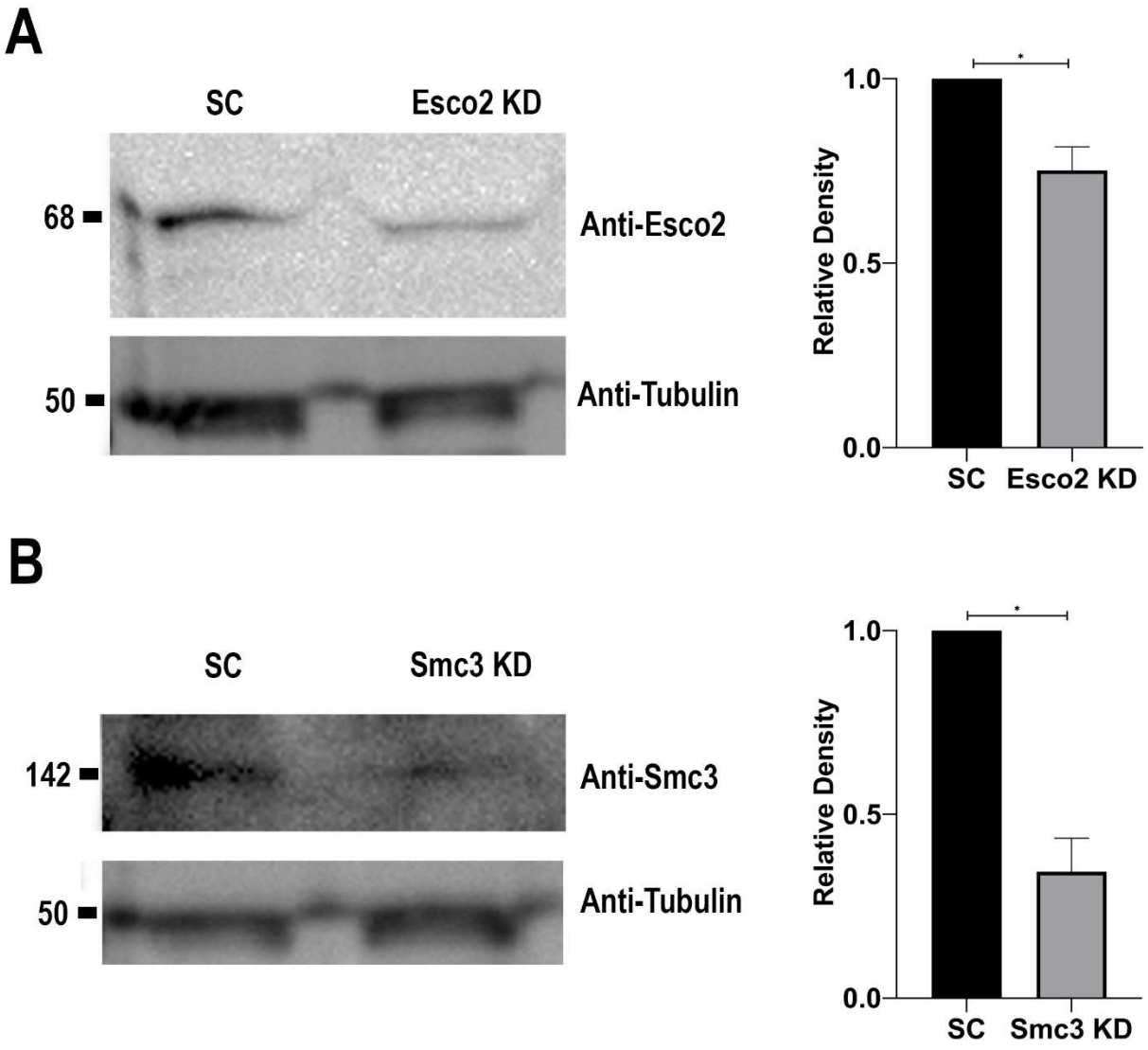

Supplemental Figure 2.1. Validation of Esco2 and Smc3 protein reduction with MO injections. (A) Western blot of SC embryo lysates compared to esco2 MO embryo lysates. Immunoblots were probed with Esco2 and Tubulin antibodies. Analysis detects Esco2 at a predicted size of 68 kDa and Tubulin at the predicted size of 50 kDa. Graph shows the average relative densities of the Esco2 bands between experimental and control sample from 3 biological replicates. Esco2 protein levels are significantly reduced by 25% with MO injection compared to SC injected embryos (error bars represent s.e.m., un-paired t-test, *P<0.05). (B) Western blot of SC embryo lysates compared to smc3 MO embryo lysates. Immunoblots were probed with Smc3 and Tubulin antibodies. Analysis detects Smc3 at a predicted size of 142 kDa and Tubulin at the predicted size of 50 kDa. Graph shows the average relative densities of the Smc3 bands between experimental and control sample from three biological replicates. Smc3 protein levels are significantly reduced by 66% with MO injection compared to SC injected embryos (error bars represent s.e.m., un-paired t-test, *P<0.05).

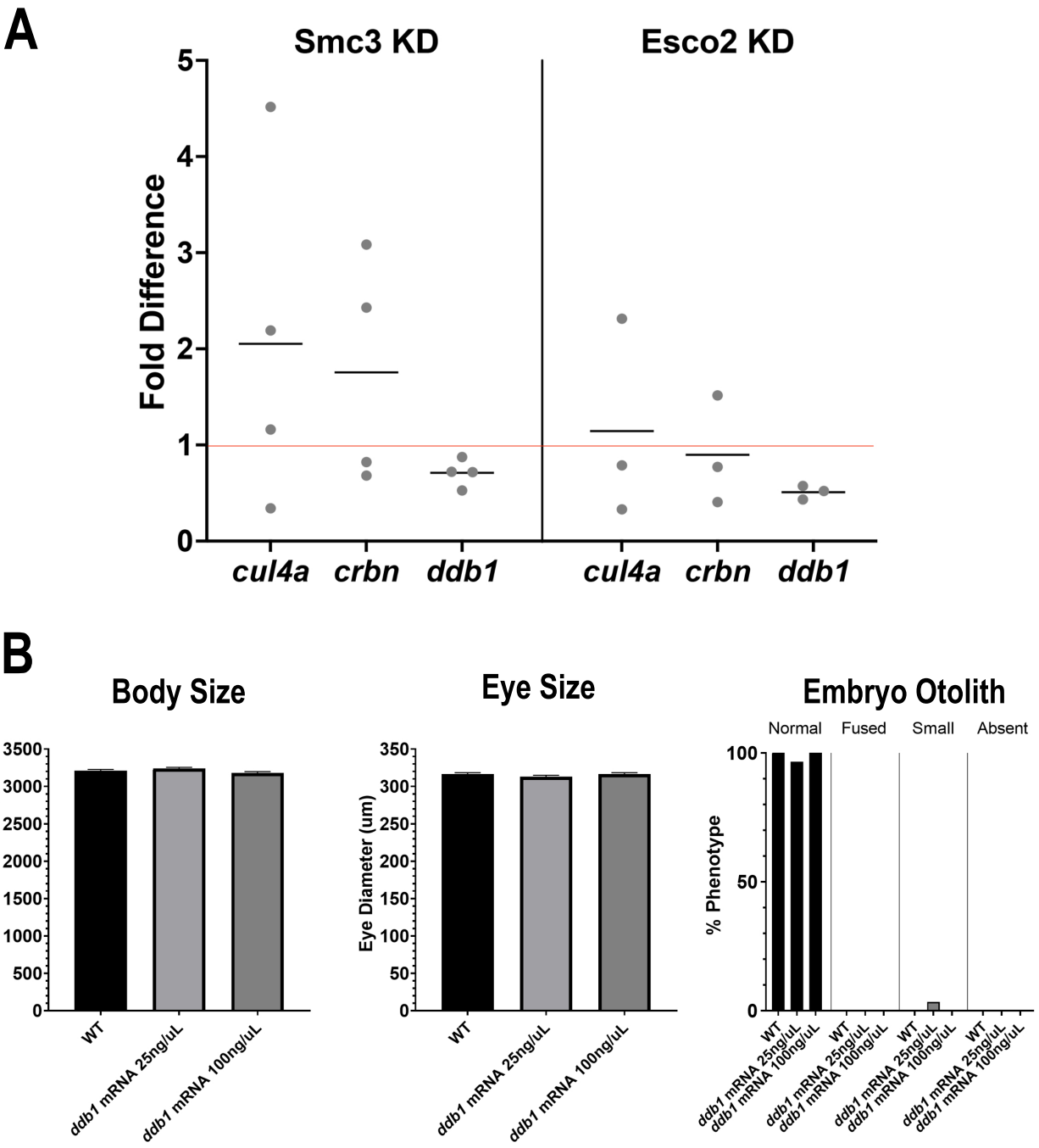
A
Smc3 KD
Esco2 KD
Fold Difference
0
1
2
3
4
5
cul4a
crbn
ddb1
cul4a
crbn
ddb1
B
Body Size
Body Length (um)
0
500
1000
1500
2000
2500
3000
3500
WT
ddb1 mRNA 25ng/uL
ddb1 mRNA 100ng/uL
Eye Size
Eye Diameter (um)
0
50
100
150
200
250
300
350
WT
ddb1 mRNA 25ng/uL
ddb1 mRNA 100ng/uL
Embryo Otolith
Normal
Fused
Small
Absent
% Phenotype
0
50
100
WT
ddb1 mRNA 25ng/uL
ddb1 mRNA 100ng/uL

Supplemental Figure 2.2. *ddb1* is downregulated in Smc3 KD and Esco2 KD embryos. (A) Gene expression levels were measured by qRT-PCR analysis in Smc3 KD and Esco2 KD embryos. Graph shows fold difference in expression levels from each replicate (grey) and the average expression (black line) for each gene. Keratin was used as the internal refence gene control for fold difference calculations. A fold difference of 1 is considered no change with respect to SC MO injected embryos (represented by red line). CRL4 component genes (*cul4a*, *crbn* and *ddb1*) were analyzed in Smc3 KD and Esco2 KD embryos. Only *ddb1* expression was significantly downregulated in both Smc3 KD and Esco2 KD embryos (un-paired t-test, $P<0.05$), while cul4a and crbn were inconsistent and not significant (un-paired t-test, $P>0.05$). (B) Exogenous *ddb1* mRNA was injected to WT embryos at the 1-cell stage. 30-46 replicates were analyzed and at least 3 independent trials were performed. Phenotypes were imaged and measured at 72 hpf. *ddb1* overexpression in WT embryos had no effect in embryo length, eye size, or embryo otolith phenotype (error bars represent s.e.m, one-way ANOVA with Turkey's multiple comparison, $P>0.05$).

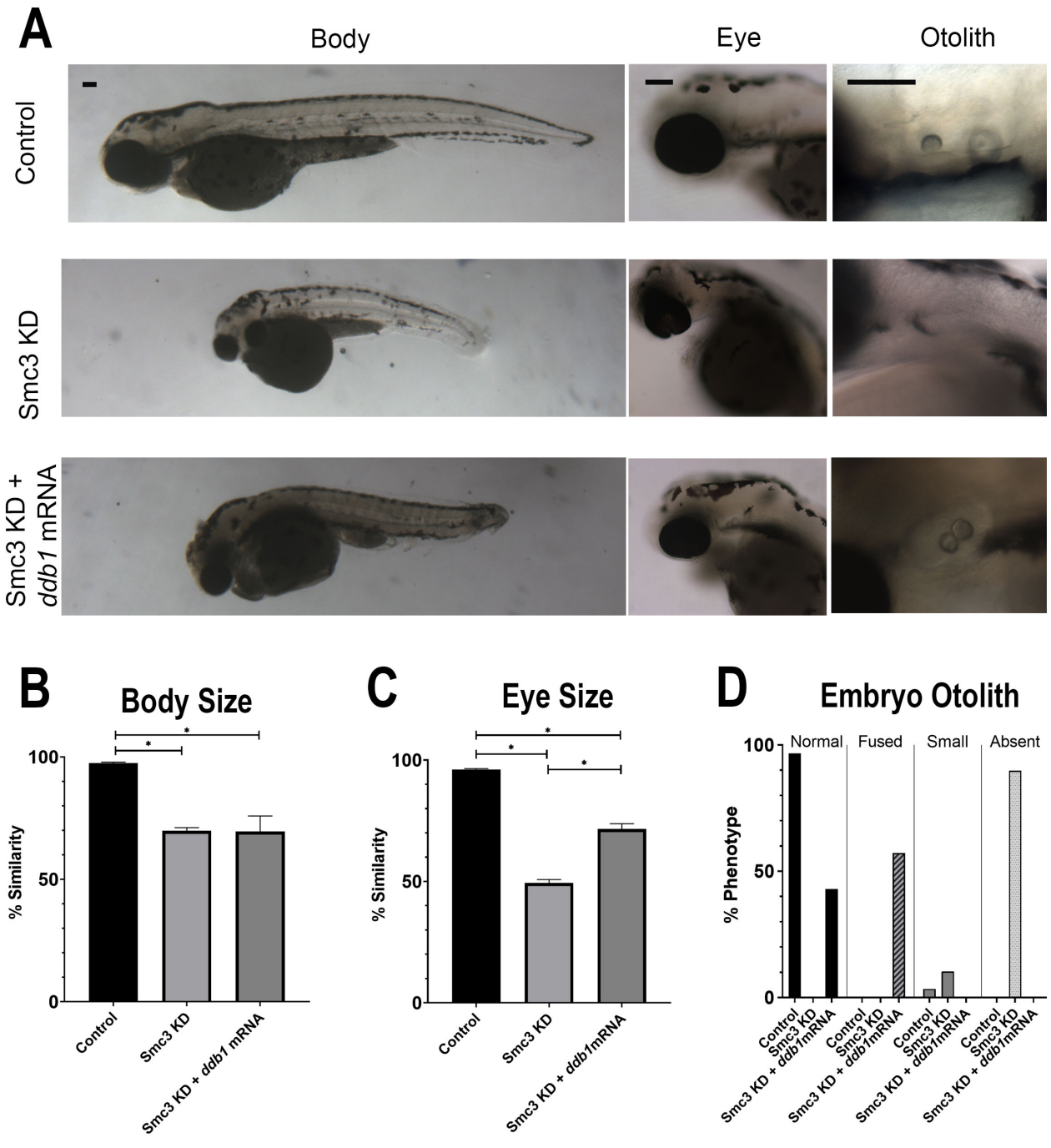
A
Body
Eye
Otolith
Control
Smc3 KD
Smc3 KD + ddb1 mRNA
B
Body Size
% Similarity
100
50
0
Control
Smc3 KD
Smc3 KD + ddb1 mRNA
C
Eye Size
% Similarity
100
50
0
Control
Smc3 KD
Smc3 KD + ddb1mRNA
D
Embryo Otolith
% Phenotype
100
50
0
Normal
Fused
Small
Absent
Control
Smc3 KD
Smc3 KD + ddb1mRNA

Supplemental Figure 2.3. Reduced levels of exogenous *ddb1* overexpression rescues eye and otolith phenotypes in Smc3 KD phenotypes. (A) Representative images of control embryos (WT injected with 25ng/µl concentration of *ddb1* mRNA), Smc3 KD (smc3-ATG MO injected) and Smc3 KD + *ddb1* mRNA (smc3-ATG MO co-injected with 25ng/µl concentration of *ddb1* mRNA) embryos. For all experiments 40-48 replicates were analyzed and at least 3 independent trials were performed. (B) Quantification of body size from injected embryos were compared to un-injected WT embryos to obtain percent similarity. Bar graph reveals no significant rescue of body length in Smc3 KD + *ddb1* mRNA compared to Smc3 KD alone (error bars represent s.e.m., one-way ANOVA with Turkey's multiple comparison, $P>0.05$). (C) Quantification of eye size from injected embryos were compared to un-injected WT embryos to obtain percent similarity. Bar graph reveals a significant rescue of eye size in Smc3 KD + *ddb1* mRNA compared to Smc3 KD alone (error bars represent s.e.m., one-way ANOVA with Turkey's multiple comparison, $*P<0.05$). (D) Graph shows percent of normal, fused, small, or absent otolith phenotypes with MO treatments. Data reveals 0% of Smc3 KD embryos exhibited normal otoliths, while 43% of Smc3 KD + *ddb1* mRNA embryo otoliths were rescued to normal levels. A decrease in absent otolith phenotypes was observed with *ddb1* mRNA co-injections compared to KD alone. Scale bar: 100µm.

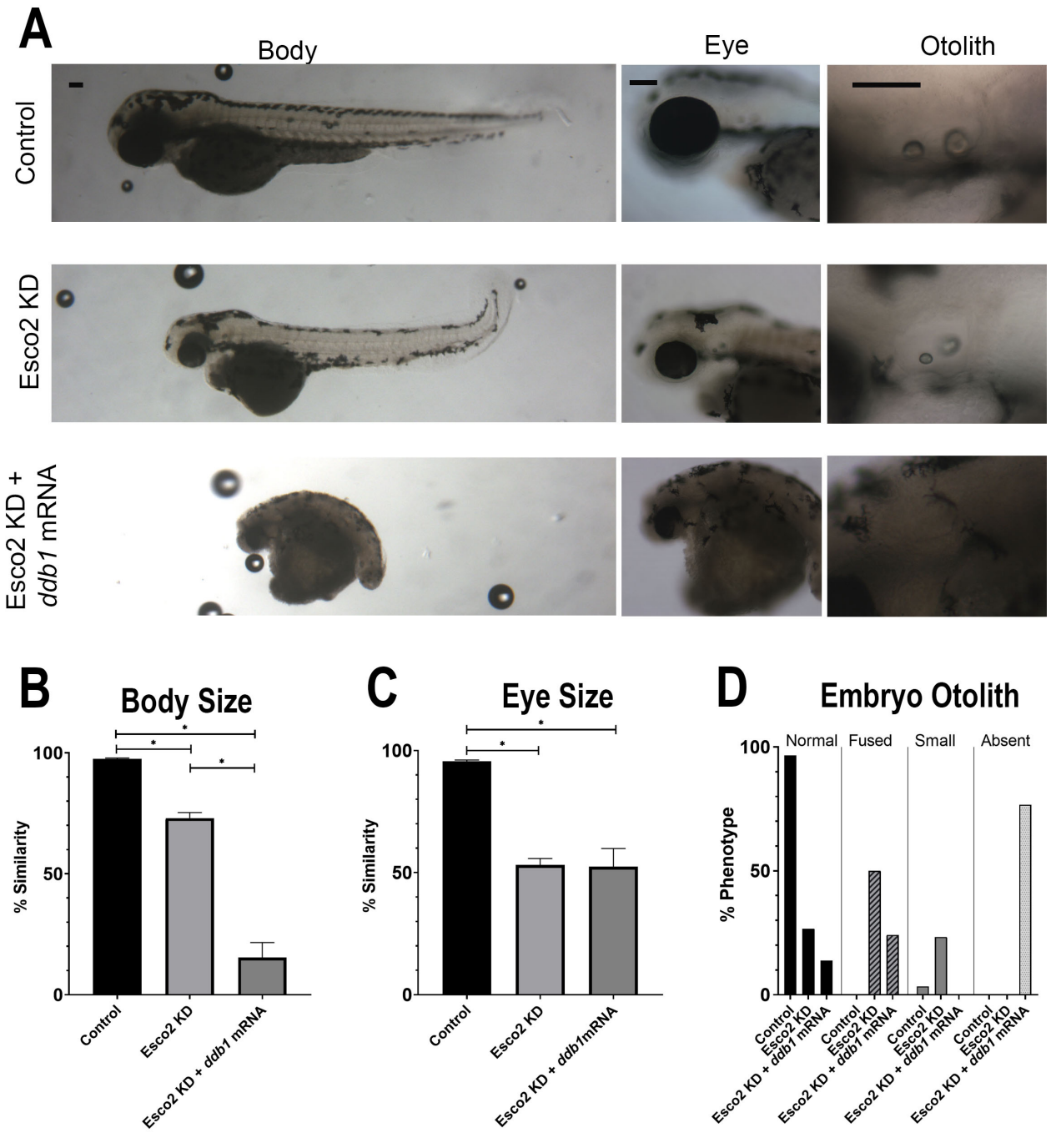
A
Body
Eye
Otolith
Control
Esco2 KD
Esco2 KD + ddb1 mRNA
B
Body Size
% Similarity
100
50
0
Control
Esco2 KD
Esco2 KD + ddb1 mRNA
C
Eye Size
% Similarity
100
50
0
Control
Esco2 KD
Esco2 KD + ddb1mRNA
D
Embryo Otolith
% Phenotype
100
50
0
Normal
Fused
Small
Absent
Control
Esco2 KD
Esco2 KD + ddb1 mRNA

Supplemental Figure 2.4. Reduced levels of exogenous ddb1 overexpression exacerbates body and otolith phenotypes in Esco2 KD phenotypes. (A) Representative images of control embryos (WT injected with 25ng/µl concentration of *ddb1* mRNA), Esco2 KD (esco2-ATG MO injected) and Esco2 KD + *ddb1* mRNA (esco2-ATG MO co-injected with 25ng/µl concentration of *ddb1* mRNA) embryos. For all experiments 27-30 replicates were analyzed and at least 3 independent trials were performed. (B) Quantification of body size from injected embryos were compared to un-injected WT embryos to obtain percent similarity. Bar graph reveals significant reduction of body length in Esco2 KD + *ddb1* mRNA compared to Esco2 KD alone (error bars represent s.e.m., one-way ANOVA with Turkey's multiple comparison, *$P<0.05$). (C) Quantification of eye size from injected embryos were compared to un-injected WT embryos to obtain percent similarity. Bar graph reveals no significant change in eye size in Esco2 KD + *ddb1* mRNA compared to Esco2 KD alone (error bars represent s.e.m., one-way ANOVA with Turkey's multiple comparison, $P>0.05$). (D) Graph shows percent of normal, fused, small, or absent otolith phenotypes with MO treatments. Data reveals 27% of Esco2 KD embryos displayed normal otoliths, while only 14% of Esco2 KD + *ddb1* mRNA embryo otoliths exhibited a normal phenotype. An increase in absent otolith phenotypes was observed with *ddb1* mRNA co-injections compared to KD alone. Scale bar: 100µm.

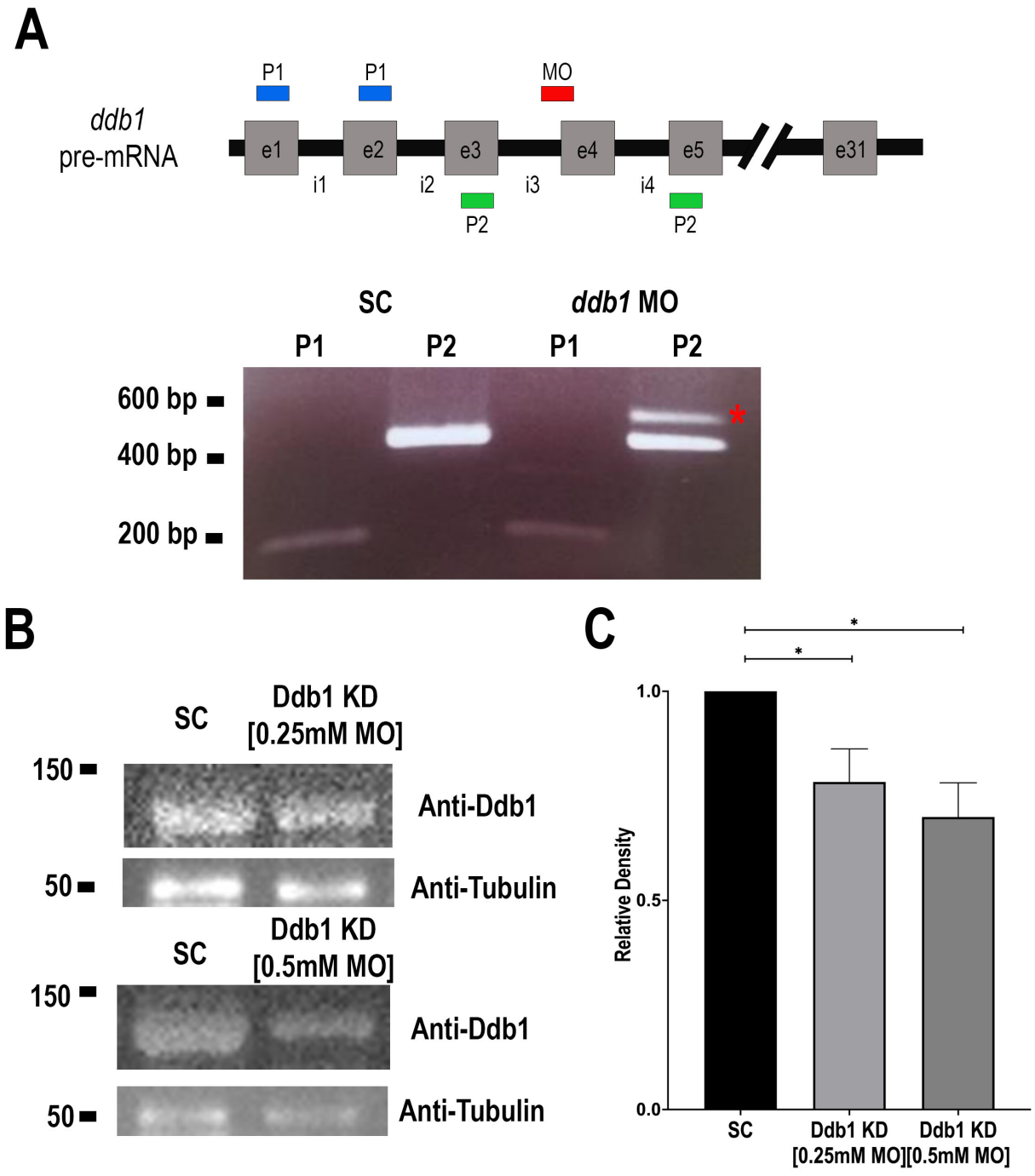

Supplemental Figure 2.5. *ddb1*-SB MO causes intron insertion and reduces Ddb1 protein levels. (A) Top: Schematic representation of the zebrafish ddb1 pre-mRNA with

exons (e) represented by gray boxes and introns (i) represented by spaces in between. The position of the ddb1 MO is represented by a red box positioned at the third intron and exon junction site (i3e4). The positions of the control primer pair (P1) are indicated by the blue boxes, while target primer pair (P2) are represented by green boxes. Bottom: Results of RT-PCR analysis using P1 and P2 primers to validate SB efficacy of ddb1 MO. The P1 primers amplified the expected 177bp product for both the SC MO cDNA and the ddb1 MO cDNA. In contrast, the P2 primers amplified a 538bp product (marked with a red *) in the ddb1 MO cDNA sample due to the inclusion of intron 3 as predicted for the ddb1-SB MO compared to the SC MO cDNA which only showed the expected 423bp product. At least 15 embryos were used per biological replicate, 3 biological replicates were performed and validated intron 3 insertion with ddb1 MO injections. (B) Western blot of SC embryo lysates compared to ddb1 MO embryo lysates. Immunoblots were probed with Ddb1 and Tubulin antibodies. Analysis detects Ddb1 at a predicted size of 130 kDa and Tubulin at the predicted size of 50 kDa. Ddb1 protein levels are reduced with ddb1 MO lysates at both 0.25mM and 0.50mM concentrations compared to the SC MO lysates. (C) Graph shows the average relative densities of the Ddb1 bands between experimental and control sample from 3 to 6 biological replicates. Ddb1 protein levels are significantly reduced by 22% and 32% with the [0.25mM] and [0.50mM] MO injections respectively, compared to SC injected embryos (error bars represent s.e.m., un-paired t-test, *$P<0.05$).

2.8 References

Asatsuma-Okumura T, Ito T, Handa H. Molecular mechanism of cereblon-based drugs. *Pharmacol Ther*. 2019 Oct;202:132-139. doi: 10.1016/j.pharmthera.2019.06.004. Epub 2019 Jun 14. PMID: 31202702

Banerji R, Eble DM, Iovine MK, Skibbens RV. Esco2 regulates cx43 expression during skeletal regeneration in the zebrafish fin. Dev Dyn. 2016 Jan;245(1):7-21. doi: 10.1002/dvdy.24354. Epub 2015 Nov 25. PMID: 26434741.

Banerji R, Skibbens RV, Iovine MK. Cohesin mediates Esco2-dependent transcriptional regulation in a zebrafish regenerating fin model of Roberts Syndrome. Biol Open. 2017. Dec 15;6(12):1802-1813. doi: 10.1242/bio.026013. PMID: 29084713; PMCID: PMC5769645.

Banerji R, Skibbens RV, Iovine MK. How many roads lead to cohesinopathies? *Dev Dyn.* 2017b Nov;246(11):881-888. doi: 10.1002/dvdy.24510. Epub 2017 May 22. PMID: 28422453.

Bavley CC, Rice RC, Fischer DK, Fakira AK, Byrne M, Kosovsky M, Rizzo BK, Del Prete D, Alaedini A, Morón JA, Higgins JJ, D'Adamio L, Rajadhyaksha AM. Rescue of Learning and Memory Deficits in the Human Nonsyndromic Intellectual Disability Cereblon Knock-Out Mouse Model by Targeting the AMP-Activated Protein Kinase-mTORC1 Translational Pathway. *J Neurosci*. 2018 Mar 14;38(11):2780-2795. doi: 10.1523/JNEUROSCI.0599-17.2018. Epub 2018 Feb 19. PMID: 29459374; PMCID: PMC5852658.

Bhadra J, Iovine MK. Hsp47 mediates Cx43-dependent skeletal growth and patterning in the regenerating fin. *Mech Dev*. 2015 Nov;138 Pt 3:364-74. doi: 10.1016/j.mod.2015.06.004. Epub 2015 Jun 20. PMID: 26103547.

Bose T, Lee KK, Lu S, Xu B, Harris B, Slaughter B, Unruh J, Garrett A, McDowell W, Box A, Li H, Peak A, Ramachandran S, Seidel C, Gerton JL. Cohesin proteins promote ribosomal RNA production and protein translation in yeast and human cells. PLoS Genet. 2012;8(6):e1002749. doi: 10.1371/journal.pgen.1002749. Epub 2012 Jun 14. PMID: 22719263; PMCID: PMC3375231.

Cheng J, Guo J, North BJ, Tao K, Zhou P, Wei W. The emerging role for Cullin 4 family of E3 ligases in tumorigenesis. *Biochim Biophys Acta Rev Cancer*. 2019 Jan;1871(1):138-159. doi: 10.1016/j.bbcan.2018.11.007. Epub 2018 Dec 30. PMID: 30602127; PMCID: PMC7179951.

Cukrov D, Newman TAC, Leask M, Leeke B, Sarogni P, Patimo A, Kline AD, Krantz ID, Horsfield JA, Musio A. Antioxidant treatment ameliorates phenotypic features of SMC1A-mutated Cornelia de Lange syndrome in vitro and in vivo. *Hum Mol Genet.* 2018 Sep 1;27(17):3002-3011. doi: 10.1093/hmg/ddy203. PMID: 29860495.

Dorsett D, Krantz ID. On the molecular etiology of Cornelia de Lange syndrome. *Ann N Y Acad Sci*. 2009 Jan;1151:22-37. doi: 10.1111/j.1749-6632.2008.03450.x. PMID: 19154515; PMCID: PMC2733214.

Ghiselli G. SMC3 knockdown triggers genomic instability and p53-dependent apoptosis in human and zebrafish cells. *Mol Cancer*. 2006 Nov 2;5:52. doi: 10.1186/1476-4598-5-52. PMID: 17081288; PMCID: PMC1636066.

Horsfield JA, Anagnostou SH, Hu JK, Cho KH, Geisler R, Lieschke G, Crosier KE, Crosier PS. Cohesin-dependent regulation of Runx genes. *Development*. 2007 Jul;134(14):2639-49. doi: 10.1242/dev.002485. Epub 2007 Jun 13. PMID: 17567667.

Hou F, Zou H. Two human orthologues of Eco1/Ctf7 acetyltransferases are both required for proper sister-chromatid cohesion. *Mol Biol Cell*. 2005 Aug;16(8):3908-18. doi: 10.1091/mbc.e04-12-1063. Epub 2005 Jun 15. PMID: 15958495; PMCID: PMC1182326.

Ito T, Ando H, Suzuki T, Ogura T, Hotta K, Imamura Y, Yamaguchi Y, Handa H. Identification of a primary target of thalidomide teratogenicity. *Science*. 2010 Mar;327(5971: 1345-50. doi: 10.1126/science.1177319. PMID: 20223979.

Jo S, Lee KH, Song S, Jung YK, Park CS. Identification and functional characterization of cereblon as a binding protein for large-conductance calcium-activated potassium channel in rat brain. J Neurochem. 2005 Sep;94(5):1212-24. doi: 10.1111/j.1471-4159.2005.03344.x. Epub 2005 Jul 25. PMID: 16045448.

Liu J, Ye J, Zou X, Xu Z, Feng Y, Zou X, Chen Z, Li Y, Cang Y. CRL4A(CRBN) E3 ubiquitin ligase restricts BK channel activity and prevents epileptogenesis. *Nat. Commun*. 2014 May;5:3924. doi.org/10.1038/ncomms4924.

Mannini L, Musio A. The dark side of cohesin: the carcinogenic point of view. *Mutat Res*. 2011 Nov-Dec;728(3):81-7. doi: 10.1016/j.mrrev.2011.07.004. PMID: 22106471.

Meier M, Grant J, Dowdle A, Thomas A, Gerton J, Collas P, O'Sullivan JM, Horsfield JA. Cohesin facilitates zygotic genome activation in zebrafish. *Development*. 2018 Jan 3;145(1):dev156521. doi: 10.1242/dev.156521. PMID: 29158440.

Minamino M, Tei S, Negishi L, Kanemaki MT, Yoshimura A, Sutani T, Bando M, Shirahige K. Temporal Regulation of ESCO2 Degradation by the MCM Complex, the CUL4-DDB1-VPRBP Complex, and the Anaphase-Promoting Complex. *Curr Biol.* 2018 Aug 20;28(16):2665-2672.e5. doi: 10.1016/j.cub.2018.06.037. Epub 2018 Aug 9. PMID: 30100344.

Mönnich M, Kuriger Z, Print CG, Horsfield JA. A zebrafish model of Roberts syndrome reveals that Esco2 depletion interferes with development by disrupting the cell cycle. *PLoS One*. 2011;6(5):e20051. doi: 10.1371/journal.pone.0020051. Epub 2011 May 26. PMID: 21637801; PMCID: PMC3102698.

Morita A, Nakahira K, Hasegawa T, Uchida K, Taniguchi Y, Takeda S, Toyoda A, Sakaki Y, Shimada A, Takeda H, Yanagihara I. Establishment and characterization of Roberts syndrome and SC phocomelia model medaka (Oryzias latipes). *Dev Growth Differ*. 2012 Jun;54(5):588-604. doi: 10.1111/j.1440-169X.2012.01362.x. PMID: 22694322.

Muto A, Calof AL, Lander AD, Schilling TF. Multifactorial origins of heart and gut defects in nipbl-deficient zebrafish, a model of Cornelia de Lange Syndrome. *PLoS Biol*. 2011 Oct;9(10):e1001181. doi: 10.1371/journal.pbio.1001181. Epub 2011 Oct 25. PMID: 22039349; PMCID: PMC3201921.

Paznekas WA, Boyadjiev SA, Shapiro RE, Daniels O, Wollnik B, Keegan CE, Innis JW, Dinulos MB, Christian C, Hannibal MC, Jabs EW. Connexin 43 (GJA1)

mutations cause the pleiotropic phenotype of oculodentodigital dysplasia. Am J Hum Genet. 2003 Feb;72(2):408-18. doi: 10.1086/346090. Epub 2002 Nov 27. PMID: 12457340; PMCID: PMC379233.

Percival SM, Parant JM. Observing Mitotic Division and Dynamics in a Live Zebrafish Embryo. *J Vis Exp.* 2016 Jul 15;(113):10.3791/54218. doi: 10.3791/54218. PMID: 27501381; PMCID: PMC6082026.

Percival SM, Thomas HR, Amsterdam A, Carroll AJ, Lees JA, Yost HJ, Parant JM. Variations in dysfunction of sister chromatid cohesion in esco2 mutant zebrafish reflect the phenotypic diversity of Roberts syndrome. *Dis Model Mech*. 2015 Aug 1;8(8):941-55. doi: 10.1242/dmm.019059. Epub 2015 Jun 4. PMID: 26044958; PMCID: PMC4527282.

Petroski MD, Deshaies RJ. Function and regulation of cullin-RING ubiquitin ligases. *Nat Rev Mol Cell Biol*. 2005 Jan;6(1):9-20. doi: 10.1038/nrm1547. PMID: 15688063.

Rolef Ben-Shahar T, Heeger S, Lehane C, East P, Flynn H, Skehel M, Uhlmann F. Eco1-dependent cohesin acetylation during establishment of sister chromatid cohesion. *Science*. 2008 Jul 25;321(5888):563-6. doi: 10.1126/science.1157774. PMID: 18653893.

Rollins RA, Korom M, Aulner N, Martens A, Dorsett D. Drosophila nipped-B protein supports sister chromatid cohesion and opposes the stromalin/Scc3 cohesion factor to facilitate long-range activation of the cut gene. Mol Cell Biol. 2004 Apr;24(8):3100-11. doi: 10.1128/mcb.24.8.3100-3111.2004. PMID: 15060134; PMCID: PMC381657.

Rollins RA, Morcillo P, Dorsett D. Nipped-B, a Drosophila homologue of chromosomal adherins, participates in activation by remote enhancers in the cut and Ultrabithorax genes. Genetics. 1999 Jun;152(2):577-93. PMID: 10353901; PMCID: PMC1460629.

Schnabel D, Castillo-Robles J, Lomeli H. Protein Purification and Western Blot Detection from Single Zebrafish Embryo. *Zebrafish*. 2019 Dec;16(6):505-507. Doi: 10.1089/zeb.2019.1761. Epub 2019 Aug 13. PMID: 31408407.

Schnabel D, Castillo-Robles J, Lomeli H. Protein Purification and Western Blot Detection from Single Zebrafish Embryo. *Zebrafish*. 2019 Dec;16(6):505-507. Doi: 10.1089/zeb.2019.1761. Epub 2019 Aug 13. PMID: 31408407.

Schuster K, Leeke B, Meier M, Wang Y, Newman T, Burgess S, Horsfield JA. A neural crest origin for cohesinopathy heart defects. *Hum Mol Genet*. 2015 Dec 15;24(24):7005-16. Doi: 10.1093/hmg/ddv402. Epub 2015 Sep 29. PMID: 26420840; PMCID: PMC4654055.

Skibbens RV, Corson LB, Koshland D, Hieter P. Ctf7p is essential for sister chromatid cohesion and links mitotic chromosome structure to the DNA replication machinery. *Genes Dev*. 1999 Feb 1;13(3):307-19. doi: 10.1101/gad.13.3.307. PMID: 9990855; PMCID: PMC316428.

Smithells RW, Newman CG. Recognition of thalidomide defects. J Med Genet. 1992 Oct;29(10):716-23. doi: 10.1136/jmg.29.10.716. PMID: 1433232; PMCID: PMC1016130.

Sun H, Zhang J, Xin S, Jiang M, Zhang J, Li Z, Cao Q, Lou H. Cul4-Ddb1 ubiquitin ligases facilitate DNA replication-coupled sister chromatid cohesion through

regulation of cohesin acetyltransferase Esco2. *PloS Genet*. 2019 Feb 19;15(2):e1007685. Doi: 10.1371/journal.pgen.1007685. PMID: 30779731; PMCID: PMC6396947.

Sun P, Zhang Q, Zhang Y, Wang F, Wang L, Yamamoto R, Sugai T, Kato N. Fear conditioning suppresses large-conductance calcium-activated potassium channels in lateral amygdala neurons. *Physiol Behav*. 2015 Jan;138:279-84. Doi: 10.1016/j.physbeh.2014.10.005. Epub 2014 Oct 20. PMID: 25447473.

Ton QV, Kathryn Iovine M. Semaphorin3d mediates Cx43-dependent phenotypes during fin regeneration. *Dev Biol.* 2012 Jun 15;366(2):195-203. doi: 10.1016/j.ydbio.2012.03.020. Epub 2012 Apr 20. PMID: 22542598; PMCID: PMC3358573.

Tóth A, Ciosk R, Uhlmann F, Galova M, Schleiffer A, Nasmyth K. Yeast cohesin complex requires a conserved protein, Eco1p(Ctf7), to establish cohesion between sister chromatids during DNA replication. *Genes Dev*. 1999 Feb 1;13(3):320-33. doi: 10.1101/gad.13.3.320. PMID: 9990856; PMCID: PMC316435.

Unal E, Heidinger-Pauli JM, Kim W, Guacci V, Onn I, Gygi SP, Koshland DE. A molecular determinant for the establishment of sister chromatid cohesion. *Science*. 2008 Jul 25;321(5888):566-9. doi: 10.1126/science.1157880. PMID: 18653894.

Xu B, Lee KK, Zhang L, Gerton JL. Stimulation of mTORC1 with L-leucine rescues defects associated with Roberts syndrome. *PLoS Genet*. 2013;9(10):e1003857. doi: 10.1371/journal.pgen.1003857. Epub 2013 Oct 3. PMID: 24098154; PMCID: PMC3789817.

Zakari M, Yuen K, Gerton JL. Etiology and pathogenesis of the cohesinopathies. *Wiley Interdiscip Rev Dev Biol*. 2015 Sep-Oct;4(5):489-504. doi: 10.1002/wdev.190. Epub 2015 Apr 7. PMID: 25847322; PMCID: PMC6680315.

Zhang J, Shi X, Li Y, Kim BJ, Jia J, Huang Z, Yang T, Fu X, Jung SY, Wang Y, Zhang P, Kim ST, Pan X, Qin J. Acetylation of Smc3 by Eco1 is required for S phase sister chromatid cohesion in both human and yeast. *Mol Cell*. 2008 Jul 11;31(1):143-51. doi: 10.1016/j.molcel.2008.06.006. PMID: 18614053.

CHAPTER 3:

PROTEIN TURNOVER DOWSTREAM OF THE COHESIN/CRL4 AXIS CONTRIBUTES TO ABNORMAL DEVELOPMENT

3.1 Abstract

Cohesinopathies, such as Cornelia de Lange Syndrome (CdLS) and Roberts Syndrome (RBS) are severe developmental syndromes that arise due to mutations that impact cohesin function. Mutations in *ESCO2* (encoding a cohesin activator) give rise to RBS, while *NIPBL* (encoding a cohesin loader) or genes that encode cohesin complex subunits (SMC proteins, or RAD21) give rise to CdLS. Of these, *NIPBL* mutations account for about 65% of CdLS cases. Here, we report on new findings that Nipbl impacts the transcription of *ddb1*, a key component of CRL4 E3 ligase in zebrafish. We additionally investigate the downstream targets of the cohesin/CRL4 axis that lead to developmental maladies.

3.2 Introduction

Cohesins are protein complexes that mediate both *trans*- and *cis*- DNA tethering important for cell cycle progression, transcriptional regulation, and DNA repair (Zakari et al., 2015; Skibbens, 2016). Although initially identified for its role in sister chromatid tethering (Guacci et al., 1997; Michaelis et al., 1997), current research is focused more on understanding the *cis*- DNA tethering mechanism of cohesins which play a critical role in gene regulation (Rollins et al., 2004; Dorsett et al., 2005; Wendt et al., 2008; Kawauchi et al., 2009; Muto et al., 2011; Muto et al., 2014; Banerji et al., 2016; Banerji et al., 2017; Sanchez et al., 2022).

Cohesin is made up of core subunits SMC1, SMC3, and RAD21, that together form a ring like structure. Cohesins are loaded and unloaded onto DNA (with the help of NIPBL, HDAC8, and PDS5 auxiliary proteins), but activated (through ESCO2 acetylation of SMC3) to stabilize DNA binding (Skibbens, 2016; Srinivasan et al., 2018). Given the pivotal role of cohesins in many cell processes, it is not surprising that cohesin mutations lead to developmental conditions that impact almost every tissue in the body. Roberts Syndrome (RBS) is a cohesinopathy that arises due to mutations in *ESCO2*, the cohesin acetyltransferase (Vega et al., 2005; Schüle et al., 2005; Gordillo et al., 2008). Cornelia de Lange Syndrome (CdLS), another cohesinopathy, arises from mutations in cohesin core subunits (*SMC1*, *SMC3* or *RAD21*) or in auxiliary factors (such as, *HDAC8 or NIPBL*) (Rollins 1999; Rollins 2004; Krantz et al., 2004; Tonkin et al., 2004; Dorssett, 2007; Horsfield et al., 2007; Wendt et al., 2008; Misulovin et al., 2008; Liu et al., 2009; Zakari et al., 2015).

While the gene mutations that lead to RBS and CdLS are well established, the downstream impacts of such mutations are largely unknown. Recent insights, however, come from the study of the teratogen thalidomide. Thalidomide poisoning, *in utero*, leads to shockingly similar phenotypes (such as phocomelia, craniofacial abnormalities, and heart malformations, etc.) to those exhibited by cohesinopathy patients (Smithells and Newman, 1992; Vargesson, 2015). Thalidomide is a drug that acts through the direct binding to a Cullin4 Ring E3 Ligase (CRL4) of the ubiquitin proteosome system (Ito et al., 2010). CRL4 is made up of ROC1, CUL4, DDB1, and a DDB1-CUL4 Associated Factor (DCAF) (McCall et al., 2008). Not surprisingly, in humans, mutations in *CUL4* or *DDB1* are associated with short stature, intellectual disabilities, and craniofacial and digit anomalies (Cabezas et al., 2000; Tarpey et al., 2007; Vulto-va Silfhout et al., 2015; White et al., 2021).While some endogenous targets of CRL4 have been identified *in-vitro* and in cell cycle studies, those functionally important for tissue malformation in development are still largely unknown (Waning et al., 2008; Leung-Pineda et al., 2009; Yu et al., 2015).

Using zebrafish embryo as a model system, we recently found that the CRL4 is targeted not only by thalidomide, but also regulated by cohesin. On the one hand, thalidomide binds CRBN subunit of CRL4 to block proper ubiquitination of endogenous targets and promote novel targets (Ito et al., 2011). On the other hand, our data revealed that Smc3 and Esco2 are both required for *ddb1* transcription (Sanchez et al., 2022). Knock downs of Smc3 or Esco2 results in reduced *ddb1* expression and produced severe phenotypes in zebrafish. Importantly, phenotypes that arise in response to Smc3 knockdown are rescued by exogenous expression of

ddb1 mRNA (Sanchez et al., 2022). *SMC3* mutations, however, account for only a small percentage of CdLS cases. *NIPBL* (Nipped-B in drosophila and Scc2 in yeast) mutations, on the other hand, account for roughly 65% of reported CdLS cases. Thus, it becomes critical to test whether Nipbl function similarly impacts *ddb1*. If CRL4 activity (regulated through cohesin-dependent transcription of *ddb1*) is downstream of many cohesinopathy phenotypes, then it similarly becomes important to identify targets downstream of this cohesin/CRL4 axis.

Here, we identify targets which may serve as treatment options for developmental malformations. These findings investigate the hypothesis that Nipbl similarly targets the CRL4 component, Ddb1, and further assess the cohesin/CRL4 axis influence on protein turnover that contribute to cohesinopathy phenotypes.

3.3 Materials and Methods

Maintenance of Zebrafish Colony

Zebrafish (Danio rerio) strains C32 and saxo2-GFP transgenic lines were used. This study was performed in accordance with the recommendations in the Guide for the Care and Use of Laboratory Animals of the National Institutes of Health. These protocols were approved by Lehigh's Institutional Animal Care and Use Committee (IACUC) (Protocol 187). Lehigh University's Animal Welfare Assurance Number is A-3877-01.

Morpholino (MO) Injections

MO purchased from GeneTools, LLC (Philomath, OR) were dissolved in sterile dH_2O, for a 1mM concentration (sequences available upon request). These were

heated to 65°C for 15 minutes prior to use. Nipbla/b MOs were mixed together for a concentration of 0.5mM each. A standard control (SC) MO with no target sequence in zebrafish was used as control. Microinjections were performed at the 1-cell stage using the Narishige IM 300 Microinjector and Nikon SMZ 800 for visualization. Zygotes were sorted for viability and fertilized embryos were kept in egg water and Ampicillin solution at 28°C. Embryos were dechorionated using pronase if needed, then harvested for lysate or cDNA preparations or fixed in 4% paraformaldehyde (PFA), and kept at 4°C overnight for phenotype analysis. Embryos were stored in 100% methanol at -20°C for long term use after fixing.

Embryo Lysates and Immunoblotting

MO injected embryo lysates were made to validate mRNA expression for *ddb1* and EGFP_Pparαa mRNAs. mRNA injected embryos were harvested at 24 hpf along with appropriate controls (phenol red injected embryos as control for *ddb1* mRNA injected, EGFP mRNA injected embryos as control for EGFP_Pparαa mRNA injected). Lysate protocol was adapted from Schabel et al., 2019. In short, embryos were de-chlorinated with pronase then washed in E3 egg water. Individual embryos were placed in 1.5mL centrifuge tubes and all excess egg water was removed. 500µL of heptane were added immediately followed by 500µL of cold methanol. Sample were fixed for 5 mins at room temperature. Embryo was washed two times with 500µL of cold methanol then 2 times with 100µL of Embryo Buffer (EB) with freshly added protease inhibitor cocktail mix. Embryos were homogenized in 20µL of EB. Three single embryo lysate preps were pulled to create one biological replicate. Lysates were stored at -80°C, 5X SDS Loading buffer was added and samples were

boiled before use for 5 minutes. A primary antibody for Ddb1 was used to detect protein levels (1:500, Abcam ab124672). Alexa 488 anti-rabbit (1:1000, Invitrogen) was used to detect Ddb1 primary antibody. An Alexa 488 conjugated antibody specific for GFP was used to detect EGFP mRNA and EGFP_Pparαa expression (1:1000, Invitrogen A-21311). Mouse anti-α-tubulin (1:1000, Sigma-Aldrich, T9026) was used as a loading control. Alexa 647 anti-mouse (1:1000, Invitrogen) was used to detect the tubulin primary antibody. For measurement of band intensities, ImageJ software (https://imagej.nih. gov/ij/) was used. Relative pixel densities of gel bands were measured using the gel analysis tool in ImageJ software as previously described in Bhadra and Iovine, 2015. Tubulin was used as a loading control and thus the relative expression calculations were based on the ratio of Ddb1 or GFP to Tubulin.

mRNA Rescue

Full length mRNA encoding for *ddb1* was designed using the sequence from the ZFin database. The plasmid was stored at -20°C until used. Plasmid was diluted to a 1:10 concentration of 0.2μg/μL in sterile water. One Shot Max Efficiency DH5α cells were transformed with the plasmid using standard procedures. The Qiagen Mini-Prep kit was used to isolate plasmid DNA from the transformed bacteria. The plasmid DNA was then linearized by performing an AvrII digest. A transcription reaction was then performed using the Invitrogen mMessage mMachine kit. The concentration of the resulting mRNA was assessed using the Thermo Scientific Nanodrop 2000. This was also run on a formaldehyde gel and imaged using the BioRad Gel Doc. The mRNA was then diluted to a concentration of 100ng/μL in phenol red. Diluted mRNA was heated at 65°C for 5 minutes prior to injections into zebrafish embryos at the 1-cell stage as

previously described. The mRNA was also co-injected into embryos that had been injected with the nipbla/b MOs. Both the mRNA injected embryos and co-injected rescue embryos were fixed at 72 hpf in 4% PFA overnight at 4°C and for phenotypes analysis. Embryos were stored in 100% methanol at -20°C for long term use after fixing.

qRT-PCR

For qRT-PCR, total mRNA was extracted from around 15 embryos to make one biological replicate using Trizol reagent and the standard protocol. The resulting mRNA pellet was resuspended in a solution of DEPC H2O and RNAse Inhibitor, then the concentration of RNA was recorded using the Thermo Scientific Nanodrop 2000. For making cDNA, 1 µg of total RNA was reverse transcribed with SuperScript III reverse transcriptase (Invitrogen) using oligo (dT) primers. The resulting cDNA was diluted 1:10 for qRT-PCR, using the Rotor-Gene 6000. cDNA was made on Nipbla/b MOs injected embryos and SC MO injected embryos. For each cDNA used, primers at a 10µM concentrations were used. Specific primers for ddb1 were used (F: 5'-GCACACTGCAGATTGATGAC-3', R: 5'-GACGACTCCACTAACACTACAG-3'). keratin4 primers (F: 5'-TCATCGACAAAGTGCGCTTC-3'; R: 5'-TCGATGTTGGAACGTGTGGT-3') were used as a housekeeping gene control. For each PCR tube, 7.5µL of Sybr Green, 3µL 10µM Primers , 3.5µL sterile H2O, and 1µL cDNA was added. Analyses of the samples were done using Rotor-Gene 6000 series software (Corbette Research) and the average cycle number (C_T) determined for each amplicon. Delta C_T (ΔC_T) between housekeeping gene and CRL4 genes were calculated to represent expression levels normalized to keratin values. $\Delta\Delta C_T$ values were

calculated to represent the relative level of gene expression and the fold difference was determined using the $\Delta\Delta C_T$ method ($2^{-\Delta\Delta C_T}$) as previously described in Iovine lab publications.

Imaging Analysis of Embryos

Zebrafish embryos fixed at 72 hpf were mounted on double cavity slides using 3% methyl cellulose for embedding. Embryo phenotypes were observed using the Nikon SMZ 1500, 1X objective at room temperature and the Nikon Eclipse 80i Microscope, 10X and 20X objectives at room temperature. Microscopes were equipped with SPOT-RTKE digital camera (Diagnostic Instruments) and SPOT software (Diagnostic Instruments) for image acquisition. Embryos fixed at 3 days post fertilization were imaged using 3% methyl cellulose on a double cavity microscope slide and positioned supine. The embryo heart was imaged at 10x, 20x, and 40x magnification on a Nikon Eclipse 80i microscope with fluorescence from a X-Cite 120 Fluorescence Imaging System. Embryos were then repositioned to lie laterally, and images of the body were taken at 4x, of the head at 10x, and of the anterior and posterior otoliths at 20x magnification. The images obtained were then used to quantify whole embryo length, eye diameter, and heart phenotypes. Heart phenotypes were scored as Type A if reduced jogging was observed and Type B if cardiac bifida was observed.

Cell Lines and Culture Conditions

GM14894 (healthy control), GM20000 (CdLS patient), and GM20466 (RBS patient) cell lines were purchased from Corriell Institute for Medical Research. LCLs were grown in RPMI 1640 with 15% fetal bovine serum (FBS), 100 U penicillin/ml, 100 μg streptomycin/ml sulfate, and 1% L-glutamine. Samples from a healthy control

of European descent, 1 clinically severe CdLS affected individual of European descent (with *NIPBL* frameshift mutation), and 1 clinically diagnosed RBS affected individual of European descent (with *ESCO2* frameshift and nonsense mutation alleles) were chosen. Cells were incubated at 37 C with 5% CO2 levels.

Cell Lysate Preparation and Western Blot

To harvest cells for lysate preparation, 5×10^6 exponentially growing cells were seeded in 15 ml media in a 75-ml Falcon flask, and fed exactly after 24 hours. After an additional 24 hours on day 3, cells were pelleted by centrifuge. Pelleted cells were washed with 1X PBS twice and resuspended in Lysate Sample Buffer. Suspension was agitated by pipetting then boiled for Western Blots. 10% SDS-PAGE gel was poured with 5% stacking.

Liquid Chromatography Mass Spectrometry

Rutgers Proteomics facility performed and analyzed mass spectrometry data on embryos knockdown for Esco2, Smc3 and Ddb1 compared to control embryos. About 100 ug of each lysate were digested using standard gel-plug protocol. Half of each sample was labeled with TMT11 plex reagent (Thermo Scientific) according to manufacturer's instructions. A test mix of 1% of individual samples were run on nano-LC-MSMS and the reporter ion intensity were used to normalize the mixing of the samples to achieve sample ratio 1:1 for all samples. After mixing, the samples were desalted with SpeC18 and dried. TMT labeled and combined sample were desalted with SPEC C18 column and solubilized in 200 µL of buffer A (20 mm ammonium, pH 10) and separated on an Xbridge column (Waters; C18; 3.5 µm, 2.1 × 150 mm) using a linear gradient of 1% B min−1, then from 2% to 45% B (20 mm ammonium in 90%

acetonitrile, pH 10) at a flow rate of 200 μL min−1 using Agilent HP1100. Fractions were collected at 1-min intervals and dried under vacuum. For total proteome analysis, 14 fractions (Fraction from 25 min to 38 min) were chosen for total proteome analysis.

All LC-MS data were analyzed with Maxquant (version 1.6.10.43) with Andromeda search engine. Type of LC-MS run was set to reporter ion MS2 with 10plex TMT as isobaric labels. Reporter ion mass tolerance was set at 0.003Da. LC-MS data were searched against the most up to date Uniprot zebrafish proteome database with addition of potential contaminants. Protease was set as trypsin/P that allowed 2 miss cuts. Carbaidomethylation of cysteine was set as fixed modification, N-terminal acetylation, oxidation at methionine were set as variable modifications. Protein with FDR<1% were reported. The protein group results were analyzed using Perseus (version 1.6.10.43). The data were 1st filtered for reverse and contaminant hits and the reporter ion intensity data were further log 2 transformed and normalized to the column median value. For group comparison, statistical significance between groups were analyzed using student T-test with equal variance on both sites and the Q value was calculated with permutation test. S0=0.1 was used to evaluate significance.

Statistical Analysis

ANOVA tests were used to determine if there was a statistically significant difference in body size, and eye size between knockdowns (KD) and controls. Statistical analysis was performed using ordinary one-way ANOVA tests. Two-tailed paired t-tests were used to determine if there was a statistically significant difference in qRT-PCR analysis between KDs and controls. Only values giving $P < 0.05$ are reported.

3.4 Results

Nipbla/b KD impact Ddb1 levels in zebrafish

Because *NIPBL* mutations account for the highest incidence of CdLS patients, we sought to determine if Nipbl-knockdown in zebrafish similarly targets CRL4. Zebrafish have two NIPBL proteins, Nipbla and Nipblb, that share 66% homology to the human protein and 70% homology to each other (Muto et al., 2011). The roles of Nipbla and Nipblb in zebrafish are at least partially redundant, as double knockdowns (KD) are required to see significant developmental impairment (Muto et al, 2011, 2014, Xu et al., 2015; Kawauchi et al., 2016). To further study the role of Nipbl in zebrafish development, we used previously well-characterized *nipbla* and *nipblb* targeting morpholinos (MO) (Muto et al, 2011, 2014, Xu et al., 2015; Kawauchi et al., 2016). A *nipbla/b* MOs mix (each at 0.5mM concentration) was injected into 1-cell stage embryos. In parallel, Standard Control (SC) MO was injected into embryos (1mM). We found that Nipbla/b-KD leads to significant defects in body length and eye size compared to SC MO embryos (Figure 3.1A-B). We additionally observed abnormal heart phenotypes (Figure 3.1C-D), similar to those previously characterized due to Nipbla/b-KD in zebrafish (Muto et al., 2011). Thus, Nipbla/b KD in zebrafish provides a robust model for CdLS and recapitulate many phenotypes that arise due to Esco2 KD and Smc3 KD.

Prior findings suggest that Esco2 and cohesin regulate *ddb1* transcription, a component of the CRL4 E3 Ligase (Sanchez et al., 2022). To investigate if *ddb1* is also impacted in *nipbla/b* MO injected embryos, we assessed *ddb1* transcript levels at 24 hours post fertilization (hpf) through qRT-PCR. cDNA obtained from *nipbla/b*

MO mix injected embryos, compared to SC MO injected embryos, was used to calculate fold changes in *ddb1* gene expression, using the housekeeping gene *keratin-4* as a control. The results show that *ddb1* is significantly downregulated in *nipbla/b* MO injected embryos compared to SC MO injected embryos (Figure 3.2A). To further assess the impact of Nipbla/b KD, we quantified Ddb1 protein levels compared to SC MO injected embryos. Consistent with a reduction in transcription, Nipbla/b KD embryos exhibited a significant decrease in Ddb1 protein levels compared to control embryos (Figure 3.2B).

If downregulation of Ddb1 plays a role in the developmental defects produced by Nipbla/b KDs, then exogenous expression of *ddb1* mRNA should rescue the abnormal phenotypes that otherwise occur. To test this hypothesis, we injected *ddb1* mRNA independent of cohesin regulation, to elevate Ddb1 protein levels (Supplemental Figure 3.1) in embryos at the 1-cell stage, along with the *nipbla/b* MO mix. Importantly, a number of phenotypes were significantly rescued by exogenous *ddb1* expression (eye and otolith phenotypes quantified in Supplemental Figure 3.2). These results support a model that cohesinopathies impact CRL4 E3 ligase, and that reduced CRL4 function underlies a significant number of CdLS phenotypes.

Mass spectrometry identifies accumulated proteins across the cohesinopathies/CRL4 axis

Given that Ddb1 is the scaffold for Cul4 upon which interchangeable DCAFs bind. In turn DCAFs act as the substrate recognition component for CRL4 ligases (McCall et al., 2008). Given the role of E3 ligases in protein degradation, we hypothesized that a subset of proteins that accumulate due to reduced CRL4 activity

play a role in producing the abnormal phenotypes observed in cohesinopathy zebrafish embryos. In an effort to identify proteins downstream of the cohesin/CRL4 axis, we performed mass spectrometry on zebrafish embryos knocked down for two independent models for cohesinopathies (Esco2 KD as a model for RBS and Smc3 KD as a model for CdLS) and also Ddb1 KD to inhibit proper CRL4 formation. Embryos individually injected with one of these 3 MOs (targeting either *esco2*, *smc3*, *ddb1*), or a SC MO, were harvested at 24hpf to obtain lysates. The resulting lysates were subjected to proteomic Liquid Chromatography Mass Spectrometry (LC-MS) to identify proteins represented at elevated levels in each of the 3 treatments, compared to SC MO (Figure 3.3A). In total, 30 proteins were identified as significantly elevated across all 3 treatments (*esco2* MO, *smc3* MO, *ddb1* MO*)* (Figure 3.3B; Table 3.1). From those 30, a top 10 candidate list was prioritized based on 1) a greater than 20% increase in all 3 knockdowns, 2) human homologs, and 3) exhibited expression profiles in tissues impacted in cohesinopathies. Of those 10, we then focused in candidates previously reported as ubiquitinated. Below, we present evidence on one of the candidates, peroxisome proliferator-activated receptor alpha a (Pparαa).

Pparαa is widely expressed in zebrafish craniofacial (eye, brain, otic placode) and heart structures during development (Collins et al., 2019; Hsieh et al., 2018; Levi et al., 2012). In murine models, PPARα plays a role in lipid metabolism and zebrafish studies show multiple deformities (including craniofacial malformation and pericardial edema) associated Pparαa modulation during development (Djouadi et al., 1998; Leone et al., 1999; Heneka et al., 2007; Hsieh et al., 2018; Venezia et al.,

2021). As noted above, PPARα is degraded in a ubiquitin dependent manner (Blanquart et al., 2002).

PPARα levels impacted in patient cell lines and *pparαa* mRNA overexpression causes abnormal phenotypes in zebrafish embryos

Pparαa is a transcription factor that regulates the expression of genes involved in cell proliferation, cell differentiation, and immune response (Peters et al., 2012). If elevated levels of PPARα contributes to cohesinopathies, we reasoned that lymphoblastoid cell lines (LCL) from individuals with known mutations in the cohesin regulator *NIPBL* (CdLS) and *ESCO2* (RBS) would similarly exhibit increased PPARα levels. Western blot probing for PPARα in lysates obtained from CdLS and RBS LCL cells, compared to lysates from healthy control LCL cells, were analyzed. Tubulin antibody was used as a loading control. Results suggest an increase of PPARα protein levels in log growing cells in both RBS cells and CdLS cells, compared to healthy control cell lysates (Figure 3.4). These results support LC-MS zebrafish findings that show increased levels of Pparαa in Smc3 KD, Esco2 KD, and Ddb1 KD embryos.

To test our model that accumulation of proteins, such as Pparαa, downstream of the cohesin/CRL4 axis are responsible for a subset of phenotypes in cohesinopathies, we injected *pparαa* mRNA in embryos at the 1-cell stage. As expected, control embryos injected with phenol red produced no abnormal phenotypes. In contrast, *pparαa* mRNA injections resulted in a significant reduction of eye size (Figure 3.4A-B). Abnormal heart phenotypes were also observed with *pparαa* mRNA injections, compared to control embryos (Figure 3.4C). Interestingly, no effect on body length

was observed with *pparαa* overexpression (Figure 3.4A-B). This suggests that an alternate target of CRL4 mediates this phenotype.

3.5 Discussion

We previously reported on a unifying mechanism for cohesinopathies and thalidomide teratogenicity that converges through the CRL4 E3 ligase (Sanchez et al., 2022). One major revelation of the current study is Nipbla/b KD regulate *ddb1* expression in zebrafish embryos, similar to Esco2 KD and Smc3 KD findings. The relevance of this pathway is supported by findings that Nipbla/b KD phenotypes are rescued by exogenous *ddb1* mRNA. We further reveal candidate proteins downstream of the cohesin/CRL4 pathway identified through proteomic mass spectrometry. Overexpression of Pparαa, one of the candidate proteins, produced eye and heart malformation in zebrafish embryos. In combination with our previous findings (Sanchez et al., 2022), these results provide evidence that cohesinopathies act on CRL4 E3 Ligase and that aberrant CRL4 function plays a role in abnormal development.

A major revelation of this study is in translating the zebrafish findings in a human cell line model. Our preliminary findings using a small number of CdLS and RBS patient cell lines suggest that PPARα protein accumulates in cohesinopathy patient lines compared to healthy control cell lines. Future experiments analyzing PPARα levels in additional patient cell lines will provide important insight into human disease mechanism. For instance, there is high degree of phenotypic variability in CdLS patients (Krantz et al., 2004; Deardoff et al., 2007). We are currently

expanding this study to include multiple CdLS cell lines with other *NIPBL* mutations. Our cross-model approach (zebrafish and human cell line) will provide insight into our the extent that our zebrafish LC-MS data translated to human cohesinopathies. Additionally, this strategy provides tangible support for future studies to identify possible therapeutics.

3.6 Figures and Tables

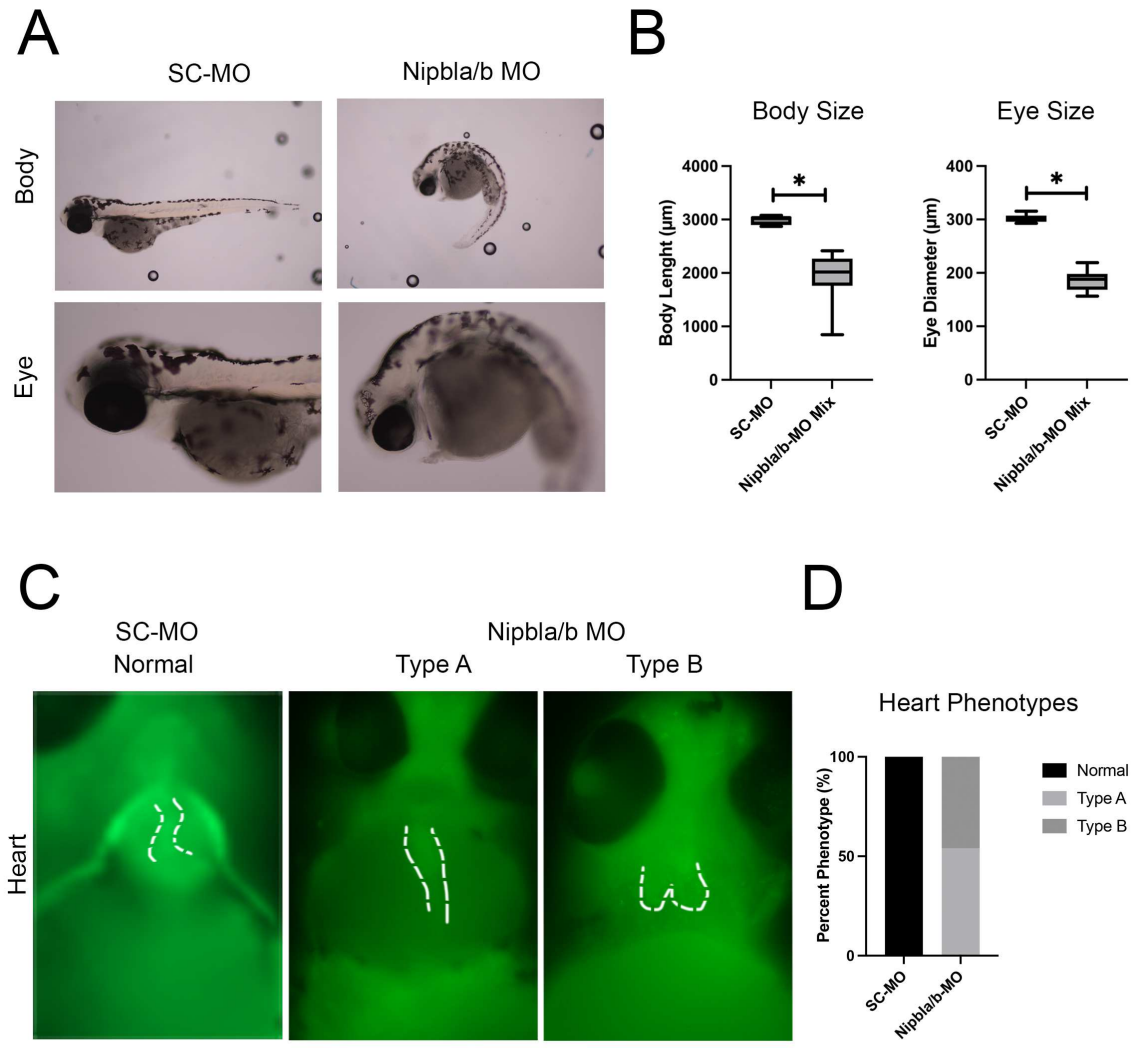

Figure 3.1. *nipbla/b* MOs phenotypes include reduced body and eye size, and abnormal heart development. (A) Representative images of control embryos (SC MO injected), *nipbla/b* MO injected embryos. For all experiments, 15-31 72hpf embryos were

analyzed from a minimum of 3 independent trials. (B) Quantification of body and eye sizes from MO injected embryos were compared to SC MO injected embryos. The graph reveals significant reductions of body length and eye diameter in *nipbla/b* MO injected embryos compared to control embryos (error bars represent s.e.m., one-way ANOVA with Turkey's multiple comparison, *P<0.05). (C) Heart looping phenotypes observed in *nipbla/b* MO injected embryos compared to SC injected embryos. cmcl2-EGFP transgenic line was used to visualize heart phenotypes. The graph shows percent phenotype observed with MO treatments. Reduced or no-jogging phenotypes were characterized as Type A, while cardiac bifida was characterized as Type B. Control embryos all exhibited normal heart looping phenotypes, while nipbla/b MO injected embryos all exhibited heart defects.

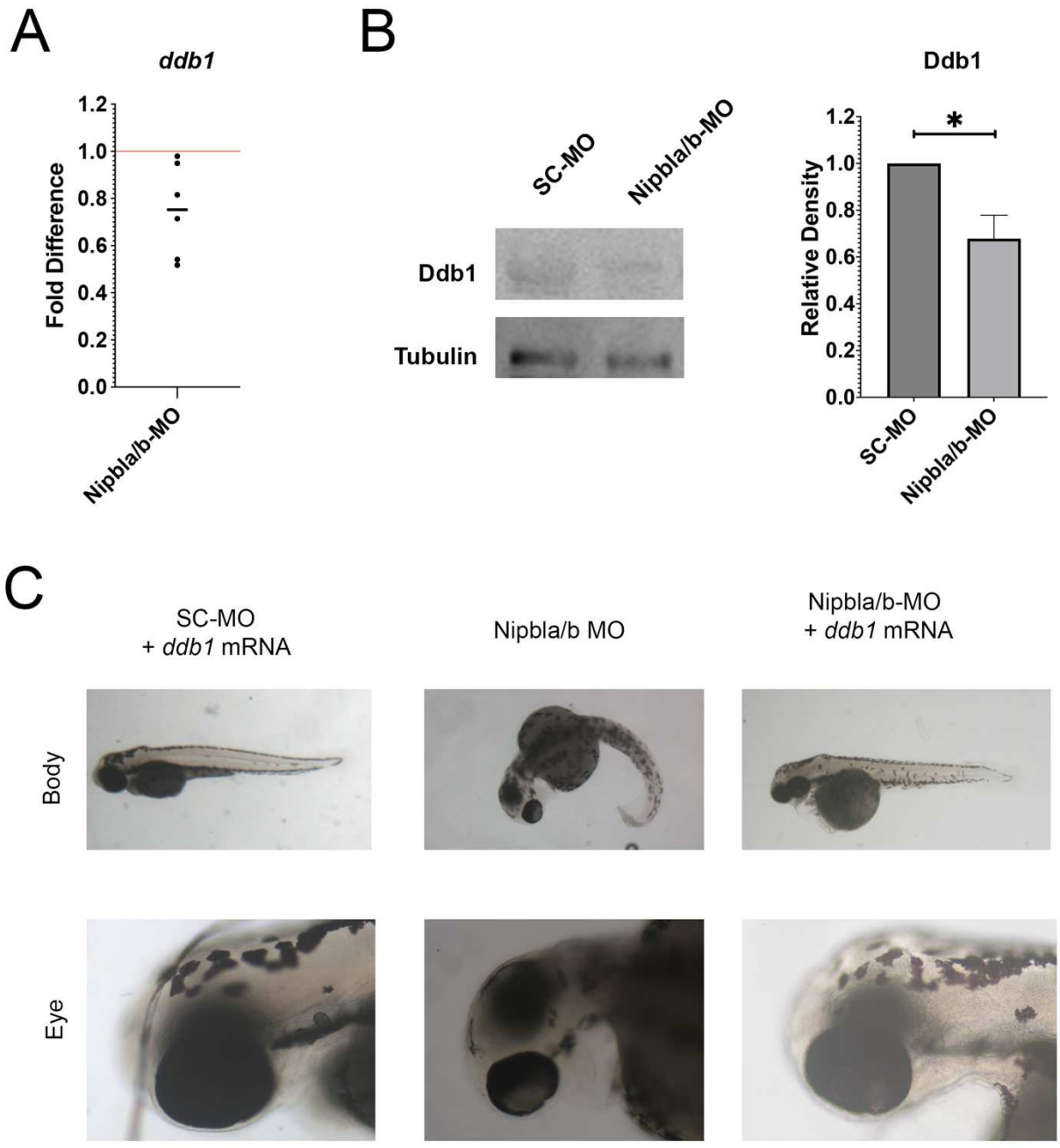

Figure 3.2. Exogenous expression of *ddb1* rescues Nipbla/b KD phenotypes. (A) Gene expression levels were measured by qRT-PCR analysis in *nipbla/*b MO injected embryos. The graph shows fold difference in expression levels from each replicate (black) and the

average expression (black line) for each gene. Keratin was used as the internal refence gene control for fold difference calculations. A fold difference of 1 is considered no change with respect to SC MO injected embryos (represented by red line). *ddb1* expression is significantly downregulated in Nipbla/b KD embryos (un-paired t-test, $P<0.05$). (B) Ddb1 protein levels were measured through Western Blot of nipbla/b MO injected embryo lysates compared to SC MO lysate controls. Immunoblots were probed with Ddb1 and Tubulin antibodies. Analysis detects Ddb1 at a predicted size of 130 kDa and Tubulin at the predicted size of 50 kDa. Graph shows the average relative densities of the Ddb1 bands between experimental and control sample from 3 biological replicates. Ddb1 protein levels are significantly reduced by 32% with MO injection compared to SC injected embryos (error bars represent s.e.m., un-paired t-test, $*P<0.05$). (C) Exogenous *ddb1* mRNA was injected to WT embryos at the 1-cell stage immediately following *nipbla/b* MO injections. Rescue of body and eye sizes observed with ddb1 overexpression. 31-35 replicates were analyzed and at least 3 independent trials were performed. Phenotypes were imaged and measured at 72 hpf.

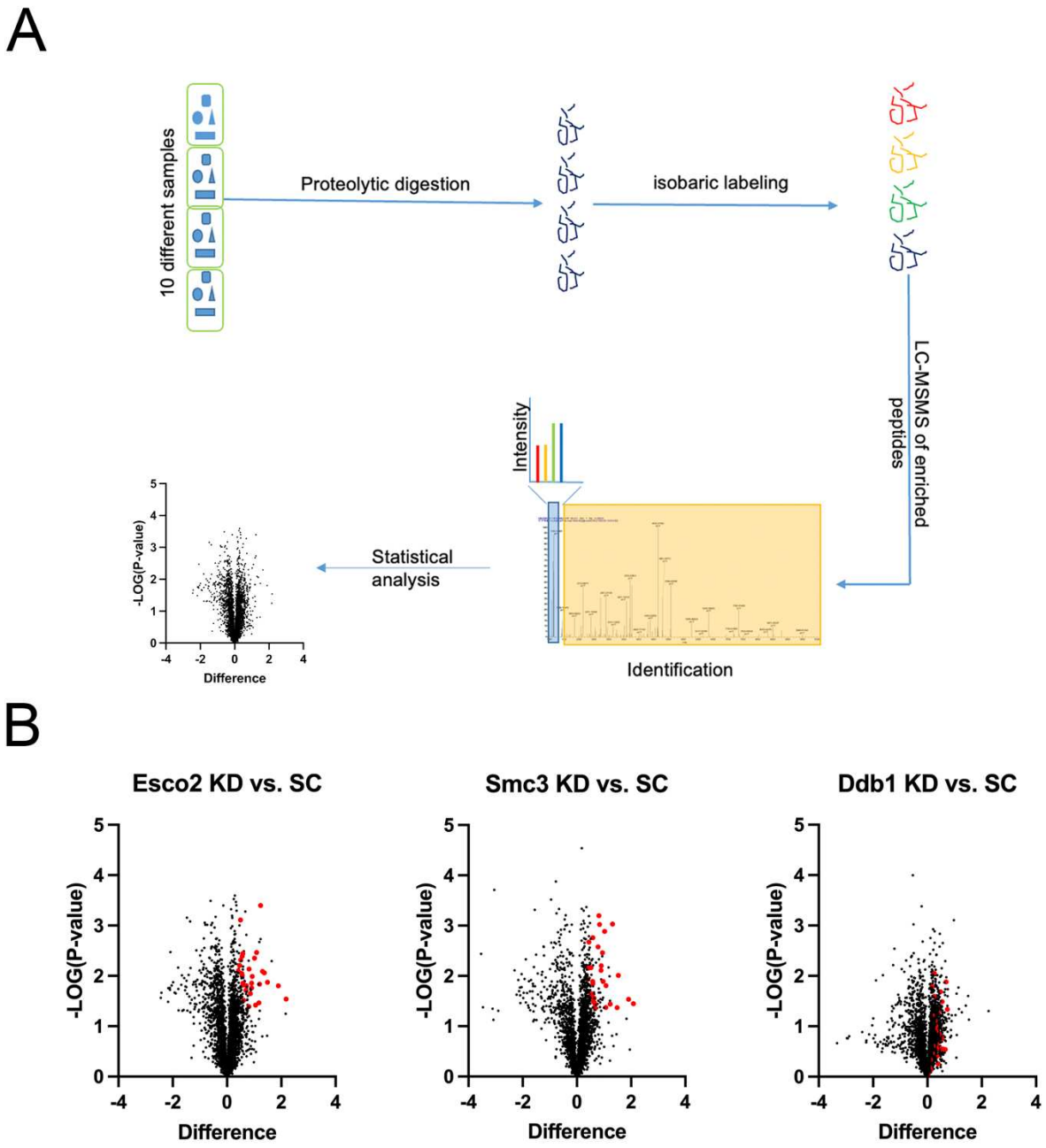

Figure 3.3. Identification of candidates coordinately regulated across Esco2/cohesin and CRL4 pathway. (A) Workflow for liquid chromatography mass spectrometry performed on 3 independent replicates of Esco2 KD embryo lysates, Smc3 KD embryo lysates, and Ddb1 KD embryo lysates. Each lysate replicate contained 3-6 embryos for a

total of 9-18 embryos analyzed per treatment. SC injected embryo lysates were used as control. About 100 ug of each lysate were digested using standard gel-plug protocol. Half of each sample was labeled with TMT11 plex reagent. 10plex TMT was used for isobaric labels. Reporter ion mass tolerance was set at 0.003Da. LC-MS data were searched against the most up to date Uniprot zebrafish proteome database with addition of potential contaminants. The protein group results were analyzed using Perseus (version 1.6.10.43). (B) Volcano plots of 3422 protein groups identified with FDR<1% proteins in esco2 MO vs. SC MO analysis, smc3 MO vs. SC MO analysis, and ddb1MO vs. SC MO analysis. Red dots represent significant accumulated significant proteins in common between the 3 treatments.

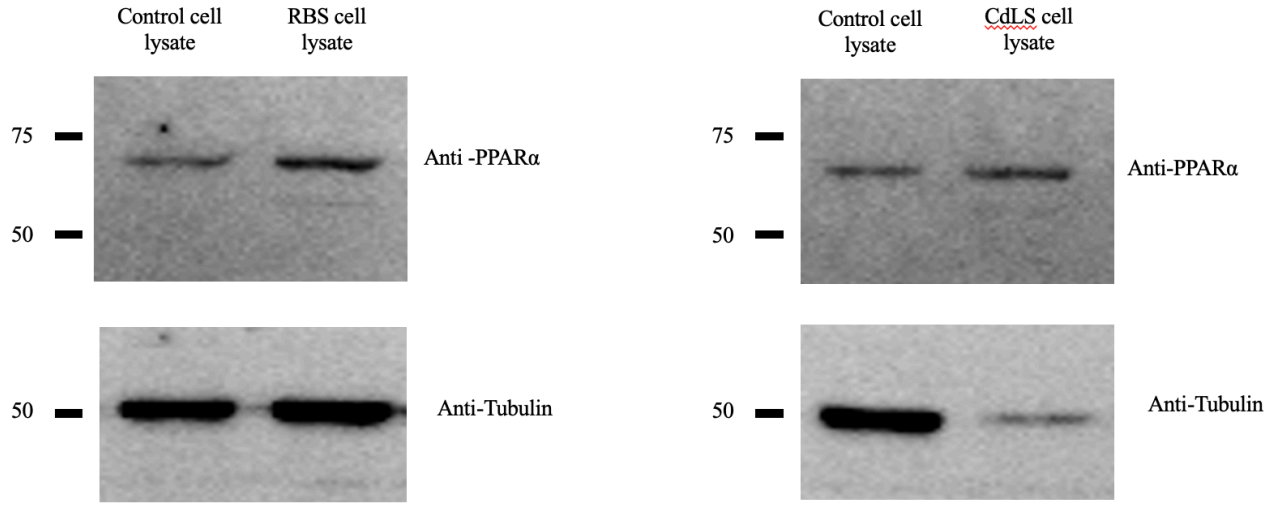

Figure 3.4. RBS and CdLS patient cell lines exhibit increased levels of PPARα.

Western Blot of PPARA protein levels were measured through Western Blot of healthy control, RBS and CdLS cell line lysate. Immunoblots were probed with PPARA and Tubulin antibodies. Analysis detects PPARα at a predicted size of 68 kDa and Tubulin at the predicted size of 50 kDa.

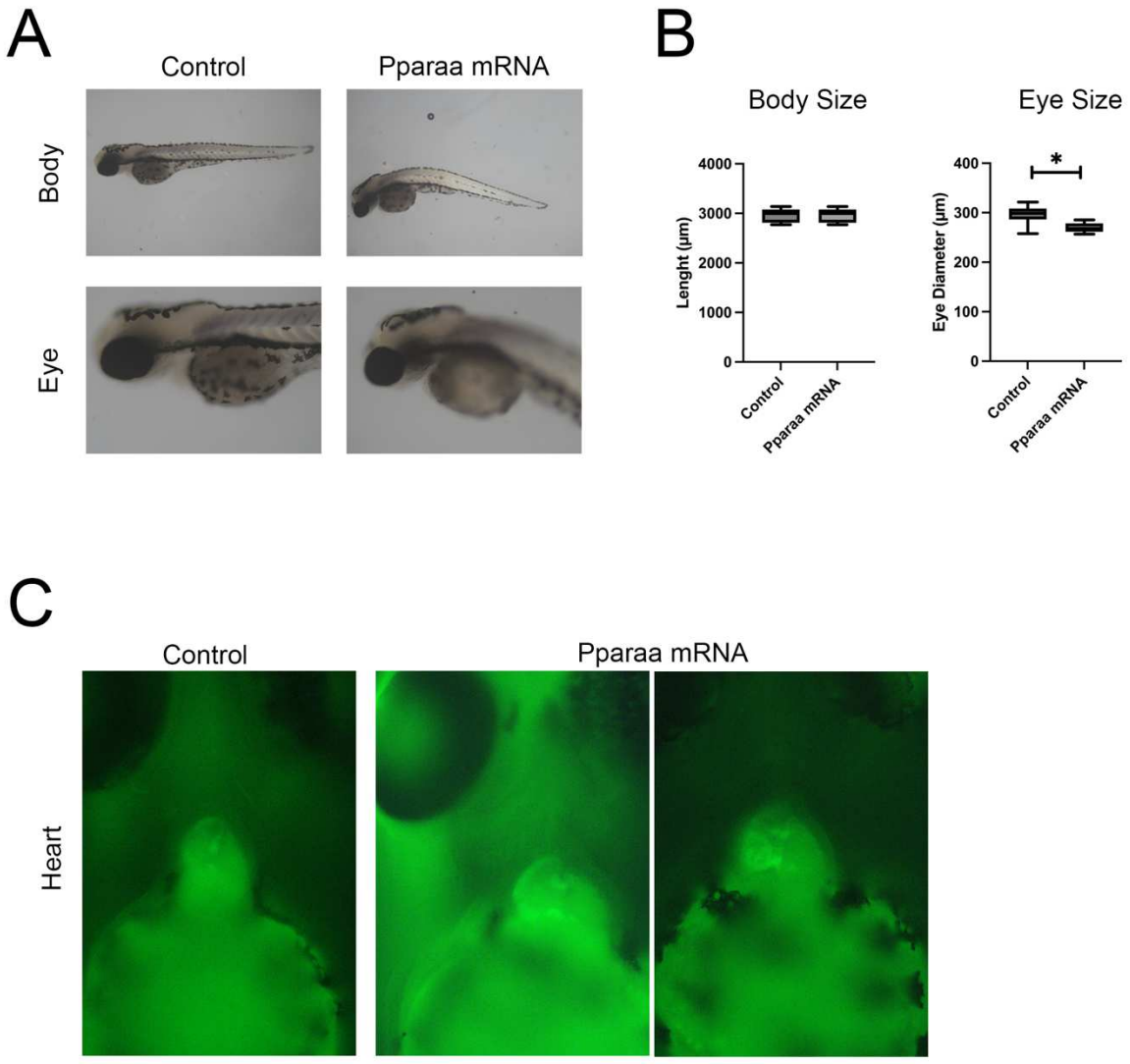

Figure 3.5. ***pparαa*** mRNA **produces abnormal phenotypes in zebrafish embryos.** (A) Representative images of control embryos (phenol red injected), and *pparαa* mRNA injected embryos. For all experiments, 11-23 72hpf embryos were analyzed from a minimum of 3 independent trials. (B) Quantification of body and eye sizes from mRNA

injected embryos compared to controls. The graph reveals significant reduction in eye diameter in *pparαa* mRNA injected embryos compared to control embryos (error bars represent s.e.m., one-way ANOVA with Turkey's multiple comparison, *P<0.05). No significant difference in body length observed between *pparαa* mRNA injected and control embryos (C) Abnormal heart phenotypes observed in *pparαa* mRNA injected embryos compared to control injected embryos. cmcl2-EGFP transgenic line was used to visualize heart phenotypes.

		Esco2 KD vs. SC	Smc3 KD vs. SC	Ddb1 KD vs. SC
Protein ID	Gene Name	Difference	Difference	Difference
Q1RLT0	mat2al	1.23655351	1.073552608	0.35800815
Q90ZZ7;I3IT92	aldh3b1	0.494288286	0.395914078	0.35357213
Q6GQM3	psma6l	1.088751316	0.837722143	0.30382752
Q4V984;F1QYB8;A0A2R8RJG0	rab1bb	0.580788771	0.813877106	0.2985847
E7FBN4	ccdc97	0.561916351	0.583009879	0.20322633
Q9PT95;A0A0R4IVC3	rbp4	1.01729695	1.019125938	0.28981805
Q6DRF3	psmb1	0.508434137	0.430668831	0.16333699
Q6P3J2	arhgdia	0.467732906	0.589079539	0.56137013
A0A2R8Q009;F1QAE8;Q6NWX7	ntmt1	0.812605063	0.784346263	0.5553925
F8W4P0;F1QSP5;F8W3U8;F1R6M3;Q8QGG8;E7EZA2	ddx4	0.41194582	0.531398455	0.19382787
A0A2R8RHW2;A0A2R8RVB7;F1R2T3;Q1MTC6;A0A2R8QQ28	vtg7	1.306207498	1.316763719	0.831429
F1QXE8;A0A2R8QN72	glb1l	1.378790855	1.532193025	0.70665479
Q804G7	anxa4	0.544283072	0.565238953	0.22565961
E7F5V3;A0A2R8Q644	fasn	0.558222294	0.521127383	0.18008065
F1Q7L0	vtg4	0.929385662	0.895548344	0.20674562
A0A2R8QA33;E7F4U1;A0A2R8Q3N3	arhgef2	1.487620831	1.232399305	0.65551162
B0R174	rbp1	0.904615879	0.672195117	0.13635087
Q5RHE5	si:dkey-90m5.4	0.583061218	0.646815459	0.31550813
F2Z4T7	lman2lb	1.200867494	1.066747983	0.67841077
F6NHA0;B8JIH2	vcla	0.598661423	0.612442493	0.20521474
Q7ZV08;F8W3F9;E9QBN9;E9QII2;F1QNP1;A0A0R4IYL9;F1Q589	scamp2	0.7122159	0.670710564	0.54768968
A0A0R4IA33;A0A0R4INF8		1.889341672	1.904612382	0.53111768

O93423;A0A2R8Q993;F1QCQ7;A0A2R8RTR5;A0A2R8QIZ7;A0A2R8QD47;A0A0R4IGK4;E9QIN9;F1R5A4;A5PLE0	stom	0.90393877	0.94673125	0.6107924
A0A2R8QPY5;A8E7G5	sfxn4	0.696242015	1.484941324	0.6757133
F1R1P4	sesn3	0.862670263	0.887174447	0.42437291
F1QC84	f13a1a.1	2.177110195	2.086372693	0.30634189
B1H1M3	prosc	0.614677588	0.441312154	0.21430326
Q6NV34	decr2	1.179144859	0.638601144	0.23723769
A0A2R8QBG3;F1QV15;A0A2R8QKR3;A0A2R8RSX9	vtg6	1.051682631	0.963767529	0.23556376
Q5RGZ2	Pparαa	0.804489772	0.586190383	0.3081305

Table 3.1. Significant accumulated proteins in independent Esco2 KD, Smc3 KD and Ddb1 KD zebrafish embryos. Zebrafish protein ID and gene name provided. Only proteins with FDR <1% were reported and student t-test was used for group comparisons.

3.7 Supplemental Figures and Tables

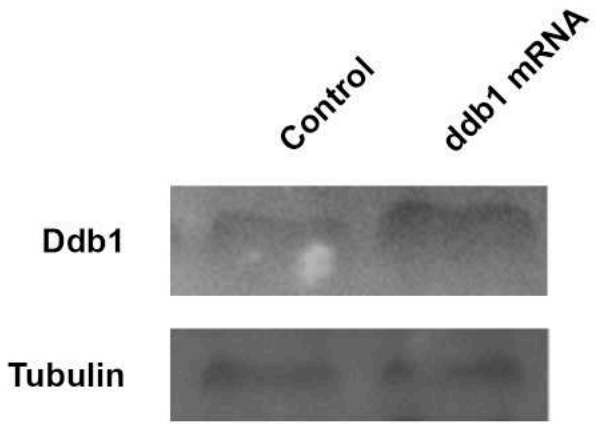

Supplemental Figure 3.1. *ddb1* mRNA **injections in zebrafish result in increased Ddb1 protein levels.** Ddb1 protein levels were measured through Western Blot of *ddb1* mRNA injected embryo lysates compared to phenol red injected embryo lysate controls. Immunoblots were probed with Ddb1 and Tubulin antibodies. Analysis detects Ddb1 at a predicted size of 130 kDa and Tubulin at the predicted size of 50 kDa.

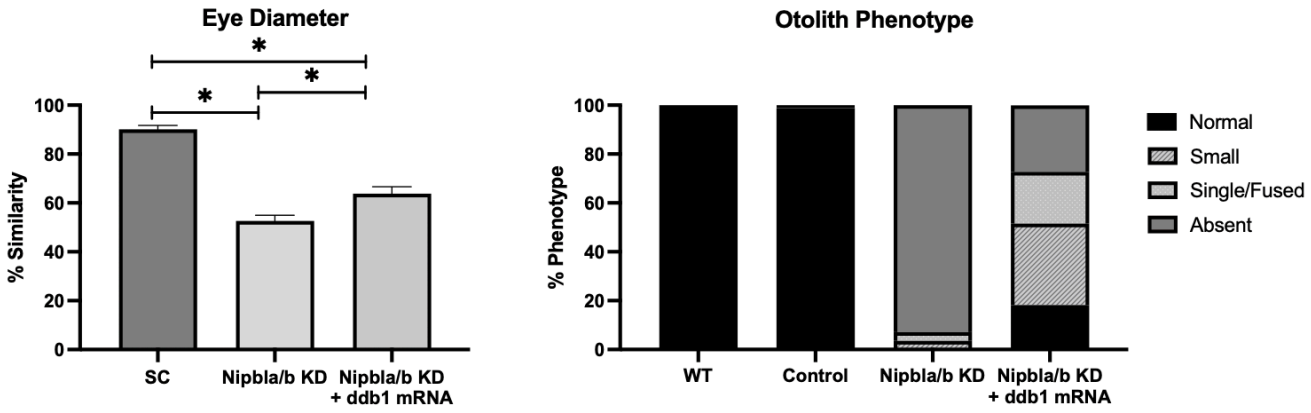

Supplemental Figure 3.2. Quantification of Nipbla/b KD phenotype rescue by *ddb1* mRNA**.** (left) Quantification of eye phenotypes from injected embryos were compared to un-injected WT embryos to obtain percent similarity. Bar graph reveals significant rescue of eye diameter in Nipbl KD + *ddb1* mRNA compared to Nipbl KD alone (error bars represent s.e.m., one-way ANOVA with Turkey's multiple comparison, *P<0.05) (right) Graph shows percent of normal, fused, small, or absent otolith phenotypes with *nipbla/b* MO treatments. Data reveals 0% of Nipbla/b KD embryos displayed normal otoliths. Nipbla/b KD + *ddb1* mRNA embryos exhibited an 18% increase in normal otoliths phenotypes compared to 0% normal otolith phenotypes in Nipbla/b KD alone.

3.8 References

Banerji R, Eble DM, Iovine MK, Skibbens RV. Esco2 regulates cx43 expression during skeletal regeneration in the zebrafish fin. Dev Dyn. 2016 Jan;245(1):7-21. doi: 10.1002/dvdy.24354. Epub 2015 Nov 25. PMID: 26434741.

Banerji R, Skibbens RV, Iovine MK. Cohesin mediates Esco2-dependent transcriptional regulation in a zebrafish regenerating fin model of Roberts Syndrome. Biol Open. 2017. Dec 15;6(12):1802-1813. doi: 10.1242/bio.026013. PMID: 29084713; PMCID: PMC5769645.

Blanquart C, Barbier O, Fruchart JC, Staels B, Glineur C. Peroxisome proliferator-activated receptor alpha (PPARalpha) turnover by the ubiquitin-proteasome system controls the ligand-induced expression level of its target genes. J Biol Chem. 2002 Oct 4;277(40):37254-9. doi: 10.1074/jbc.M110598200. Epub 2002 Jul 12. PMID: 12118000.

Cabezas DA, Slaugh R, Abidi F, Arena JF, Stevenson RE, Schwartz CE, Lubs HA. A new X linked mental retardation (XLMR) syndrome with short stature, small testes, muscle wasting, and tremor localises to Xq24-q25. J Med Genet. 2000 Sep;37(9):663-8. doi: 10.1136/jmg.37.9.663. PMID: 10978355; PMCID: PMC1734699.

Collins MM, Ahlberg G, Hansen CV, Guenther S, Marín-Juez R, Sokol AM, El-Sammak H, Piesker J, Hellsten Y, Olesen MS, Stainier DYR, Lundegaard PR. Early sarcomere and metabolic defects in a zebrafish *pitx2c* cardiac arrhythmia model. PNAS. 2019 Aug 12 116(48): 24114-24121. doi: 10.1073/pnas.1913905116.

Djouadi F, Weinheimer CJ, Saffitz JE, Pitchford C, Bastin J, Gonzalez FJ, Kelly DP. A gender-related defect in lipid metabolism and glucose homeostasis in peroxisome proliferator- activated receptor alpha- deficient mice. J Clin Invest. 1998 Sep 15;102(6):1083-91. doi: 10.1172/JCI3949. PMID: 9739042; PMCID: PMC509091.

Dorsett D, Eissenberg JC, Misulovin Z, Martens A, Redding B, McKim K. Effects of sister chromatid cohesion proteins on cut gene expression during wing development in Drosophila. Development. 2005 Nov;132(21):4743-53. doi: 10.1242/dev.02064. Epub 2005 Oct 5. PMID: 16207752; PMCID: PMC1635493.

Dorsett D. Roles of the sister chromatid cohesion apparatus in gene expression, development, and human syndromes. Chromosoma. 2007 Feb;116(1):1-13. doi: 10.1007/s00412-006-0072-6. Epub 2006 Jul 4. PMID: 16819604; PMCID: PMC1783675.

Gordillo M, Vega H, Trainer AH, Hou F, Sakai N, Luque R, Kayserili H, Basaran S, Skovby F, Hennekam RC, Uzielli ML, Schnur RE, Manouvrier S, Chang S, Blair E, Hurst JA, Forzano F, Meins M, Simola KO, Raas-Rothschild A, Schultz RA, McDaniel LD, Ozono K, Inui K, Zou H, Jabs EW. The molecular mechanism underlying Roberts syndrome involves loss of ESCO2 acetyltransferase activity. Hum Mol Genet. 2008 Jul 15;17(14):2172-80. doi: 10.1093/hmg/ddn116. PMID: 18411254

Guacci V, Koshland D, Strunnikov A. A direct link between sister chromatid cohesion and chromosome condensation revealed through the analysis of MCD1 in S.

cerevisiae. Cell. 1997 Oct 3;91(1):47-57. doi: 10.1016/s0092-8674(01)80008-8. PMID: 9335334; PMCID: PMC2670185.

Heneka MT, Landreth GE, Hüll M. Drug insight: effects mediated by peroxisome proliferator-activated receptor-gamma in CNS disorders. Nat Clin Pract Neurol. 2007 Sep;3(9):496-504. doi: 10.1038/ncpneuro0586. PMID: 17805244.

Horsfield JA, Anagnostou SH, Hu JK, Cho KH, Geisler R, Lieschke G, Crosier KE, Crosier PS. Cohesin-dependent regulation of Runx genes. Development. 2007 Jul;134(14):2639-49. doi: 10.1242/dev.002485. Epub 2007 Jun 13. PMID: 17567667.

Hsieh YC, Chiang MC, Huang YC, Yeh TH, Shih HY, Liu HF, Chen HY, Wang CP, Cheng YC. Pparα deficiency inhibits the proliferation of neuronal and glial precursors in the zebrafish central nervous system. Dev Dyn. 2018 Dec;247(12):1264-1275. doi: 10.1002/dvdy.24683. Epub 2018 Nov 26. PMID: 30358936.

Ito T, Ando H, Handa H. Teratogenic effects of thalidomide: molecular mechanisms. Cell Mol Life Sci. 2011 May;68(9):1569-79. doi: 10.1007/s00018-010-0619-9. Epub 2011 Jan 5. PMID: 21207098.

Ito T, Ando H, Suzuki T, Ogura T, Hotta K, Imamura Y, Yamaguchi Y, Handa H. Identification of a primary target of thalidomide teratogenicity. Science. 2010 Mar;327(5971: 1345-50. doi: 10.1126/science.1177319. PMID: 20223979.

Kawauchi S, Calof AL, Santos R, Lopez-Burks ME, Young CM, Hoang MP, Chua A, Lao T, Lechner MS, Daniel JA, Nussenzweig A, Kitzes L, Yokomori K, Hallgrimsson B, Lander AD. Multiple organ system defects and transcriptional

dysregulation in the Nipbl(+/-) mouse, a model of Cornelia de Lange Syndrome. PLoS Genet. 2009 Sep;5(9):e1000650. doi: 10.1371/journal.pgen.1000650. Epub 2009 Sep 18. PMID: 19763162; PMCID: PMC2730539.

Kawauchi S, Santos R, Muto A, Lopez-Burks ME, Schilling TF, Lander AD, Calof AL. Using mouse and zebrafish models to understand the etiology of developmental defects in Cornelia de Lange Syndrome. Am J Med Genet C Semin Med Genet. 2016 Jun;172(2):138-45. doi: 10.1002/ajmg.c.31484. Epub 2016 Apr 27. PMID: 27120001; PMCID: PMC4924516.

Krantz ID, McCallum J, DeScipio C, Kaur M, Gillis LA, Yaeger D, Jukofsky L, Wasserman N, Bottani A, Morris CA, Nowaczyk MJ, Toriello H, Bamshad MJ, Carey JC, Rappaport E, Kawauchi S, Lander AD, Calof AL, Li HH, Devoto M, Jackson LG. Cornelia de Lange syndrome is caused by mutations in NIPBL, the human homolog of Drosophila melanogaster Nipped-B. Nat Genet. 2004 Jun;36(6):631-5. doi: 10.1038/ng1364. Epub 2004 May 16. PMID: 15146186; PMCID: PMC4902017.

Leone TC, Weinheimer CJ, Kelly DP. A critical role for the peroxisome proliferator-activated receptor alpha (PPARalpha) in the cellular fasting response: the PPARalpha-null mouse as a model of fatty acid oxidation disorders. Proc Natl Acad Sci U S A. 1999 Jun 22;96(13):7473-8. doi: 10.1073/pnas.96.13.7473. PMID: 10377439; PMCID: PMC22110.

Leung-Pineda V, Huh J, Piwnica-Worms H. DDB1 targets Chk1 to the Cul4 E3 ligase complex in normal cycling cells and in cells experiencing replication stress.

Cancer Res. 2009 Mar 15;69(6):2630-7. doi: 10.1158/0008-5472.CAN-08-3382. Epub 2009 Mar 10. PMID: 19276361; PMCID: PMC2776040.

Levi L, Ziv T, Admon A, Levavi-Sivan B, Lubzens E. Insight into molecular pathways of retinal metabolism, associated with vitellogenesis in zebrafish. Am J Physiol Endocrinol Metab. 2012 Mar 15;302(6):E626-44. doi: 10.1152/ajpendo.00310.2011. Epub 2011 Dec 28. PMID: 22205629.

Liu J, Zhang Z, Bando M, Itoh T, Deardorff MA, Clark D, Kaur M, Tandy S, Kondoh T, Rappaport E, Spinner NB, Vega H, Jackson LG, Shirahige K, Krantz ID. Transcriptional dysregulation in NIPBL and cohesin mutant human cells. PLoS Biol. 2009 May 5;7(5):e1000119. doi: 10.1371/journal.pbio.1000119. Epub 2009 May 26. PMID: 19468298; PMCID: PMC2680332.

Liu J, Zhang Z, Bando M, Itoh T, Deardorff MA, Clark D, Kaur M, Tandy S, Kondoh T, Rappaport E, Spinner NB, Vega H, Jackson LG, Shirahige K, Krantz ID. Transcriptional dysregulation in NIPBL and cohesin mutant human cells. PLoS Biol. 2009 May 5;7(5):e1000119. doi: 10.1371/journal.pbio.1000119. Epub 2009 May 26. PMID: 19468298; PMCID: PMC2680332.

McCall CM, Miliani de Marval PL, Chastain PD 2nd, Jackson SC, He YJ, Kotake Y, Cook JG, Xiong Y. Human immunodeficiency virus type 1 Vpr-binding protein VprBP, a WD40 protein associated with the DDB1-CUL4 E3 ubiquitin ligase, is essential for DNA replication and embryonic development. Mol Cell Biol. 2008 Sep;28(18):5621-33. doi: 10.1128/MCB.00232-08. Epub 2008 Jul 7. PMID: 18606781; PMCID: PMC2546929.

Michaelis C, Ciosk R, Nasmyth K. Cohesins: chromosomal proteins that prevent premature separation of sister chromatids. Cell. 1997 Oct 3;91(1):35-45. doi: 10.1016/s0092-8674(01)80007-6. PMID: 9335333.

Misulovin Z, Schwartz YB, Li XY, Kahn TG, Gause M, MacArthur S, Fay JC, Eisen MB, Pirrotta V, Biggin MD, Dorsett D. Association of cohesin and Nipped-B with transcriptionally active regions of the Drosophila melanogaster genome. Chromosoma. 2008 Feb;117(1):89-102. doi: 10.1007/s00412-007-0129-1. Epub 2007 Oct 27. PMID: 17965872; PMCID: PMC2258211.

Muto A, Calof AL, Lander AD, Schilling TF. Multifactorial origins of heart and gut defects in nipbl-deficient zebrafish, a model of Cornelia de Lange Syndrome. PLoS Biol. 2011 Oct;9(10):e1001181. doi: 10.1371/journal.pbio.1001181. Epub 2011 Oct 25. PMID: 22039349; PMCID: PMC3201921.

Muto A, Ikeda S, Lopez-Burks ME, Kikuchi Y, Calof AL, Lander AD, Schilling TF. Nipbl and mediator cooperatively regulate gene expression to control limb development. PLoS Genet. 2014 Sep 25;10(9):e1004671. doi: 10.1371/journal.pgen.1004671. PMID: 25255084; PMCID: PMC4177752.

Peters JM, Shah YM, Gonzalez FJ. The role of peroxisome proliferator-activated receptors in carcinogenesis and chemoprevention. Nat Rev Cancer. 2012 Feb 9;12(3):181-95. doi: 10.1038/nrc3214. PMID: 22318237; PMCID: PMC3322353.

Rollins RA, Korom M, Aulner N, Martens A, Dorsett D. Drosophila nipped-B protein supports sister chromatid cohesion and opposes the stromalin/Scc3 cohesion factor to facilitate long-range activation of the cut gene. Mol Cell Biol. 2004

Apr;24(8):3100-11. doi: 10.1128/mcb.24.8.3100-3111.2004. PMID: 15060134; PMCID: PMC381657.

Rollins RA, Morcillo P, Dorsett D. Nipped-B, a Drosophila homologue of chromosomal adherins, participates in activation by remote enhancers in the cut and Ultrabithorax genes. Genetics. 1999 Jun;152(2):577-93. PMID: 10353901; PMCID: PMC1460629.

Sanchez AC, Thren ED, Iovine MK, Skibbens RV. Esco2 and cohesin regulate CRL4 ubiquitin ligase *ddb1* expression and thalidomide teratogenicity. Cell Cycle. 2022 Mar;21(5):501-513. doi: 10.1080/15384101.2021.2023304. Epub 2022 Jan 6. PMID: 34989322; PMCID: PMC8942496.

Schnabel D, Castillo-Robles J, Lomeli H. Protein Purification and Western Blot Detection from Single Zebrafish Embryo. *Zebrafish*. 2019 Dec;16(6):505-507. doi: 10.1089/zeb.2019.1761. Epub 2019 Aug 13. PMID: 31408407.

Schüle B, Oviedo A, Johnston K, Pai S, Francke U. Inactivating mutations in ESCO2 cause SC phocomelia and Roberts syndrome: no phenotype-genotype correlation. Am J Hum Genet. 2005 Dec;77(6):1117-28. doi: 10.1086/498695. Epub 2005 Oct 31. PMID: 16380922; PMCID: PMC1285169.

Skibbens RV. Of Rings and Rods: Regulating Cohesin Entrapment of DNA to Generate Intra- and Intermolecular Tethers. PLoS Genet. 2016 Oct 27;12(10):e1006337. doi: 10.1371/journal.pgen.1006337. Erratum in: PLoS Genet. 2016 Dec 1;12 (12):e1006478. PMID: 27788133; PMCID: PMC5082857.

Smithells RW, Newman CG. Recognition of thalidomide defects. J Med Genet. 1992 Oct;29(10):716-23. doi: 10.1136/jmg.29.10.716. PMID: 1433232; PMCID: PMC1016130.

Srinivasan M, Scheinost JC, Petela NJ, Gligoris TG, Wissler M, Ogushi S, Collier JE, Voulgaris M, Kurze A, Chan KL, Hu B, Costanzo V, Nasmyth KA. The Cohesin Ring Uses Its Hinge to Organize DNA Using Non-topological as well as Topological Mechanisms. Cell. 2018 May 31;173(6):1508-1519.e18. doi: 10.1016/j.cell.2018.04.015. Epub 2018 May 10. PMID: 29754816; PMCID: PMC6371919.

Tarpey PS, Raymond FL, O'Meara S, Edkins S, Teague J, Butler A, Dicks E, Stevens C, Tofts C, Avis T, Barthorpe S, Buck G, Cole J, Gray K, Halliday K, Harrison R, Hills K, Jenkinson A, Jones D, Menzies A, Mironenko T, Perry J, Raine K, Richardson D, Shepherd R, Small A, Varian J, West S, Widaa S, Mallya U, Moon J, Luo Y, Holder S, Smithson SF, Hurst JA, Clayton-Smith J, Kerr B, Boyle J, Shaw M, Vandeleur L, Rodriguez J, Slaugh R, Easton DF, Wooster R, Bobrow M, Srivastava AK, Stevenson RE, Schwartz CE, Turner G, Gecz J, Futreal PA, Stratton MR, Partington M. Mutations in CUL4B, which encodes a ubiquitin E3 ligase subunit, cause an X-linked mental retardation syndrome associated with aggressive outbursts, seizures, relative macrocephaly, central obesity, hypogonadism, pes cavus, and tremor. Am J Hum Genet. 2007 Feb;80(2):345-52. doi: 10.1086/511134. Epub 2007 Jan 4. PMID: 17236139; PMCID: PMC1785336.

Tonkin ET, Wang TJ, Lisgo S, Bamshad MJ, Strachan T. NIPBL, encoding a homolog of fungal Scc2-type sister chromatid cohesion proteins and fly Nipped-B, is mutated in Cornelia de Lange syndrome. Nat Genet. 2004 Jun;36(6):636-41. Epub 2004 May 16. doi: 10.1038/ng1363 PMID: 15146185

Vargesson N. Thalidomide-induced teratogenesis: history and mechanisms. Birth Defects Res C Embryo Today. 2015 Jun;105(2):140-56. doi: 10.1002/bdrc.21096. Epub 2015 Jun 4. PMID: 26043938; PMCID: PMC4737249.

Vega H, Waisfisz Q, Gordillo M, Sakai N, Yanagihara I, Yamada M, van Gosliga D, Kayserili H, Xu C, Ozono K, Jabs EW, Inui K, Joenje H. Roberts syndrome is caused by mutations in ESCO2, a human homolog of yeast ECO1 that is essential for the establishment of sister chromatid cohesion. Nat Genet. 2005 May;37(5):468-70. Epub 2005 Apr 10. doi: 10.1038/ng1548. PMID: 15821733

Venezia O, Islam S, Cho C, Timme-Laragy AR, Sant KE. Modulation of PPAR signaling disrupts pancreas development in the zebrafish, Danio rerio. Toxicol Appl Pharmacol. 2021 Sep 1;426:115653. doi: 10.1016/j.taap.2021.115653. Epub 2021 Jul 21. PMID: 34302850; PMCID: PMC8588802.

Vulto-van Silfhout AT, Nakagawa T, Bahi-Buisson N, Haas SA, Hu H, Bienek M, Vissers LE, Gilissen C, Tzschach A, Busche A, Müsebeck J, Rump P, Mathijssen IB, Avela K, Somer M, Doagu F, Philips AK, Rauch A, Baumer A, Voesenek K, Poirier K, Vigneron J, Amram D, Odent S, Nawara M, Obersztyn E, Lenart J, Charzewska A, Lebrun N, Fischer U, Nillesen WM, Yntema HG, Järvelä I, Ropers HH, de Vries BB, Brunner HG, van Bokhoven H, Raymond FL, Willemsen MA, Chelly J, Xiong Y, Barkovich AJ, Kalscheuer VM, Kleefstra T,

de Brouwer AP. Variants in CUL4B are associated with cerebral malformations. Hum Mutat. 2015 Jan;36(1):106-17. doi: 10.1002/humu.22718. PMID: 25385192; PMCID: PMC4608231.

Waning DL, Li B, Jia N, Naaldijk Y, Goebel WS, HogenEsch H, Chun KT. Cul4A is required for hematopoietic cell viability and its deficiency leads to apoptosis. Blood. 2008 Jul 15;112(2):320-9. doi: 10.1182/blood-2007-11-126300. Epub 2008 Mar 13. PMID: 18339895; PMCID: PMC2442743.

Wendt KS, Peters JM. How cohesin and CTCF cooperate in regulating gene expression. Chromosome Res. 2009;17(2):201-14. doi: 10.1007/s10577-008-9017-7. Epub 2009 Mar 24. PMID: 19308701.

Wendt KS, Yoshida K, Itoh T, Bando M, Koch B, Schirghuber E, Tsutsumi S, Nagae G, Ishihara K, Mishiro T, Yahata K, Imamoto F, Aburatani H, Nakao M, Imamoto N, Maeshima K, Shirahige K, Peters JM. Cohesin mediates transcriptional insulation by CCCTC-binding factor. Nature. 2008 Feb 14;451(7180):796-801. doi: 10.1038/nature06634. Epub 2008 Jan 30. PMID: 18235444.

White SM, Bhoj E, Nellåker C, Lachmeijer AMA, Marshall AE, Boycott KM, Li D, Smith W, Hartley T, McBride A, Ernst ME, May AS, Wieczorek D, Abou Jamra R, Koch-Hogrebe M, Õunap K, Pajusalu S, van Gassen KLI, Sadedin S, Ellingwood S, Tan TY, Christodoulou J, Barea J, Lockhart PJ; Care4Rare Canada Consortium; Nezarati MM, Kernohan KD. A DNA repair disorder caused by de novo monoallelic DDB1 variants is associated with a neurodevelopmental syndrome. Am J Hum Genet. 2021 Apr 1;108(4):749-756. doi:

10.1016/j.ajhg.2021.03.007. Epub 2021 Mar 19. PMID: 33743206; PMCID: PMC8059373.

Xu B, Sowa N, Cardenas ME, Gerton JL. L-leucine partially rescues translational and developmental defects associated with zebrafish models of Cornelia de Lange syndrome. Hum. Mol. Genet. 2015 March 24(15). 12:1540-1555. doi: 10.1093/hmg/ddu565.

Yu C, Ji SY, Sha QQ, Sun QY, Fan HY. CRL4-DCAF1 ubiquitin E3 ligase directs protein phosphatase 2A degradation to control oocyte meiotic maturation. Nat Commun. 2015 Aug 18;6:8017. doi: 10.1038/ncomms9017. PMID: 26281983; PMCID: PMC4557334

Zakari M, Yuen K, Gerton JL. Etiology and pathogenesis of the cohesinopathies. Wiley Interdiscip Rev Dev Biol. 2015 Sep-Oct;4(5):489-504. doi: 10.1002/wdev.190. Epub 2015 Apr 7. PMID: 25847322; PMCID: PMC6680315.

CHAPTER 4

REMAINING QUESTIONS AND FUTURE DIRECTIONS

4.1 Introduction

The focus of my thesis dissertation revealed new mechanisms in developmental pathways. Here, we revealed a unifying molecular pathway contributing to abnormal development in cohesinopathies and thalidomide teratogenicity. In Chapters 2 and 3, I provide evidence that cohesin and auxiliary proteins regulate the expression of *ddb1*, a subunit of the CRL4 E3 ligase that thalidomide targets. In this model (Figure 4.1), we proposed that decreased expression of *ddb1* in cohesinopathies inhibits the proper formation of CRL4 E3. In turn, less CRL4 function results in accumulated proteins that would otherwise be targeted for degradation during normal development.

My research next provides insight into potential endogenous targets of CRL4 and, importantly, those in common with cohesinopathies that impact specific developmental processes. I obtained potential protein targets of the cohesin/CRL4 pathway through LC-MS. I performed independent MO-mediated knockdowns of the cohesin subunit, Smc3, the cohesin activator, Esco2, and the CRL4 component, Ddb1, to compare differentially regulated proteins with each knockdown compared to controls (detailed method outlined in Chapter 3). Accumulated proteins were relevant, given the role of E3 ligases in targeting proteins for degradation. A list of prioritized proteins was made from the significant accumulated proteins in independent Esco2 KD, Smc3 KD, and Ddb1 KD zebrafish embryos (listed in Table 3.1). This list of top 10 proteins for further studies was based on evidence of developmental process involvement, localization of gene expression, and evidence for ubiquitination (Table 4.1).

Still, several questions remain unsolved regarding (1) the downstream targets of cohesin/CRL4 E3 ligase axis that are necessary for proper development, (2) the extent of unifying mechanism leading to organ malformation in similar multi-spectrum syndromes. This chapter provides a synopsis of my preliminary work to start addressing these questions.

4.2 LC-MS Identifies promising common targets of CRL4 and cohesin

In Chapter 3, I focused on Pparαa and provided preliminary evidence of PPARα levels increased in patient cell lines. We have additional patient cell lines with severe clinically diagnosed CdLS and characterized NIPBL frameshift and nonsense mutations (Table 4.2). Cell lysates from these new CdLS lines will be obtained, and PPARα levels will be analyzed with an appropriate loading control. Assessing DDB1 protein levels in our patient cell lines will also be necessary. These results will provide insight into the extent that human NIPBL mutations regulate CRL4.

From the list of prioritized proteins (Table 4.1), additional candidates should be pursued, some which have associated human conditions may be of interest. For instance, *ARHGDIA* mutations in humans have been associated with necrotic syndrome type 8, a developmental abnormality of kidney malformation (Gupta et al., 2013; Gee et al., 2013). *ARHGEF2* mutations are associated with neurodevelopmental disorder with midbrain and hindbrain malformations and unilateral focal polymicrogyria (Ravindran et al., 2017). *RBP4* mutations result in vision impairment and eye malformation, including retinal dystrophy and microphthalmia (Seelinger et al., 1999; Cukras et al., 2012; Chou et al., 2015). All

these tissues are impacted in both cohesinopathies and thalidomide teratogenicity syndromes.

Evidence of ubiquitination in almost all the proteins in our list of prioritized proteins has been found in humans (Wagner et al., 2011; Danielsen et al., 2011; Udeshi et al., 2013; Blanquart et al., 2002). However, one important hypothesis to test is whether our LC-MS candidate proteins are direct or indirect targets of the CRL4 E3 Ligase. At least in one case, the mechanism ubiquitination is known, MAT2A is targeted for degradation by a Cullin family E3 ligase based on studies performed in HEK293T cells (Wang et al., 2016). Thus, it's important to test if CRL4, specifically, plays a role in direct regulation of this, and other candidate proteins. This could be achieved by co-immunoprecipitation or fluorescence resonance energy transfer (FRET) experiments in LCL cell lines. These experiments would provide novel endogenous substrates of the CRL4.

Our model hinges on the role of poly ubiquitination for proteasomal targeting of the CRL4 E3 ligases, yet mono ubiquitination of substrates can regulate signal transduction, transcription, DNA repair, and many other cellular processes (Chen and Mallampalli, 2009; Zeng et al., 2016; Braten et al., 2016). While my focus has been on accumulated proteins due to the role of CRL4 degradation, other downstream impacts of the cohesin/CRL4 pathway, outside of the ubiquitin-proteasome system, must be assessed. For instance, using the LC-MS results to identify aberrant regulation of proteins in a tissue-specific manner. For instance, searching for known eye development markers or cilia related proteins from the data set, would provide insight into tissue-specific impacts of cohesin/CRL4 pathway. Similarly, finding the

independently regulated proteins between cohesin pathway knockdowns and Ddb1 knockdowns can provide clues as to the extent of the shared mechanisms.

4.3 Evidence that cx43 is a common target of CRL4 and cohesin

A promising indirect cohesin/CRL4 target for further study is connexin43 (*cx43*), a gap junction important for bone and joint development. Our lab previously implicated downregulation of *cx43* in RBS and CdLS models in the zebrafish regenerating fin (Banerji et al., 2016; Banerji et al., 2017). I performed *smc3*-MO injection at the 1-cell stage of zebrafish embryos and extracted RNA at 24hpf. Through qRT-PCR using *cx43* specific primers and *keratin-4* primers as my housekeeping control, I found downregulation of *cx43* transcript levels in *smc3*-MO injected embryos (Figure 4.1). However, I additionally investigated the effect of Ddb1 knockdown in *cx43* expression. Fist, using *ddb1*-MO and SC-MO, I injected zebrafish embryos at the 1-cell stage. RNA of injected embryos was extracted and tested using qRT-PCR to look for *cx43* transcript levels. My results showed that *cx43* is significantly downregulated in Ddb1 knockdown embryos, compared to SC MO injected embryos (data not shown).

To assess the role of Ddb1 in the developmental phenotypes that arise due to decreased *cx43* levels, I used embryos obtained from our *sof*^{b123} transgenic line. The *sof*^{b123} line exhibits reduced levels of Cx43 due to hypomorphic mutations of *cx43* (Iovine et al., 2005). If Ddb1plays a role in phenotypes that arise due to reduced *cx43* levels, then exogenous expression of *ddb1* should rescue such phenotypes. The overexpression of *ddb1* mRNA in *sof*^{b123} resulted in

an increase of eye size, resembling wild-type eye size levels (Figure 4.1). *sof*^{b123} embryos, on the other hand, do not impact *ddb1* transcription, as assessed through qRT PCR (data not shown). Taken together, this provides evidence that CRL4 may be upstream of *cx43* expression important for eye development that should be further investigated.

A possible molecular pathway regulated by cohesin/CRL4 for proper eye development is the Wnt signaling pathway. Disruption in canonical Wnt signal impact eye development in zebrafish embryos (Cheng et al. 2003; Cavodeassi et al. 2005). CRL4 subunit mutations cause eye malformation in drosophila through dysregulation of Wnt signaling (Tare et al., 2016). Moreover, Cx43 is highly expressed in zebrafish eyes during development, and it has been shown to regulate Wnt signaling in other tissues (Cheng et al. 2003; Cavodeassi et al. 2005; Bhattacharya et al. 2018). Future studies are required to test the extent to which CRL4 regulates cx43 and whether the canonical Wnt signaling is involved in this pathway for eye development.

4.4 Possible interplay between cohesins and cilia

In some instances, the phenotypic similarities between cohesinopathies and other multi-spectrum syndromes have revealed shared disease mechanisms. For example, my research implicates shared molecular mechanisms of cohesinopathies with the thalidomide drug pathway. Additionally, ribosomopathies, such as Diamond–Blackfan Anemia and Treacher–Collins Syndrome, share striking similarities to a subset of clinical presentations in

cohesinopathies. Studies find that ribosomal RNA production and protein synthesis deficiency, a hallmark of ribosomopathies, is also implicated in RBS/CdLS (Bose et al., 2012; Xu et al., 2013; Zakari et al., 2015; Xu et al., 2016). Another family of syndromes resembling cohesinopathies is ciliopathies, which arise due to genetic mutations that result in abnormal cilia formation or function (Waters and Beales, 2011). Primary cilia are found in nearly all eukaryotic cells and function in motility, transduction of sensory information, and transduction of signaling pathways (May-Simera and Kelley, 2012, Bangs and Anderson, 2017; Ishikawa and Marshall, 2011). Cilia comprise 9 doublet microtubules called the axoneme extending from the cell surface (Zhao et al., 2023). Cells in sensory organs have specialized cilia. For instance, hair cells in the vertebrate auditory and vestibular systems have specialized cilia termed kinocilia (Whitfield, 2020). Hair cell kinocilia play a significant role in otolith formation in zebrafish development. Kinocilia guide otolith particle tethering to the otic vesicle poles. Disruption in hair cells leads to abnormal otoliths, such as missing or added otolith and untethered otoliths (Stooke-Vaughan et al., 2012).

My findings show that RBS (Esco2 KD) and CdLS (Smc3 KD and Nipbla/b KD) models in zebrafish embryos exhibit otolith malformation phenotypes (see Figures 2.1 and Supplemental Figure 3.2). Thus, I hypothesize that cohesinopathy models in zebrafish impact kinocilia function. Cohesin proteins have previously been observed in axonemes and basal bodies of cilia in the retina and oviduct tissues (Khanna et al., 2005; Guan et al. 2008). The question as to whether cohesin is present in the hair cell kinocilia is something I

sought to address. The cohesin subunit, Smc3, is indeed localized to the kinocilia (Figure 4.3). If Smc3 is important for kinocilia formation or stabilization, then knockdowns of Smc3 would result in kinocilia malformation. To test this model, I performed Smc3 KD and compared the kinocilia phenotypes control embryos. Results show shorter kinocilia in Smc3 KD embryos compared to controls (Figure 4.4). This suggests a functional role of cohesins in kinocilia development.

A previous study found SMC3 interacts with the cilia protein RPGR, in retina cells (Khanna et al., 2005). A yeast-2-hybrid screen, using cilia related protein library, would provide evidence as to whether SMC3 only interacts with RPGR or multiple cilia proteins. Additionally, zebrafish can be a useful model to study cohesin localization throughout kinocilia development. A transgenic line carrying a cohesin reporter (such as an inducible mCherry tagged Smc3 protein) can help visualize cohesin protein in early development. These experiments would give insight into a possible role of cohesin outside of the nucleus, as others report extra-nuclear pools of cohesin proteins (Sadano et al., 2000; Gregson et al. 2001). Additionally, mechanistically linking cohesinopathies to ciliopathies, unifies efforts in the understanding of these etiologies. Future studies should aim to understand cohesin interaction with cilia-related proteins.

4.5 Discussion

The mechanisms for developmental diseases are complex and often tissue specific. Using molecular and biochemical approaches, downstream targets of the cohesin/CRL4 pathway that may contribute to organ malformations were identified.

Future work to further explore the common downstream targets between CRL4 and cohesin, both in patient cell lines and zebrafish, may elucidate new developmental pathways. Additionally, cohesin colocalization and its impact on zebrafish kinocilia suggest a relationship between cohesin and cilia. Future work to explore this connection may reveal novel extra-nuclear roles of cohesin. Understanding the downstream events of cohesin in development can influence the future development of therapeutic approaches for cohesinopathies and related etiologies.

4.6 Figures and Tables

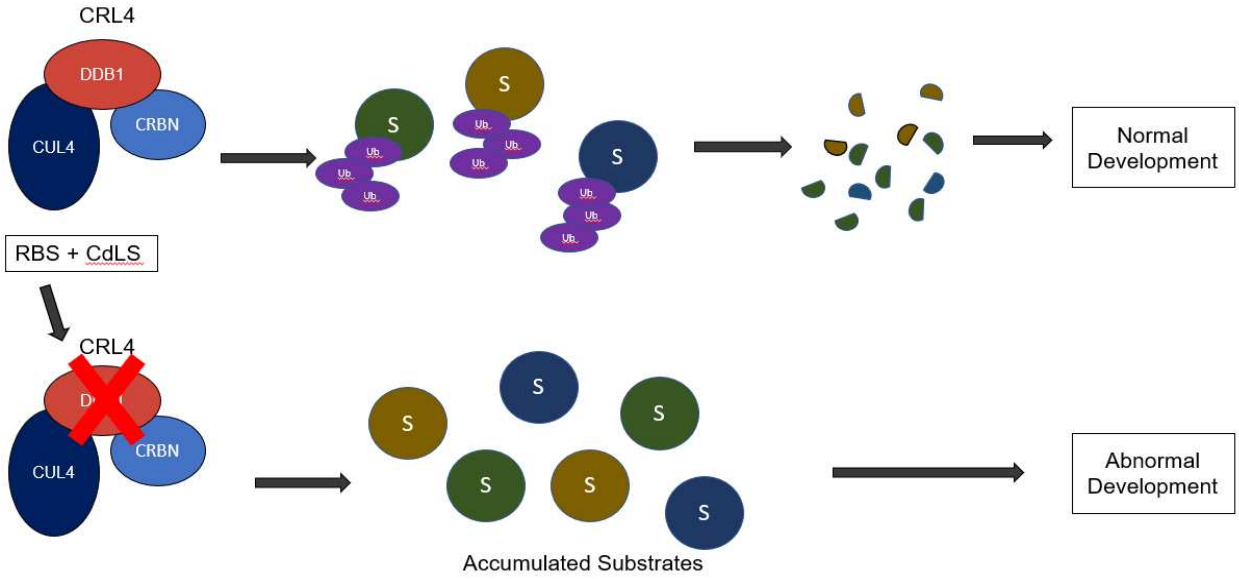

Figure 4.1. Proposed model for inhibition of CRL4 function in RBS and CdLS. CRL4 ubiquitinates substrates for targeted degradation, a process important for normal development. Both Esco2 knockdowns and Smc3 knockdowns in zebrafish, models for RBS and CdLS respectively, downregulate expression of *ddb1*, an essential component of CRL4. Improper CRL4 function fails to clear substrates from the embryo and accumulation of these leads to improper development, a similar mechanism that gives rise to thalidomide teratogenicity.

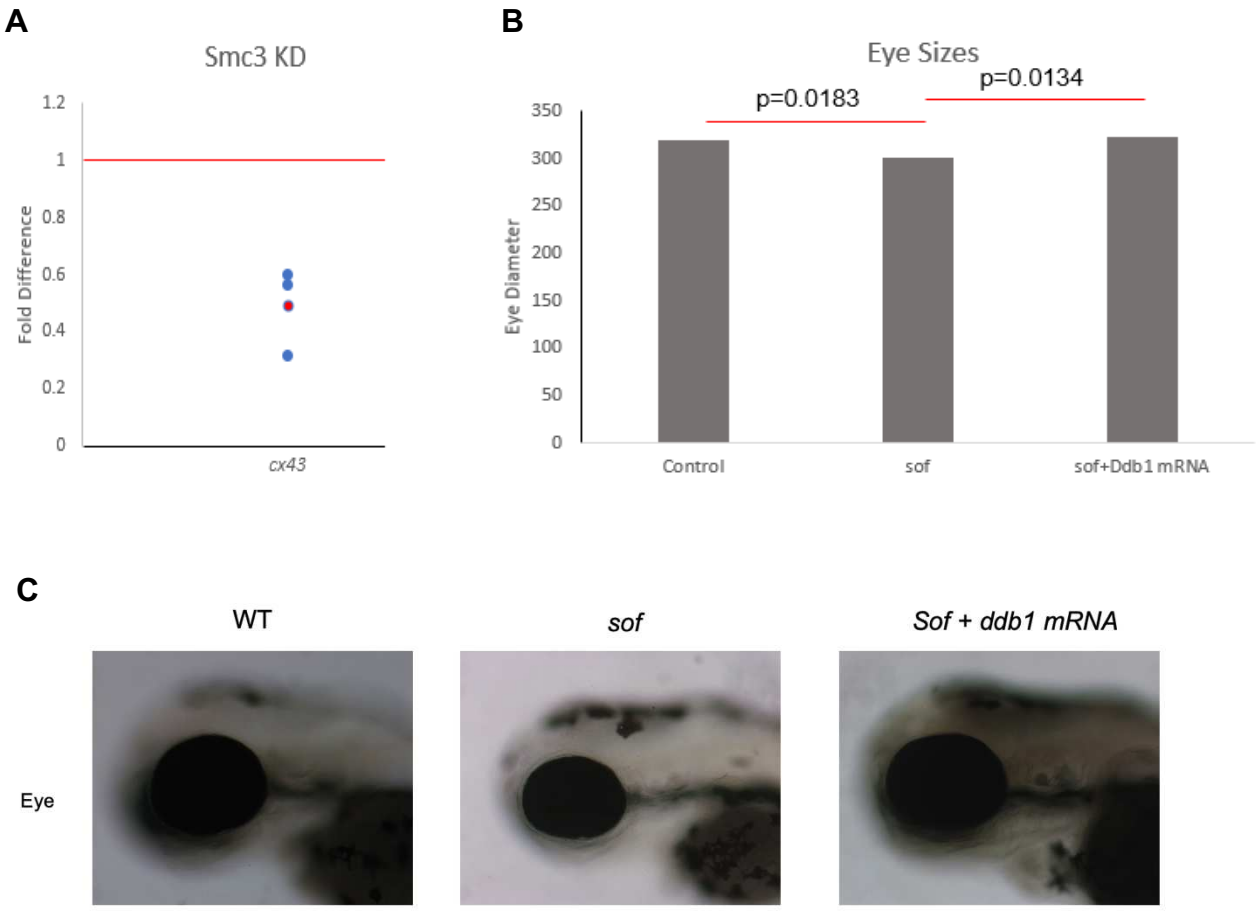

Figure 4.2. Cohesin and CRL4 impact cx43 pathway. (A) qRT-PCR of whole embryo RNA isolation shows downregulation of *cx43* expression in cohesin subunit, Smc3, knockdowns (KD). T-test = 0.0049 (B-C) *sof*^{b123} embryos, which exhibits decreased *cx43* expression levels, show a significant reduction in eye size compared to wild-type control at 72hpf. Overexpression of CRL4 subunit, Ddb1, through mRNA injection significantly increases eye sizes in *sof*^{b123} embryos.

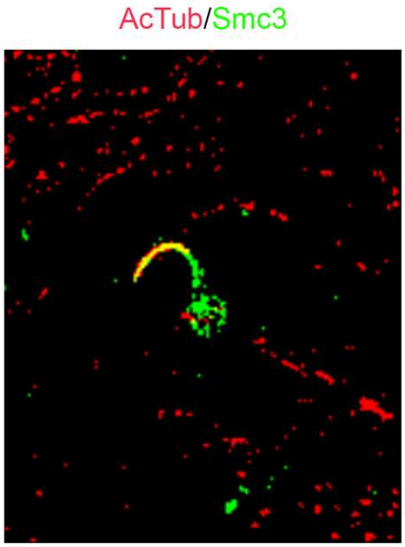

Figure 4.3. Smc3 is present at hair cell kinocilia in zebrafish. Cohesin subunit, Smc3 (green), colocalizes (yellow) to acetylated tubulin (red) in immunofluorescence imaging. Similar findings in other tissues and model organisms have been previously reported. Results suggest a role of cohesin in cilia function or development.

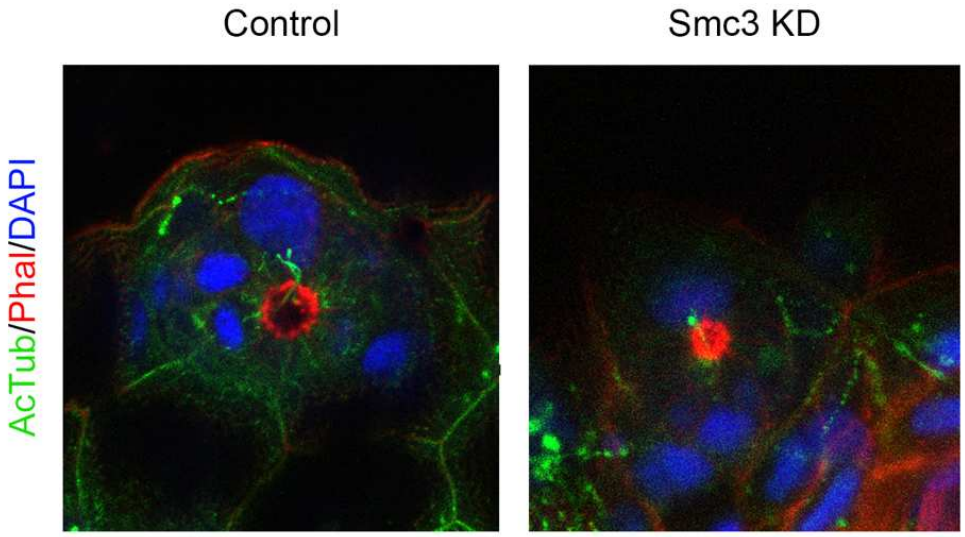

Figure 4.4. Cohesin knockdowns impact hair cell kinocilia in zebrafish embryos. Immunofluorescence of Acetylated Tubulin (green; labels kinocilia), Phalloidin (red, labels stereocilia) and DAPI (blue, labels nucleus), show shorter kinocilia in Smc3 KD zebrafish embryos.

D. rerio	Function	Tissue Expression	Expression Timeline	Human Homolog
Arhgdia	Rho GDP Dissociation Factor	Eye (Veldman et al., 2007)	48hpf	**ARHGDIA**
Mat2al	S-adenosylmethionine synthase	Eye, brain, otic placode (Lee et al., 2012)	5hpf-72hpf	**MAT2A**
Ntmt1	N-Methyltransferase 1	Eye, brain, muscles (Thisse et al., 2005)	5hpf-48hpf	**NTMT1**
Pparαa	Transcription factor	Eye, brain, jaw, heart, intestine (Collins et al., 2019; Hsieh et al., 2018; Levi et al., 2012)	All stages	**PPARA**
Aldh3b1	ROS response, dehydrogenase	Otic placode, pharynx (Thisse et al., 2001)	5hpf-48hpf	**ALDH3B1**
Arhgef2	Rho GTPase	Heart (Lu et al., 2019)	24hpf	**ARHGEF2**
Rab1bb	Ras-like GTPase	Brain, otic placode (Thisse et al., 2004)	10hpf-48hpf	RAB1B
Rbp4	Retinol Binding Protein	All anatomical structures (Tingaud-Seeira et al., 2006; Li et al., 2007; Sumanas et al., 2005)	All stages	RBP4
Sesn3	Sestrin Stress (ROS)-induced	Brain, otic placode (Thisse et al., 2001)	5hpf-72hpf	**SESN3**
Sfxn2	Mitochondrial AA transporter	All anatomical structures (Thisse et al., 2004)	All stages	**SFXN2**

Table 4.1. Prioritized list of cohesin/CRL targets identified using LC-MS. Candidate proteins downstream of the Esco2-cohesin-CRL4 axis of regulation. Each gene is conserved (human homolog shown at far right). Protein names in bold reflect evidence of Ubiquitination (shown only for human homologs).

ID	Sex	Age	Genotype	Clinical Evaluation
C1	F	12	WT	None
C1	M	8	WT	None
C3	F	7	WT	None
C4	M	8	WT	None
C5	M	5	WT	None
C6	M	12	WT	None
C7	F	25	WT	None
PT1	M	6.9	6407insA / Frameshift	CdLS / Severe
PT2	M	11.9	5167C>T / Nonsense	CdLS / Severe
PT3	F	5.3	4193C>G / Nonsense	CdLS / Severe
PT4	F	7	742_743delCT / Frameshift	CdLS / Severe
PT5	M	10.5	2969delG / Frameshift	CdLS / Severe
PT6	M	6.7	1902_1903insA / Frameshift	CdLS / Severe
PT7	F	8.3	2494C>T / nonsense	CdLS / Severe
PT8	F	9	4606C>T / Nonsense	CdLS / Severe
PT9	M	1	5721_5726del / Frameshift	CdLS / Severe
PT10	F	37	603C>T / Nonsense 752del / Frameshift	RBS / Severe

Table 4.2. Description of control and cohesinopathy patient cell lines. C1-C6 and PT1-PT8 cell lines previously obtained from Dr. Ian Krantz at CHOP and used in Liu et al., 2008. C7 and PT9-PT10 cell lines obtained from Corriel Institute.

4.7 References

Banerji R, Eble DM, Iovine MK, Skibbens RV. Esco2 regulates cx43 expression during skeletal regeneration in the zebrafish fin. Dev Dyn. 2016 Jan;245(1):7-21. doi: 10.1002/dvdy.24354. Epub 2015 Nov 25. PMID: 26434741.

Banerji R, Skibbens RV, Iovine MK. Cohesin mediates Esco2-dependent transcriptional regulation in a zebrafish regenerating fin model of Roberts Syndrome. Biol Open. 2017a Dec 15;6(12):1802-1813. doi: 10.1242/bio.026013. PMID: 29084713; PMCID: PMC5769645.

Bangs F, Anderson KV. Primary Cilia and Mammalian Hedgehog Signaling. Cold Spring Harb Perspect Biol. 2017 May 1;9(5):a028175. doi: 10.1101/cshperspect.a028175. PMID: 27881449; PMCID: PMC5411695.

Bhattacharya S, Gargiulo D, Iovine MK. Simplet-dependent regulation of β-catenin signaling influences skeletal patterning downstream of Cx43. Development. 2018 Nov 30;145(23):dev166975. doi: 10.1242/dev.166975. PMID: 30377172; PMCID: PMC6288381.

Blanquart C, Barbier O, Fruchart JC, Staels B, Glineur C. Peroxisome proliferator-activated receptor alpha (PPARα) turnover by the ubiquitin-proteasome system controls the ligand-induced expression level of its target genes. J Biol Chem. 2002 Oct 4;277(40):37254-9. doi: 10.1074/jbc.M110598200. Epub 2002 Jul 12. PMID: 12118000.

Bose T, Lee KK, Lu S, Xu B, Harris B, Slaughter B, Unruh J, Garrett A, McDowell W, Box A, Li H, Peak A, Ramachandran S, Seidel C, Gerton JL. Cohesin proteins promote ribosomal RNA production and protein translation in yeast and human

cells. PLoS Genet. 2012;8(6):e1002749. doi: 10.1371/journal.pgen.1002749. Epub 2012 Jun 14. PMID: 22719263; PMCID: PMC3375231.

Braten O, Livneh I, Ziv T, Admon A, Kehat I, Caspi LH, Gonen H, Bercovich B, Godzik A, Jahandideh S, Jaroszewski L, Sommer T, Kwon YT, Guharoy M, Tompa P, Ciechanover A. Numerous proteins with unique characteristics are degraded by the 26S proteasome following monoubiquitination. Proc Natl Acad Sci U S A. 2016 Aug 9;113(32):E4639-47. doi: 10.1073/pnas.1608644113. Epub 2016 Jul 6. PMID: 27385826; PMCID: PMC4987823.

Cavodeassi F, Carreira-Barbosa F, Young RM, Concha ML, Allende ML, Houart C, Tada M, Wilson SW. Early stages of zebrafish eye formation require the coordinated activity of Wnt11, Fz5, and the Wnt/beta-catenin pathway. Neuron. 2005 Jul 7;47(1):43-56. doi: 10.1016/j.neuron.2005.05.026. PMID: 15996547; PMCID: PMC2790414.

Chen B, Dodge ME, Tang W, Lu J, Ma Z, Fan CW, Wei S, Hao W, Kilgore J, Williams NS, Roth MG, Amatruda JF, Chen C, Lum L. Small molecule-mediated disruption of Wnt-dependent signaling in tissue regeneration and cancer. Nat Chem Biol. 2009 Feb;5(2):100-7. doi: 10.1038/nchembio.137. Epub 2009 Jan 4. PMID: 19125156; PMCID: PMC2628455.

Chen BB, Mallampalli RK. Masking of a nuclear signal motif by monoubiquitination leads to mislocalization and degradation of the regulatory enzyme cytidylyltransferase. Mol Cell Biol. 2009 Jun;29(11):3062-75. doi: 10.1128/MCB.01824-08. Epub 2009 Mar 30. PMID: 19332566; PMCID: PMC2682000.

Cheng S, Christie T, Valdimarsson G. Expression of connexin48.5, connexin44.1, and connexin43 during zebrafish (Danio rerio) lens development. Dev Dyn. 2003 Dec;228(4):709-15. DOI: 10.1002/dvdy.10436. PMID: 14648847

Chou CM, Nelson C, Tarlé SA, Pribila JT, Bardakjian T, Woods S, Schneider A, Glaser T. Biochemical Basis for Dominant Inheritance, Variable Penetrance, and Maternal Effects in RBP4 Congenital Eye Disease. Cell. 2015 Apr 23;161(3):634-646. doi: 10.1016/j.cell.2015.03.006. PMID: 25910211; PMCID: PMC4409664.

Cukras CA, Petrou P, Chew EY, Meyerle CB, Wong WT. Oral minocycline for the treatment of diabetic macular edema (DME): results of a phase I/II clinical study. Invest Ophthalmol Vis Sci. 2012 Jun 22;53(7):3865-74. doi: 10.1167/iovs.11-9413. PMID: 22589436; PMCID: PMC3390218.

Danielsen JM, Sylvestersen KB, Bekker-Jensen S, Szklarczyk D, Poulsen JW, Horn H, Jensen LJ, Mailand N, Nielsen ML. Mass spectrometric analysis of lysine ubiquitylation reveals promiscuity at site level. Mol Cell Proteomics. 2011 Mar;10(3):M110.003590. doi: 10.1074/mcp.M110.003590. Epub 2010 Dec 7. PMID: 21139048; PMCID: PMC3047152.

Gee HY, Saisawat P, Ashraf S, Hurd TW, Vega-Warner V, Fang H, Beck BB, Gribouval O, Zhou W, Diaz KA, Natarajan S, Wiggins RC, Lovric S, Chernin G, Schoeb DS, Ovunc B, Frishberg Y, Soliman NA, Fathy HM, Goebel H, Hoefele J, Weber LT, Innis JW, Faul C, Han Z, Washburn J, Antignac C, Levy S, Otto EA, Hildebrandt F. ARHGDIA mutations cause nephrotic syndrome via defective RHO GTPase signaling. J Clin Invest. 2013 Aug;123(8):3243-53. doi: 10.1172/JCI69134. Epub 2013 Jul 8. PMID: 23867502; PMCID: PMC3726174.

Gregson HC, Schmiesing JA, Kim JS, Kobayashi T, Zhou S, Yokomori K. A potential role for human cohesin in mitotic spindle aster assembly. J Biol Chem. 2001 Dec 14;276(50):47575-82. doi: 10.1074/jbc.M103364200. Epub 2001 Oct 4. PMID: 11590136.

Guan J, Ekwurtzel E, Kvist U, Yuan L. Cohesin protein SMC1 is a centrosomal protein. Biochem Biophys Res Commun. 2008 Aug 8;372(4):761-4. doi: 10.1016/j.bbrc.2008.05.120. Epub 2008 Jun 2. PMID: 18515072.

Gupta IR, Baldwin C, Auguste D, Ha KC, El Andalousi J, Fahiminiya S, Bitzan M, Bernard C, Akbari MR, Narod SA, Rosenblatt DS, Majewski J, Takano T. ARHGDIA: a novel gene implicated in nephrotic syndrome. J Med Genet. 2013 May;50(5):330-8. doi: 10.1136/jmedgenet-2012-101442. Epub 2013 Feb 22. PMID: 23434736; PMCID: PMC3625828.

Iovine MK, Higgins EP, Hindes A, Coblitz B, Johnson SL. Mutations in connexin43 (GJA1) perturb bone growth in zebrafish fins. Dev Biol. 2005 Feb 1;278(1):208-19. doi: 10.1016/j.ydbio.2004.11.005 PMID: 15649473

Ishikawa H, Marshall WF. Ciliogenesis: building the cell's antenna. Nat Rev Mol Cell Biol. 2011 Apr;12(4):222-34. doi: 10.1038/nrm3085. PMID: 21427764.

Khanna H, Hurd TW, Lillo C, Shu X, Parapuram SK, He S, Akimoto M, Wright AF, Margolis B, Williams DS, Swaroop A. RPGR-ORF15, which is mutated in retinitis pigmentosa, associates with SMC1, SMC3, and microtubule transport proteins. J Biol Chem. 2005 Sep 30;280(39):33580-7. doi: 10.1074/jbc.M505827200. Epub 2005 Jul 25. PMID: 16043481; PMCID: PMC1249479.

Liu J, Zhang Z, Bando M, Itoh T, Deardorff MA, Clark D, Kaur M, Tandy S, Kondoh T, Rappaport E, Spinner NB, Vega H, Jackson LG, Shirahige K, Krantz ID. Transcriptional dysregulation in NIPBL and cohesin mutant human cells. PLoS Biol. 2009 May 5;7(5):e1000119. doi: 10.1371/journal.pbio.1000119. Epub 2009 May 26. PMID: 19468298; PMCID: PMC2680332.

May-Simera HL, Kelley MW. Cilia, Wnt signaling, and the cytoskeleton. Cilia. 2012 May 2;1(1):7. doi: 10.1186/2046-2530-1-7. PMID: 23351924; PMCID: PMC3555707.

Moreira AL, Sampaio EP, Zmuidzinas A, Frindt P, Smith KA, Kaplan G. Thalidomide exerts its inhibitory action on tumor necrosis factor alpha by enhancing mRNA degradation. J Exp Med. 1993 Jun 1;177(6):1675-80. doi: 10.1084/jem.177.6.1675. PMID: 8496685; PMCID: PMC2191046.

Ravindran E, Hu H, Yuzwa SA, Hernandez-Miranda LR, Kraemer N, Ninnemann O, Musante L, Boltshauser E, Schindler D, Hübner A, Reinecker HC, Ropers HH, Birchmeier C, Miller FD, Wienker TF, Hübner C, Kaindl AM. Homozygous ARHGEF2 mutation causes intellectual disability and midbrain-hindbrain malformation. PLoS Genet. 2017 Apr 28;13(4):e1006746. doi: 10.1371/journal.pgen.1006746. PMID: 28453519; PMCID: PMC5428974.

Sadano H, Sugimoto H, Sakai F, Nomura N, Osumi T. NXP-1, a human protein related to Rad21/Scc1/Mcd1, is a component of the nuclear matrix. Biochem Biophys Res Commun. 2000 Jan 7;267(1):418-22. doi: 10.1006/bbrc.1999.1969. PMID: 10623634.

Seeliger MW, Biesalski HK, Wissinger B, Gollnick H, Gielen S, Frank J, Beck S, Zrenner E. Phenotype in retinol deficiency due to a hereditary defect in retinol binding protein synthesis. Invest Ophthalmol Vis Sci. 1999 Jan;40(1):3-11. PMID: 9888420.

Stooke-Vaughan GA, Huang P, Hammond KL, Schier AF, Whitfield TT. The role of hair cells, cilia and ciliary motility in otolith formation in the zebrafish otic vesicle. Development. 2012 May;139(10):1777-87. doi: 10.1242/dev.079947. Epub 2012 Mar 29. PMID: 22461562; PMCID: PMC3328178.

Tare M, Sarkar A, Bedi S, Kango-Singh M, Singh A. Cullin-4 regulates Wingless and JNK signaling-mediated cell death in the Drosophila eye. Cell Death Dis. 2016 Dec 29;7(12):e2566. doi: 10.1038/cddis.2016.338. PMID: 28032862; PMCID: PMC5261020.

Udeshi ND, Mertins P, Svinkina T, Carr SA. Large-scale identification of ubiquitination sites by mass spectrometry. Nat Protoc. 2013 Oct;8(10):1950-60. doi: 10.1038/nprot.2013.120. Epub 2013 Sep 19. PMID: 24051958; PMCID: PMC4725055

Wagner SA, Beli P, Weinert BT, Nielsen ML, Cox J, Mann M, Choudhary C. A proteome-wide, quantitative survey of in vivo ubiquitylation sites reveals widespread regulatory roles. Mol Cell Proteomics. 2011 Oct;10(10):M111.013284. doi: 10.1074/mcp.M111.013284. Epub 2011 Sep 1. PMID: 21890473; PMCID: PMC3205876.

Wang J, Zhu ZH, Yang HB, Zhang Y, Zhao XN, Zhang M, Liu YB, Xu YY, Lei QY. Cullin 3 targets methionine adenosyltransferase IIα for ubiquitylation-mediated

degradation and regulates colorectal cancer cell proliferation. FEBS J. 2016 Jul;283(13):2390-402. doi: 10.1111/febs.13759. Epub 2016 Jun 6. PMID: 27213918.

Waters AM, Beales PL. Ciliopathies: an expanding disease spectrum. Pediatr Nephrol. 2011 Jul;26(7):1039-56. doi: 10.1007/s00467-010-1731-7. Epub 2011 Jan 6. PMID: 21210154; PMCID: PMC3098370.

Whitfield TT. Cilia in the developing zebrafish ear. Philos Trans R Soc Lond B Biol Sci. 2020 Feb 17;375(1792):20190163. doi: 10.1098/rstb.2019.0163. Epub 2019 Dec 30. PMID: 31884918; PMCID: PMC7017339.

Xu B, Gogol M, Gaudenz K, Gerton JL. Improved transcription and translation with L-leucine stimulation of mTORC1 in Roberts syndrome. BMC Genomics. 2016 Jan 5;17:25. doi: 10.1186/s12864-015-2354-y. PMID: 26729373; PMCID: PMC4700579.

Xu B, Lee KK, Zhang L, Gerton JL. Stimulation of mTORC1 with L-leucine rescues defects associated with Roberts syndrome. PLoS Genet. 2013;9(10):e1003857. doi: 10.1371/journal.pgen.1003857. Epub 2013 Oct 3. PMID: 24098154; PMCID: PMC3789817.

Zakari M, Yuen K, Gerton JL. Etiology and pathogenesis of the cohesinopathies. Wiley Interdiscip Rev Dev Biol. 2015 Sep-Oct;4(5):489-504. doi: 10.1002/wdev.190. Epub 2015 Apr 7. PMID: 25847322; PMCID: PMC6680315.

Zeng M, Ren L, Mizuno K, Nestoras K, Wang H, Tang Z, Guo L, Kong D, Hu Q, He Q, Du L, Carr AM, Liu C. CRL4(Wdr70) regulates H2B monoubiquitination and

facilitates Exo1-dependent resection. Nat Commun. 2016 Apr 21;7:11364. doi: 10.1038/ncomms11364. PMID: 27098497; PMCID: PMC4844679.

Zhao H, Khan Z, Westlake CJ. Ciliogenesis membrane dynamics and organization. Semin Cell Dev Biol. 2023 Jan 15;133:20-31. doi: 10.1016/j.semcdb.2022.03.021. Epub 2022 Mar 26. PMID: 35351373; PMCID: PMC9510604.

ANNIE C. SANCHEZ
Curriculum Vitae
29 West Greenwich Street, Bethlehem, PA 18018
(718) 473-5522 | anniesanchez526@gmail.com

EDUCATION

Lehigh University, Bethlehem, PA
PhD. Cellular and Molecular Biology — March 2023
Thesis: "The Molecular Link Between Cohesinopathies and Thalidomide Teratogenicity in Zebrafish Embryo Development."

Shippensburg University, Shippensburg, PA
B.A. Biology — May 2014
Research: "The Effects of Green Tea Extract on the Growth of Streptococcus mutans, the primary causative agent of human dental caries."

LANGUAGES

Spanish– native language
English– speak, read, and write fluently

GRANTS, FELLOWSHIPS, AND AWARDS

Lehigh College of Arts and Sciences Dean's Fellowship	August 2022
Doctoral Travel Grants for Global Opportunities	June 2022
Lehigh College of Arts and Sciences Travel Grant	April 2020,2022
Lehigh University 3 Minute Thesis Runner-Up	March 2022
Nemes Graduate Student Fellowship	August 2020,2021
American Society for Cell Biology Virtual Conference Grant	December 2020
Lehigh College of Arts and Sciences Summer Dean's Fellowship	June 2020
Lehigh CITL Teaching Certificate I	December 2019
Shippensburg University Undergraduate Research Achievement	April 2014
Certified Tutor	December 2013

RESEARCH PUBLICATIONS AND PRESENTATIONS

Articles

1. M.G. Mfarej, C.A. Hyland, A.C. Sanchez, M.M. Falk, M.K Iovine, R.V. Skibbens. Cohesin: An Emerging Master Regulator at the Heart of Cardiac Development. Mol.Biol. Cell. Mol Biol Cell. mbcE2212055, March 2023. PMID: 36947206.
2. A. Sanchez, E. Thren, M.K. Iovine, R. Skibbens. Esco2 and Cohesin Regulate CRL4 Ubiquitin Ligase ddb1 Expression and Thalidomide Teratogenicity. Cell Cycle, 1-13, January 2022. PMID: 34989322.
3. A. Sanchez, M. Hastings, E. Albán Cano, N. Yen, E. Michnowski, R. Zahrouni, S. Brabender. Mitigating the effects of COVID-19 on Wage Earnings for Female Domestic Workers in the Informal Economy in Ecuador and Brazil. Martindale Center Policy Brief on the Future of Work, 1, 38-41, February 2021.

Oral Presentations

1. Presenter. Inclusion of Indigenous Voices in Public Health Solutions. Life for a Child - Our Rights to Health in Latin America: A Type 1 Diabetes Advocacy Workshop. September 5, 2022.
2. Presenter. CRL4 Links Cohesinopathies to Thalidomide Teratogenicity. The 17th International Zebrafish Conference - Gene Regulation: Central Dogma/GRNs/Epigenetics Plenary Session. June 23, 2002.
3. Moderator. Maximizing Access to Essential Supplies for Kids (MATES4Kids): Global Multi-Stakeholder Collaboration and Partnership to #LeaveNoChildBehind. United Nations High Level Political Forum Parallel Event. July 13, 2022.
4. Moderator. The Nexus Between Climate Change and NCDs: Indigenous Women Led Solutions. United Nations NGO/CSW Parallel Event. March 17, 2022.
5. Moderator. The Impact of COVID19 on Obesity and Diabetes in the Asia-Pacific Region. NCD Child Asia Pacific Region Workshop. October 23, 2021.
6. Presenter. Drugs and Genes: A Link Between Thalidomide and Cohesinopathies. Lehigh University Biological Sciences Colloquium Seminar. April 22, 2022.
7. Presenter. Drugs, Genes, and Developmental Disabilities. Lehigh University 3-minute thesis competition. March 23, 2022. (2nd Place Winner).
8. Presenter. Fishing for a Cure: Pharmacological and Genetic Mechanisms of Birth Defects. Lehigh University Biological Sciences Colloquium Seminar. April 30, 2021.
9. Presenter. Lab Safety and Research in Times of COVID. Annual National Association for Graduate and Professional Studies Northeast Regional Conference. February 27, 2021.
10. Presenter. Mitigating the effects of COVID-19 on Wage Earnings for Female Domestic Workers in the Informal Economy in Ecuador and Brazil. United Nations International Labor Organization and Lehigh University Externship - Living Wage Research Symposium. January 29, 2021.

Poster Presentations

1. A. Sanchez, E. Anderson, M.K. Iovine, R.V. Skibbens. CRL4 Links Cohesinopathies to Thalidomide Teratogenicity. The 17th International Zebrafish Conference at Montreal, Canada. June 2022.
2. A. Sanchez, E. Anderson, M.K. Iovine, R.V. Skibbens. Cohesinopathies Disrupt ddb1 Expression in Zebrafish Embryos. Mid Atlantic Society for Developmental Biology Meeting at Lehigh University. May 2022.
3. B. Adams, M. G. Allen, N. Baban, M. C. Boffi, E. Greenholt, K. Harper, M. Hawes, B. Moskal, K. Parsa, J. Rotay, A. Sanchez, O. Schulman, R. Sequeira, I. Shin, V. C. Ware, M. R. Kuchka. Elucidating Mycobacteriophage Taptic Gene Functions with the SEA-GENES Research Project at Lehigh University. Howard Hughes Medical Institute Annual SEA Symposium. April 2022.
4. E. Anderson, A. Sanchez, M. K. Iovine, R. V. Skibbens. Drugs, Genes and Birth Defects – a Zebrafish model. Poster presented at: The Research Day Summer Expo at Lehigh University, August 2021.
5. S. Andryshak, A. Boyer, G. Ciabattoni, H. Cho, N. Clarke, P. Demetriades, N. DesGranges, B. Dubyna, M. Dunterman, E. El-Halawani, M. Fehrenbach, G. Forsyth, A. Fucile, S. Haab, A. Iftikhar, R. Kyle, R. Milelli, C. Murphy, N. Novak, R. O'Toole, R. Roberts, S. Rosenthal, A. Sanchez, J. Skrapits, M. Sorbello, G. Stephenson, N. Weaver and M. Kuchka. Elucidating mycobacteriophage Butters

Gene Functions with the SEA-GENES Research Project at Lehigh. Poster presented at: Howard Hughes Medical Institute SEA-GENES Virtual Research Symposium. April 2021.

6. A. Sanchez, E. Thren, M.K. Iovine, R. Skibbens. Cohesin Defects Disrupt Expression of an Essential Component of the CRL4 Ubiquitin Ligase Involved in the Thalidomide Teratogenicity Pathway. Poster presented at: ASCB/EMBO Virtual Cell Biology Conference. December 2020.
7. A. Sanchez, M.K. Iovine, R. Skibbens. Involvement of Cohesin in Skeletal Development of Zebrafish Embryos. Presented at: Lehigh University Department of Biological Sciences Graduate Student Poster Session. February 2019. Bethlehem, PA.
8. J. Keller, A. Sanchez, J. Myslowski, B. Quinto, M. Lehman. The Effects of Green Tea Extract on the Growth of Streptococcus mutans, the primary causative agent of human dental caries. Poster presented at: Shippensburg University Research Symposium. April 2014. Shippensburg, PA.

RESEARCH EXPERIENCE

Lehigh University
Graduate Research Assistant,
Advisors: Dr. Kathryn Iovine and Dr. Robert Skibbens January 2018 – Present
Investigated the role of the cohesin complex and the Cullin-4 Ring Ligase in developmental processes in zebrafish embryos and human patient cell lines. Utilized molecular biology and biochemistry techniques such as PCR, RT-PCR, DNA and RNA extraction, in-situ hybridization, lysate preparations, plasmid cloning, transformations, in vitro transcription, microinjections, in vitro fertilization, Western blots, luciferase reporter assay, and mass spectrometry. Findings have led to multiple poster presentations and oral presentations with Lehigh University Biological Sciences department and at national and international conferences. Mentored 3 undergraduate students under this project.

Lehigh and United Nations Externship,

Advisors: Kira Mendez and Bill Hunter January 2020 – February 2020
Participated in inaugural Lehigh/United Nations International Labor Organization externship program. Performed research on living wage policies and effective legislative practices for minimum wage implementation. Collaborated with the Universidad de San Francisco de Quito in Ecuador on research. Findings were presented to United Nations International Labor Union expert panel and brief was published in book developed by Lehigh/United Nations Partnership.

Graduate Research Assistant,

Advisor: Dr. Robert Skibbens January 2018 – May 2018
Investigated the role of an E3 ubiquitin ligase on chromosome cohesion and condensation in Saccharomyces cerevisiae. Utilized sterile technique, poured plates, performed cell cycle arrest, flow cytometry, condensation assay and imaging, PCR, DNA extractions, plasmid cloning, and transformations.

Graduate Research Assistant,

Advisor: Dr. Kathryn Iovine August 2017 – December 2017
Studied the Effects of Axin2, a Wnt pathway product of Beta catenin, in joint formation. Findings contributed to Bhattacharya et al. Simplet-dependent regulation of β-catenin signaling influences skeletal patterning downstream of Cx43. Development. October 24, 2018. Performed PCR, RNA probe preparation, in-situ hybridization, zebrafish fin clips, zebrafish fin microinjections and electroporation.

Eurofins Lancaster Laboratories
Scientist August 2014 – July 2017
Performed pharmaceutical testing in Antimicrobial Effectiveness Studies, Microbial Limits Testing, Water Testing, and Microbial Organism Identification Studies. Trained in LIMS, cGMP, GLP, and controlled and hazardous substance testing. Findings contributed to FDA regulatory standard decisions and furthered research on novel antimicrobial product effectiveness and development.

Shippensburg University
Undergraduate Research Assistant,
Advisor: Dr. Marci Lehman August 2013 – May 2014
The Effects of Green Tea Extract on the Growth of Streptococcus mutans, the primary causative agent of human dental cavities. Study received undergraduate research achievement award from Shippensburg University. Utilized sterile technique, poured plates, performed antimicrobial studies, and spectrophotometer readings.

LEADERSHIP EXPERIENCE

IndigenousNCDs
Board of Directors Member January 2022 – Present
Supported and advocated for the inclusion of Indigenous voices in the Non-Communicable Diseases (NCD) global discourse. Served on steering committee meetings with the CEO and represented IndigenousNCDs as a panelist and moderator for panelist discussion at NCD Child Asia-Pacific and Latin America Workshops on Type I Diabetes. Led, organized, and translated from Spanish to English a parallel event to the Commission on the Status of Women on Indigenous women-led solutions to climate change impacts.

Lehigh University
United Nations Youth Representative for
Caring and Living as Neighbours (CLAN) May 2021 – Present
Advocated CLAN's mission of maximizing the quality of life of children living with chronic health conditions in low- and middle-income countries at the UN and relevant events. Drafted communication and comments for the UN Commission on the Status of Women, the Draft Convention on the Rights to Development, and High-Level Political Forum on behalf of CLAN which holds ECOSOC consultative status. Created and implemented 2-year strategic framework of action to amplify CLAN's Lehigh/UN Youth Rep Program partnership. Drafted comments for the Workplan from Global Coordination

Mechanism on the prevention and control of noncommunicable disease submitted to the 74th World Health Assembly.

National Association for Graduate and Professional Studies
Northeast Director for Social Justice Concerns March 2021 – Present
Contributed to association outreach projects, including the development of a mentorship guide for graduate students. Worked with the National Social Justice Concerns Chair and served on the Social Justice Concerns Committee. Reported activities of committee to the regional board. Brough up regional concerns and issues to the NAGPS National Advocacy Committee and recruited students from regional member schools to serve on committee. Created agenda and organized events for NAGPS northeast conference at Northeastern University.

National Science Policy Network
SciPol Scholar April 2022 – May 2022
Selected to participated in six-week bootcamp on science policy themes and networked with leaders in the field. Collaborated with other scholars on weekly activities and professional development. Researched and wrote policy memo on climate change impacts on indigenous communities' health. Currently developing a residence position with host office for hands on experience in science policy.

Hillcrest Pharmacy and Compounding
COVID19 Vaccination Center Administrative Volunteer March 2021 – May 2021
Assisted in patient entry into Pennsylvania Statewide Immunization Information System for COVID19 vaccine distribution tracking. Prepared and logged patient medical records and insurance information into pharmacy record system. Translated communication to Spanish speaking patients.

College of Arts and Sciences at Lehigh University
CAS Dean Graduate Student Council May 2020 – August 2021
Served in graduate student advisory board for the college dean. Aided in proposal review for CAS Summer, Fall and Spring Fellowship applications. Brought concerns and advocated for graduate students in the Biological Sciences Department and College of Arts and Sciences. Communicated relevant information and upcoming opportunities to graduate students.

Graduate Student Senate at Lehigh University
External Affairs Officer April 2020 – April 2021
Elected to serve in COVID response team meetings and Graduate Student Senate executive board. Increased collaborations and communications for political advocacy with the Associate Vice President for Government Relations and associated offices. Informed Lehigh's graduate student population of governmental policies pertaining to their studies and issued statements on executive senate positions. Coordinated and implemented communication with organizations outside of Lehigh University, including NAGPS, the graduate student coalitions, and graduate student governments. Effectively led the distribution and drafting of executive and legislative letters sent to government

officials and the local and national level as well as Graduate Student senate position statements and legislative action items statements sent to government relations offices. Continue to serve as external affairs committee member where I researched and compiled data on legislature changes affecting graduate students.

Lehigh University Creative Inquiry
Creative Scholarship Institute Scholar October 2022- February2021
Selected to be a part of the 2020 cohort for the Creative Scholarship Institute Mountaintop Initiative. Participated in immersive workshops and roundtables covering topics such as creativity and innovation, building a professional identity, communicating your research, authentic leadership, inclusive excellence, ethics and integrity and negotiating and resolving conflicts.

Graduate Life Office at Lehigh University
Provost Diversity, Inclusion and Equity Advisory Board August 2020 – December 2020
Advised and contributed to discussions on diversity, inclusion, and equity for the Provost for Graduate Studies. Shared resources and contributed to idea and project developments. Reviewed university diversity, equity and inclusion workplan and provided feedback.

Graduate Student Orientation Ambassador August 2020 – January 2021
Contributed to incoming graduate student orientation development with the Dean of Graduate Studies. Participated in orientation videos and contributed to content. Assisted incoming graduate students with questions or concerns.

Biological Organization of Graduate Students at Lehigh University
President June 2019 – May 2020
Facilitate and handle logistics of the organization, such as scheduling, budgeting, and meetings. Developed an officer's responsibility and budget tracking documents for future officers. Served as head of graduate student representative for the Biological Sciences Department. Successfully led and planned educational workshops and social events for all graduate students in the Biological Sciences department and university wide.

Health Sciences Club at Shippensburg University
Vice President April 2013 – April 2014
Collaborated with President to create and organize club schedules and budgets. Led and organized scheduled meetings, fundraisers, and student activities. Successfully led and organized trips and events to health-related museum for over 20 members.

Tri-Beta Biological Honor's Society at Shippensburg University
Treasurer March 2013 – April 2014
Maintained accurate financial records and managed organizations funds. Worked alongside faculty advisor to properly allocate funds for the organization.

Alpha Phi International Fraternity at Shippensburg University
Director of Finance November 2012 – November 2013

Collaborated with vice president of chapter operations to manage and collect chapter funds. Led new member meetings and developed computer-based payment options for all members.

TEACHING AND MENTORING EXPERIENCE

Mentor Collective
Mentor August 2020 – August 2022
Served as mentor for two first-year Lehigh University College of Arts and Sciences graduate students. Met regularly and provided advice and resources for students. Provided mentor collective and the graduate life office feedback and areas of focus.

Lehigh University
Teaching Assistant for Dr. Michael Kuchka February 2021 – May 2022
Howard Hughes Medical Institute SEA-GENES Lab and January 2020 – May 2020
Collaborated in the research and implementation of the Howard Hughes Medical Institute SEA-GENES course. Graded all lab reports, prepared equipment and reagents, and contributed to data analysis. Aided in transition to online learning due to COVID-19 pandemic. Troubleshooted and explained laboratory molecular biology techniques such as PCR, molecular cloning, bacterial transformations, isothermal assembly, super immunity assays and cytotoxicity assays.

Teaching Assistant for Dr. Lynne Cassimeris August 2019 – December 2019
Cell Biology
Graded and proctored exams and assignments. Assisted students with course material and met with students upon request. Worked alongside professor and assisted during lectures when needed.

Teaching Assistant for Dr. Katie Hoffman January 2019 – May 2019
Principles of Cell Biology
Collaborated and led in the development of active learning activities, led recitations and assisted professor during lectures, met with students upon request, administered exam grades for the course.

Teaching Assistant for Dr. Margaret Kenna August 2017-December 2017
Principle of Cell Biology Lab and Introduction to Genetics Lab and January 2018 – May 2018
Collaborated on curriculum and exam development, led laboratory lectures and explained protocols, met with students upon request, administered all grades for the course. Explained laboratory techniques such as bacterial and yeast transformations, complementation experiments, tumor suppressor activity identification in yeast, spontaneous mutations through evolution experiments, UV damage experiments and mutation screens.

Nationalities Service Center
Homework Help Tutor August 2020 – December 2020
Assisted high school student transition to online learning environment for all their courses. Shared resources with student and family members. Received training from the

Philadelphia Nationalities Service Center for implementing effective tutor strategies for their diverse population of students.

Eurofins Lancaster Laboratories
New Employee Trainer February 2016 – July 2017
Pharmaceutical Microbiology Department
Trained new employees on autoclave and water content equipment use. Assisted in Microbial Limits Testing, Antimicrobial Effectiveness Study and MALDI Sequencing Protocol training to new employees. Created and updated laboratory procedures to meet regulatory requirements.

Shippensburg University
Tutor January 2012 – May 2014
University Learning Center
Met with student for one-on-one or group sessions to assist with class material understanding for their beginning or advanced Spanish courses as well as pre-calculus and calculus courses, scheduled tutor meetings for the learning center.

PROFFESIONAL SOCIETIES

Society for Research in Child Development
Society for Developmental Biology
National Association for Graduate and Professional Studies
American Society for Cell Biology
Genetics Society of America
Biological Organization of Graduate Students at Lehigh University
Graduate Student Senate at Lehigh University
Beta Beta Beta Honor's Biological Society Rho Epsilon Chapter
Order of Omega Leadership Honor Society Eta Upsilon Chapter
Alpha Phi International Fraternity Theta Xi Chapter